ELECTRON SPIN RESONANCE AND OPTICAL SPECTROSCOPY OF HYDROCARBON RADICALS AT 4°K IN RARE-GAS MATRICES

by

KEITH INGRAM DISMUKE

A DISSERTATION PRESENTED TO THE GRADUATE COUNCIL OF
THE UNIVERSITY OF FLORIDA
IN PARTIAL FULFILLMENT OF THE REQUIREMENTS FOR THE
DEGREE OF DOCTOR OF PHILOSOPHY

UNIVERSITY OF FLORIDA

1975

to

My Family

ACKNOWLEDGEMENTS

The author extends his deep appreciation to Professor William Weltner, Jr., whose professional guidance and support made this research possible. The author acknowledges a special debt of gratitude to Dr. W. R. M. Graham, for his collaboration and informative discussions during the entire period of this work.

The author would also like to thank the members of Professor Weltner's research group as well as the staff of the machine and glass shops for the fabrication of experimental apparatus.

The completion of this dissertation would not have been possible without the love, support, and professional typing ability of the author's wife, Lin, to whom the author extends a very special appreciation.

The author would also like to acknowledge the support of the Air Force Office of Scientific Research and the National Science Foundation during this work.

TABLE OF CONTENTS

LIST OF TABLES

LIST OF FIGURES

Abstract of Dissertation Presented to
the Graduate Council of the University of Florida
in Partial Fulfillment of the Requirements for
the Degree of Doctor of Philosophy

ELECTRON SPIN RESONANCE AND OPTICAL SPECTROSCOPY OF HYDROCARBON RADICALS AT 4°K IN RARE-GAS MATRICES

by

KEITH INGRAM DISMUKE

March, 1975

Chairman: Professor William Weltner, Jr.
Major Department: Chemistry

Radical and molecular species including C_2H, C_2^-, C_4H, C_4, and $M^+C_2^-$, where M^+ represents various alkali metal cations, have been studied by the methods of electron spin resonance (ESR) and optical spectroscopy. This work employed the techniques of matrix isolation whereby the radicals to be studied were trapped in inert, solid rare-gas matrices at liquid helium temperatures.

From ESR spectra, magnetic parameters of the radicals such as g tensors, hyperfine interaction tensors (hf), and zero-field-splitting tensors (D) are determined. The value of these quantities allows the derivation of fundamental quantities such as the spin-doubling constant, γ, the electronic spin density at the site of a nucleus, $|\Psi(0)^2|$, coefficients of the wavefunctions, and others. This is supplemented by optical measurements taken

in the infrared, visible, and ultraviolet regions from which vibrational and electronic energy level separations can be determined.

The ethynyl radical, C_2H, was prepared by the high-energy photolysis of two different parent molecules, acetylene and monoiodoacetylene. This research led to the detailed characterization of the electronic and magnetic properties of C_2H, including complete spin density data of the ground state and the identification of several excited electronic states. It was determined that C_2H, in the ground state, is a linear $^2\Sigma$ molecule with the unpaired electron localized largely on the end carbon nucleus. The possibility is also proposed that C_2H undergoes bent ↔ linear electronic transitions. The results obtained in this work make possible the identification of the previously unobserved C_2H radical in interstellar clouds.

Previous matrix isolation studies have shown that the optical spectrum of C_2^- is enhanced upon the addition of the alkali metal atoms (M). When the alkali metal concentration is increased, it was found that C_2^- and the alkali metal cations form ion-pairs ($M^+C_2^-$). Analysis has demonstrated that the C≡C vibrational frequency in the excited state is dependent on both size and polarizability of the alkali metal used. Approximate ground state hf

coupling constants were determined. The shape of $M^+C_2^-$, based on ESR analysis, is a triangular conformation with C_{2v} symmetry.

The previously unidentified C_4H radical, predicted to be a relatively abundant polyatomic species in the atmospheres of carbon-rich stars, has been produced by the high-energy photolysis of diacetylene (C_4H_2). The ESR spectrum consisted of a doublet at g = 2.0004 due to the magnetic interactions of the unpaired electron and the hydrogen nucleus indicating an expected $^2\Sigma$ ground state. C_4H absorbs strongly in the 3000 Å region, with progressions attributed to excitation of the C-H, C-C, and two C≡C symmetric vibrations. A C≡C-H bending mode was also excited in the 3000 Å system. The identification was confirmed by the effects of isotopic substitution. From the value of $g_\perp$ of C_4H, a predicted value of γ has been determined, a value which may aid in the future observation of C_4H in interstellar atmospheres.

C_4 has been prepared by two completely different methods including the photolysis of C_4H_2 with high-energy radiation and the vaporization of graphite. The ESR spectra of both $^{12}C_4$ and $^{13}C_4$ have been observed and analyzed, confirming that the ground state of C_4 is $^3\Sigma$. From this analysis, the D value has been determined for various conditions illustrating that the derived D value is dependent upon the matrix environment, isotopic composition, and temperature. From $g_\perp$ = 2.0042, γ for C_4 is predicted to be -0.0006 cm^{-1}.

CHAPTER I
INTRODUCTION

The Matrix Isolation Technique

Optical and electron spin resonance spectroscopy are routinely used in the investigation of molecules in the gas phase. Some molecules are very difficult or even impossible to observe in the gas phase because of their short lifetimes, reactivity, and/or method of preparation. Some molecules are observed only under high temperature conditions, for example in the atmospheres of stars or in arcs, so that as a result of thermal excitation into many rotational, vibrational, and low-lying electronic states, the optical spectra are often quite complicated and difficult to interpret. Even if the analysis problems are solved, ambiguities may arise in the assignment of the ground state because of the population of low-lying electronic states. Other short-lived species, such as free radicals, may be highly reactive or have very short lifetimes thus making it impossible to produce a large enough concentration for gas-phase observations.

In the matrix isolation technique, high temperature species, reactive molecules, or free radicals are prepared and trapped as isolated entities in inert, transparent solids, or matrices, at cryogenic temperatures. These

trapped species can then be studied by optical or electron spin resonance techniques more or less at leisure. The isolated species do not undergo translational motion--i.e., diffusion--and are usually prevented from rotating, but may vibrate with frequencies within a few percent of the gas-phase values when excited with electromagnetic radiation. Thus, the spectra of the material in these matrices are frequently much simpler than those for any other state of matter as they will show no rotational structure and all absorptions will occur from the lowest vibrational state of the ground state.

Several methods are employed for the production of these species. A typical method used is the evaporation of an active species from a Knudsen cell. The evaporated species can then be deposited simultaneously with the inert matrix material. The formation of many radicals does not involve evaporation but the photolytic dissociation of a parent molecule during deposition. If the parent is a gas, then standard gas-handling techniques are employed and one may either mix the gas with the matrix gas in the desired proportion prior to spraying onto the cryogenic surface or co-condense the materials from separate gas inlets. Photolytic dissociation may be carried out by subjecting the material to radiation by high-energy sources such as microwave or electric discharges, ultraviolet lamps, or gamma rays, or by electron

or ion bombardment. It is evident from this discussion that if the isotopically-substituted parent species is available, the investigation of the isotopically-substituted radical or molecule presents no problem.

The matrix material can be any gas which will not react with the trapped species and which can be conveniently and rigidly solidified; however, it should be chosen to have little effect on the trapped species so that they will be in as nearly a gas-like condition as possible. The solid rare gases are usually used as matrices since they are relatively inert chemically, transparent to light over a wide wavelength region, and offer a wide range of melting points and atomic sizes. Since a neon matrix has the least polarizable atoms, it is expected to perturb the molecule least and is usually found to be the best matrix. However, since it melts at $24^{\circ}K$ and diffusion in the solid state probably begins at about $12^{\circ}K$, it can only be used with liquid helium as a refrigerant. It is found that, in general, the heavier rare gases perturb the trapped molecules more then argon and neon and therefore are less desirable as matrix media.

There are some disadvantages to the matrix isolation technique. The principal disadvantage is the effect of the matrix on trapped species. Such effects caused by the matrix environment, usually manifested as small

frequency shifts, multiplet structures, and variation in absorption intensities, are often complicating factors in the initial spectral interpretation. A quantitative explanation of the precise nature of the interactions causing these perturbations is still lacking although much work has been directed toward this problem. For examples of theoretical treatments of matrix effects, see (1-6).

This introduction is not designed to discuss in depth the subject of matrix isolation techniques. However, several very good review articles and books have been written on this technique and many aspects of the methods used. Extensive details and reviews on matrix isolation as applied to atomic and molecular studies have been given by Bass and Broida (7), Jacox and Milligan (8), Weltner (9), and Hastie, Hauge, and Margrave (10).

References - Chapter I

1. G. C. Pimentel and S. W. Charles, Pure Appl. Chem. 7, 111 (1963).

2. E. D. Becker and G. E. Pimentel, J. Chem. Phys. 25, 224 (1956).

3. M. J. Linevsky, J. Chem. Phys. 34, 587 (1961).

4. M. McCarty, Jr. and G. W. Robinson, Mol. Phys. 2, 415 (1959).

5. E. S. Pysh, S. A. Rice, and J. Jortner, J. Chem. Phys. 43, 2997 (1965).

6. D. McLeod, Jr. and W. Weltner, Jr., J. Phys. Chem. 70, 3293 (1966).

7. A. M. Bass and H. P. Broida, Formation and Trapping of Free Radicals, New York: Academic Press, Inc., 1960.

8. M. E. Jacox and D. E. Milligan, Appl. Opt., 3, 873 (1964).

9. W. Weltner, Jr., Advances in High Temperature Chemistry, New York: Academic Press, Inc., 1970, Vol. 2, p. 85.

10. J. W. Hastie, R. H. Hauge, and J. L. Margrave, Spectroscopy in Inorganic Chemistry, New York: Academic Press, Inc., 1970, Vol. 1, p. 57.

CHAPTER II
EXPERIMENTAL

Introduction

The general experimental procedure including apparatus, reagents and techniques employed in this research will be treated in this section and specific details relevant to the study of a species will be presented under that given species.

Experimental

Reagents

In a typical experiment, a sample of some small organic gas molecule was premixed by standard manometric procedures with a gas which was to be used as the inert solid when trapped for observations at $4^{\circ}K$. The inert gases employed were research grade rare gases (99.999% pure), usually argon and occasionally neon or krypton, which were obtained from commercial sources and used without further purification.

Apparatus and General Technique

In this research all experiments were carried out on two separate dewars both of which were adapted from the design of Jen, Foner, Cochran, and Bowers (1). One dewar is designed primarily for ESR experiments and the

other for optical experiments. Both systems are comprised of an outer liquid nitrogen dewar which acts as a heat shield and an inner liquid helium dewar which is in good thermal contact with the trapping surface. The inner dewar is positioned such that the trapping surface is directly in the path of the sample inlets. Both systems are designed so that the inner dewar is interchangeable in order to hold either a variable temperature or constant temperature liquid helium dewar.

For constant temperature optical studies, the inner dewar consists of a deposition window which is in contact on all four sides with a copper holder filled with liquid helium. The holder is designed so that the deposition windows are interchangeable and rotatable through 360°. By rotating the inner dewar by approximately 90°, the deposition window is directly in line with two windows in the wall of the outer container so that optical studies are made possible. By rotating the window approximately 90° more, the trapping surface is now in line with another window in the outer container which can be used for photolysis of the sample.

The material of the outer window and deposition window will depend upon which optical region is to be studied. For an infrared study, all windows should be made of cesium iodide (CsI) which transmit radiation through the visible out to about 60μ. Calcium fluoride

(CaF_2) windows are used for study in the ultraviolet and visible regions with either a CaF_2 or sapphire deposition window.

Figure 1 shows the basic features of the variable temperature dewar used for optical studies. The liquid helium reservoir is connected to a copper block by 1/8 inch stainless steel tubing. Again a deposition window is fitted into the copper block so as to be in contact on all four sides with the cooled block. The reservoir is pressurized to about 2.5 psi causing the liquid helium to flow through channels in the copper block cooling it to liquid helium temperature. The rate of flow of the helium is regulated by a Hoke micrometer needle valve at the outlet. A thermocouple (Constantan vs. Au - 0.02 at.% Fe) is connected as closely as possible to the deposition window for temperature measurements. Temperature measurements are made using the thermocouple in conjunction with a Leeds and Northrup potentiometer.

To vary the temperature of the window, the micrometer needle valve can be closed to limit the flow of liquid helium into the lower chamber. As the helium evaporates, it forces the liquid out of the channels in the copper block thereby causing a rise in the temperature. The temperature change is carefully followed by monitoring both the temperature and pressure in the dewar. The

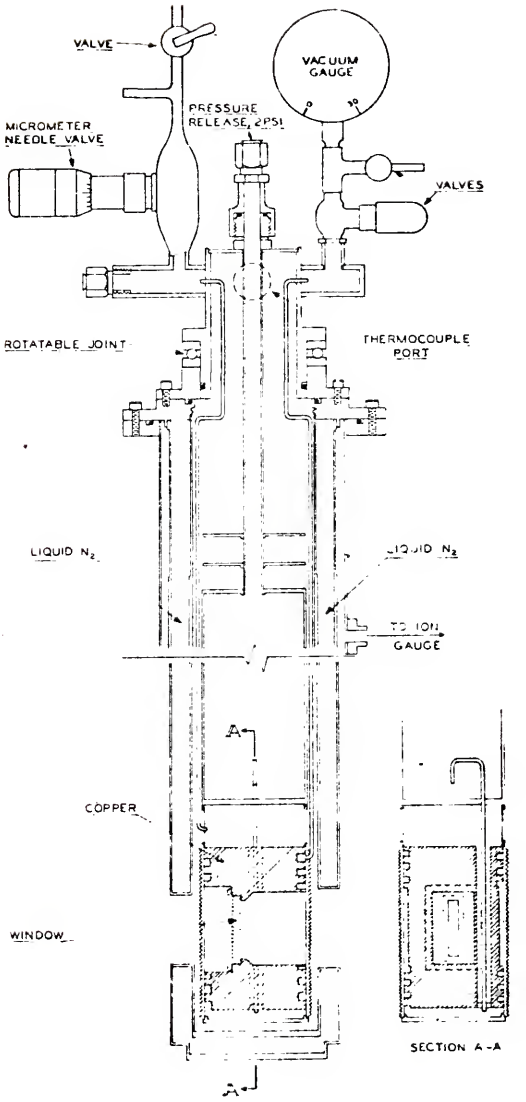

Figure 1: Basic design features of variable-temperature liquid-helium dewar used for optical studies.

window and matrix can be quickly quenched back to liquid helium temperature by opening the needle valve and allowing the liquid to flow again.

Figure 2 shows the dewar arrangement as well as the furnace system used for constant temperature ESR experiments. The trapping surface is single crystal sapphire (1-1/4" long, 1/8" wide, 3/64" thick) with one end securely embedded by Wood's metal solder into the inner dewar which is cooled to $4^{\circ}K$. By means of a vacuum-tight bellows assembly located at the top of the dewar (not shown in the Figure) the sapphire rod can be lowered or raised and rotated 360° inside or outside of the microwave cavity. When the rod is in the raised position, it is directly in line with the gas inlet and any beam of high temperature molecules being produced in the furnace. When the rod is in this position, it is in the optical path of two interchangeable windows in the outer container which makes it possible to photolyze a sample during or after deposition or to study a sample optically. If the furnace section has been used, after deposition of a sample, the entire furnace assembly may be uncoupled from the dewar by a double gate valve system without breaking the vacuum in either section. Then the rod can be lowered into the microwave cavity and the entire dewar can be rolled on fixed tracks between the pole faces of the ESR magnet.

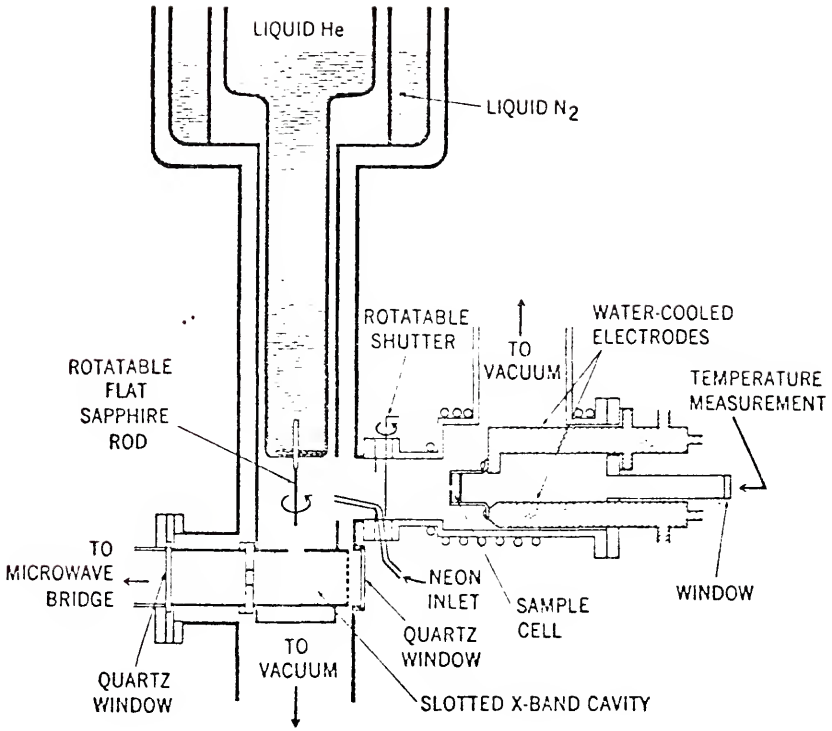

Figure 2: Basic design features of liquid-helium dewar used for ESR studies.

The inner dewar design for variable temperature ESR experiments is shown in Figure 3. As in the optical variable temperature dewar, the desired temperature is obtained by controlling the rate of helium flow through a copper section at the bottom of the pressurized liquid helium reservoir. A thermocouple (Chromel vs. Au - 0.02 at.% Fe) is connected to the copper section for temperature measurements.

In preparing a matrix for study several different techniques were employed depending upon the required species. In some cases the substance to be isolated could be prepared by photolysis of a gaseous parent molecule. In other cases, the substance to be isolated could only be prepared from a nonvolatile parent species. And in some instances it was required to isolate both volatile and nonvolatile species together.

If the species to be isolated could be prepared from a volatile parent compound, standard manometric techniques were employed to premix the inert gas with the volatile parent compound in the desired proportion. The gases could then be sprayed onto the cryogenic surface and photolyzed either during or after the deposition. The rate at which the gases are introduced is controlled by a needle valve adjustment and monitored by a Heise Manometer.

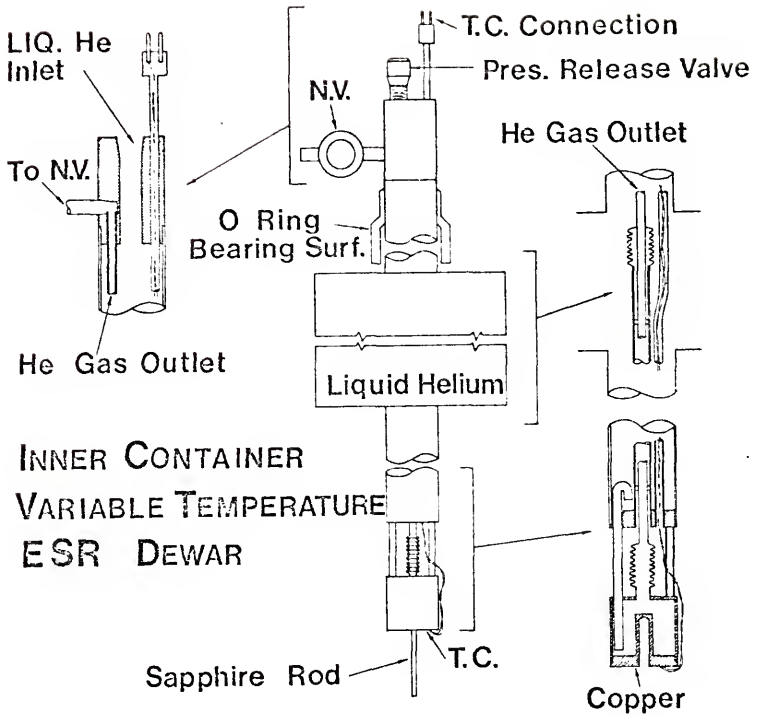

Figure 3: Basic design features of variable-temperature liquid-helium dewar used for ESR studies.

When the species to be isolated could be prepared only from a nonvolatile substance, a Knudsen cell was used to produce a molecular beam from a parent substance which was codeposited with the inert gas. Figure 2 shows how the furnace section containing the Knudsen cell was designed so that the trapping surface was directly in line with the molecular beam. The cell to be resistance heated was constructed of tantalum tubing which was filled with the nonvolatile species. The cell was supported on water cooled copper electrodes and heated to the desired temperature. The temperature was measured with either a vanishing filament optical pyrometer through an 0-ring sealed glass viewing port equipped with a magnetic shutter to prevent film formation on the glass or a (Chromel vs. Alumel) thermocouple in conjunction with a Leeds and Northrup potentiometer connected directly to the tantalum cell. The distance between the Knudsen cells in the furnace and the trapping surface was approximately twelve centimeters.

The furnace and dewar are independently pumped by mechanical and two inch silicone oil diffusion pumps. When the dewar contains liquid nitrogen in the outer shield and liquid helium in the inner dewar, pressures as low as 3×10^{-8} mm Hg are obtained while pressures down to 1×10^{-6} mm Hg were obtained with liquid nitrogen in the furnace systems. Pressures were monitored by Bayert-Alpert ionization gauges.

Some experiments require premixed gas to be co-deposited with a nonvolatile substance in which case a combination of the two techniques described above was employed.

Two basic techniques were used for the production of the desired molecular species or radical species. One technique employed the previously discussed high-temperature Knudsen cell while in the other technique, various parent materials were photolyzed with radiation from high-energy sources including either a flowing hydrogen-helium electrodeless discharge lamp or a high pressure mercury lamp.

The mercury lamp consists of water cooled mercury capillary lamp operated at 1000 watts (type A-H6 obtained from G. W. Gates & Co., Inc., N.Y., water jacket is PEK-SEB type single ended water jacket obtained from PEK labs). This lamp radiates energy in the ultraviolet and visible region which is composed of two principal components: (a) characteristic mercury line spectra and (b) a strong base continuum.

To limit heating effect of the mercury lamp, it was usually operated in conjunction with an ultraviolet transmitting filter which was non-transmitting in the visible and infrared regions. Normally a Corning 7-54 filter was employed. For photolysis of a sample with the mercury lamp, the dewar was equipped with a quartz optical window to transmit the ultraviolet radiation.

The flowing hydrogen-helium electrodeless discharge lamp radiates high energy radiation in the vacuum ultraviolet region. The lamp, shown schematically in Figure 4, is constructed after the design of David and Braun (2). A cylinder of the hydrogen-helium gas mixture (approximately 10 percent hydrogen by volume) was attached to the lamp gas inlet. A mechanical forepump was employed to evacuate the entire system to a pressure of about 30μ which effectively seals the lamp to a LiF window by means of a brass fitting with two "O" rings. The gas flow was then adjusted with a Hoke needle valve to a pressure of approximately 1 torr. The gas mixture is led into and out of the lamp with flexible Tygon tubing. The LiF window was positioned in the dewar so that the incoming parent material would be photolyzed by the radiation produced by this lamp.

A Raytheon PGM 10, 85 W, 2450 MHz microwave generator in conjunction with a tunable cavity was used to excite the discharge in the flowing gas. Figure 5 shows the emission spectrum from the lamp in the vacuum ultraviolet region measured through a LiF optical window.

Due to the very high energy radiation being transmitted by the LiF windows yellow color centers were noticeable after five to ten hours of normal use of the lamp. This cut the efficiency of the lamp measurably. In order to rid the LiF windows of these color centers

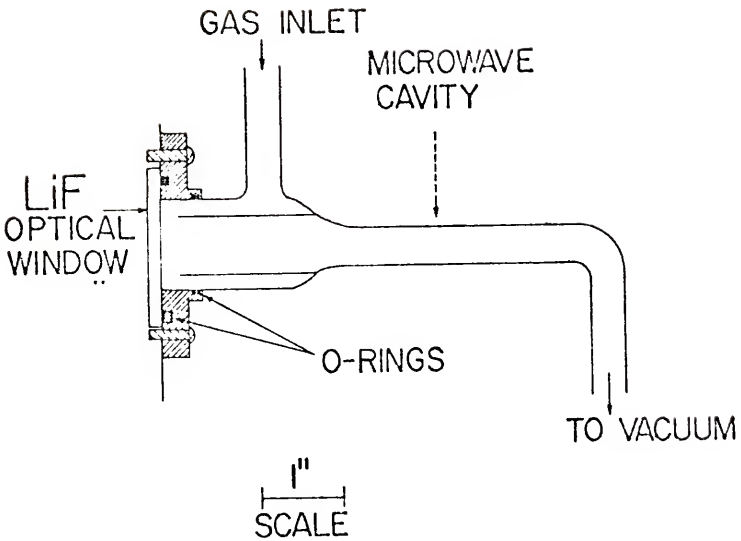

Figure 4: Schematic drawing of flowing hydrogen-helium quartz electrodeless discharge lamp.

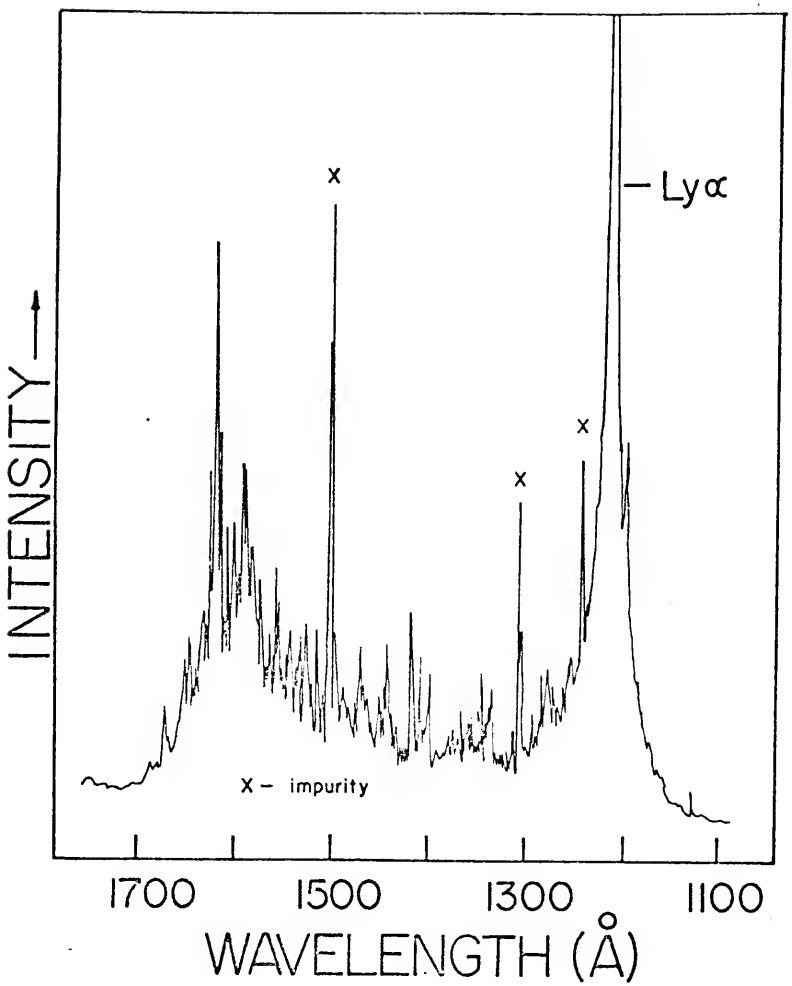

Figure 5: Emission spectrum from hydrogen-helium flowing discharge lamp measured through a LiF optical window.

these windows were removed from the dewars and annealed at approximately 800°F for one to two hours. LiF windows were changed and annealed normally after every two or three experiments to maximize the efficiency of photolysis and the yield of products.

As stated previously, the optical dewar could be equipped with various windows and trapping surfaces in order to analyze the prepared matrix in the regions ranging from the infrared to the far ultraviolet.

For investigations of the infrared region (4000-200 cm^{-1}), a Perkin Elmer 621 spectrophotometer with interchangeable grating and calcium fluoride prism optics was used. Optical spectra in the range 3500 to 10,500 Å were recorded using a Jarrell-Ash 0.5 m Ebert scanning spectrometer with gratings blazed at 5000 Å and 10,000 Å and fitted with RCA 1P21 or 7102 photomultipliers. A GE tungsten lamp provided the continuum and spectra were calibrated with mercury lines from a low pressure Pen Ray Quartz mercury lamp source. From 2000 to 3500 Å an evacuated McPherson monochromator with a RCA 941 photomultiplier monitoring the radiation from the exit slits through a sodium salicylate window was employed. The continuum was provided by a microwave discharge through a lamp filled with xenon to a pressure of approximately 400 torr.

ESR spectra were recorded on a Mosely 2D-2 XY recorder with the Varian V-4500 instrument employing superheterodyne detection. The magnetic field was measured by using an Alpha Scientific Model 675 NMR fluxmeter whose frequency was determined with a Beckman 6121 counter. The X-band microwave cavity frequency ($\nu \simeq 9.4$ GHz) was measured with a Hewlett Packard high Q wavemeter.

For a typical experiment the area around the trapping surface was evacuated to a pressure as low as possible ($\simeq 2 \times 10^{-5}$ mm of Hg) with a mechanical and a silicone oil diffusion pump. The outer dewar was filled with liquid nitrogen and then the inner dewar was pre-cooled with liquid nitrogen prior to filling with liquid helium. After the inner dewar was filled with liquid helium, the temperature of the trapping surface was near $4^{o}K$.

The matrix gas was deposited at a rate of 0.1 to 0.3 l-atm/hr with a total consumption of approximately 300 cc (STP). The rate of deposition was maintained at a steady rate throughout by needle valve adjustment with the rate depending upon the effectiveness of production of the desired species. If a metal was codeposited, the temperature of the cell was adjusted such that the vapor pressure of the metal produced in the furnace was approximately 10^{-3} mm of Hg. Matrix components could

be photolyzed during or after deposition, or both, with either the electrodeless discharge flow lamp or the mercury lamp.

The products were then analyzed by means of optical or electron spin resonance spectroscopy. If it was necessary, experiments were performed on the variable temperature dewars so that the matrices could be annealed to any desired temperature and then observed again.

References - Chapter II

1. C. K. Jen, S. N. Foner, E. L. Cochran, and V. A. Bowers, Phys. Rev. 112, 1169 (1958).

2. D. David and W. Braun, Appl. Opt. 7, 2071 (1968).

CHAPTER III
ESR THEORY

Introduction

The principles of ESR spectroscopy have been thoroughly studied and are discussed in detail in a number of excellent references (1-9). The basic principles of ESR theory will be presented for molecules of $^2\Sigma$ type and in a later section, for molecules of $^3\Sigma$ type.

A $^2\Sigma$ molecule is a linear molecule with zero orbital angular momentum and one unpaired electron ($S = 1/2$, $L = 0$). In the presence of an externally applied magnetic field, the degenerate spin state will be split and the difference in energy of the states will be approximately equal to $g_e \beta_o H$, where g_e is the free electron g-factor (2.0023), β_o is the Bohr magneton ($eh/4\pi mc = 9.2732 \times 10^{-21}$ erg/G) and H is the strength of the magnetic field. If electromagnetic radiation of frequency ν_o is present which satisfies the resonance condition,

$$\Delta E = h\nu_o = g_e \beta_o H, \qquad (1)$$

where h is Planck's constant (6.6256×10^{-27} erg-sec), transitions between these Zeeman levels can occur.

Resonances for a given microwave frequency do not always occur at the same magnetic field strength so that g may be taken as a parameter which governs the position of the resonance absorption. In this study, an X-band instrument with $\nu_o \simeq 9400$ MHz was employed.

Spin Hamiltonian for $^2\Sigma$ Molecules

The terms in the general Hamiltonian for those molecules in an external magnetic field can be written as

$$H = H_E + H_{LS} + H_{SI} + H_{SH} + H_{IH} \qquad (2)$$

where:

H_E is a composite term expressing the total kinetic energy of the electrons, the coulombic attraction between the electron and nuclei, and the repulsions between the electrons

$$H_E = \sum_i \left(\frac{p_i^2}{2m} - \frac{Ze^2}{r_i} \right) + \sum_i \sum_j \frac{e^2}{r_{ij}} \qquad (3)$$

where p_i is the momentum of the ith electron, and r_i is its distance from the nucleus. Z is the nuclear charge. r_{ij} is the distance between electron i and electron j. H_{LS} represents the potential energy due to spin-orbit coupling usually expressed in the form

$$H_{LS} = \lambda \underline{L} \cdot \underline{S} \qquad (4)$$

where $\underline{L}$ and $\underline{S}$ are the orbital and electron-spin angular momentum operators. λ is the molecular spin-orbit coupling constant.

H_{SI} represents the hyperfine interaction arising from the electron-spin orbital angular momentum and magnetic moment interacting with any nuclear magnetic moment present in the molecule and may be expressed

$$H_{SI} = g_I \beta_N g_e \beta_o \left[\frac{\underline{L}\cdot\underline{I}}{r^3} + \frac{3(\underline{S}\cdot\underline{r})(\underline{r}\cdot\underline{I})}{r^5} - \frac{\underline{S}\cdot\underline{I}}{r^3} + \frac{8\pi\delta(r)\underline{S}\cdot\underline{I}}{3} \right] = \underline{I}\cdot\underline{A}\cdot\underline{S} \qquad (5)$$

where $\underline{I}$ is the nuclear-spin angular momentum operator, β_N is the nuclear magneton, g_e and g_N are the electronic and nuclear g factors and $\underline{A}$ is a second order tensor (see discussion of $\underline{A}$ tensor below).

This interaction consists of three parts. The first involves a $\underline{L}\cdot\underline{I}$ interaction between the magnetic field produced by the orbital momentum of the electron with the nuclear moment. For a $^2\Sigma$ molecule in which L = 0, this term will be zero except for any small orbital angular momentum entering through the $\underline{L}\cdot\underline{S}$ interaction. The next two terms are the Hamiltonian

for the interaction of the two magnetic dipoles of the nuclear magnetic moment and the magnetic moment produced by the electron spin. This produces an angularly dependent term varying as r^{-3} and depends upon the p or d character of the odd electron. The last term represents the isotropic Fermi (contact) term and depends on the spin density at the nucleus i.e., on the s character of the odd electron. The Dirac δ-function indicates that this term has a non-zero value only at the nucleus.

H_{SH} (Electron Zeeman term) represents the interaction of the spin and orbital angular momenta of the electrons with the externally applied magnetic field written

$$H_{SH} = \beta_o(\underline{L} + g_e\underline{S})\cdot\underline{H} \tag{6}$$

where $\underline{H}$ is the magnetic field.

H_{IH} (Nuclear Zeeman term) represents the interaction of the angular momenta of the nuclei with the externally applied magnetic field written

$$H_{IH} = \frac{h}{2\pi} \sum_i - \gamma_i \cdot \underline{I}_i \cdot \underline{H} \tag{7}$$

where γ_i is the magnetogyric ratio of the ith nucleus.

The energy contributions from the various terms vary over a wide range and it is obvious that H_E and H_{LS}

involve too much energy for excitation by ESR. H_{SI}, H_{SH} and H_{IH} involve energies ideally suited for ESR and frequently H_{IH} energies are too small to be observed in the presence of H_{SI}. Due to the magnitude of these various interactions, other types of interactions are neglected here since in general they are much smaller. For detailed discussions of these terms, see references (1-13).

Calculations with the general Hamiltonian are very difficult; therefore, a simplified accounting of the more likely interactions is performed with a spin Hamiltonian (H_{spin}). In the spin Hamiltonian the terms H_E, H_{LS}, and H_{SH} are replaced by a single term $-\beta \underline{H}_o \cdot \underline{g} \cdot \underline{S}$ where $\underline{S}$ is the effective electronic spin and $\underline{g}$ is a second order tensor (see discussion on $\underline{g}$ tensor below) (1). By convention S is assigned a value that makes the observed number of energy levels equal to (2S + 1). Thus we can relate all the magnetic properties of a system to this effective spin by the spin Hamiltonian since it combines all the terms of the general Hamiltonian which are sensitive to spin.

If the nuclear Zeeman term (H_{IH}) is neglected the spin Hamiltonian can be written

$$H_{spin} = \beta \underline{H}_o \cdot \underline{g} \cdot \underline{S} + H_{SI}$$

$$= \beta \underline{H}_o \cdot \underline{g} \cdot \underline{S} + \underline{I} \cdot \underline{A} \cdot \underline{S} . \qquad (8)$$

g Tensor

In the absence of hyperfine interaction, the spin Hamiltonian for S = 1/2 is

$$H_{spin} = \beta \underline{S} \cdot \underline{g} \cdot \underline{H}. \tag{9}$$

The complete interaction of $\underline{S}$ and $\underline{H}$ must take into account the effect of each component of $\underline{S}$ on each component of $\underline{H}$. For an arbitrary set (x,y,z) of orthogonal axes then

$$\beta \underline{S} \cdot \underline{g} \cdot \underline{H} = \beta \begin{bmatrix} S_x S_y S_z \end{bmatrix} \begin{bmatrix} g_{xx} g_{xy} g_{xz} \\ g_{yx} g_{yy} g_{yz} \\ g_{zx} g_{zy} g_{zz} \end{bmatrix} \begin{bmatrix} H_x \\ H_y \\ H_z \end{bmatrix}. \tag{10}$$

S_x, S_y, and S_z are components of the effective spin along the x, y, and z axes. $\underline{g}$ is strictly a 3 x 3 matrix and is referred to as a symmetrical tensor of the second order (6). The double subscripts on the g-tensor may be interpreted as follows. g_{xy} may be considered as the contribution to g along the x-axis when the magnetic field is applied along the y-axis. In general these axes (x, y, z) are not the principal directions of the g tensor, but by a suitable rotation of axes the off-diagonal elements of the g-tensor can be made equal to zero. When the g-tensor is so diagonalized the components along the diagonal, g_{xx}, g_{yy}, and g_{zz}, then are the principal directions of the g-tensor with respect to the molecule.

As alluded to previously, the anisotropy of the g-tensor arises from the orbital angular momentum of the electron through spin-orbit coupling. The intrinsic spin angular momentum of a free electron is associated with a g factor of 2.0023 (14). However the electron in a molecule may also possess orbital angular momentum. The corresponding orbital angular momentum adds vectorially to the spin angular momentum. Since the ground states of many linear molecules have zero orbital angular momentum (Σ states), it is likely that in these cases the g-factor would have precisely the free-electron value. However, the interaction of a presumably "pure spin" ground state with certain excited states can admix a small amount of orbital angular momentum into the ground state. This interaction is usually inversely proportional to the energy separation of the states and results in a change in the components of the g-factor.

The orbital and spin angular momenta will be coupled through the spin-orbit interaction term, which may be given as

$$H_{LS} = \lambda \underline{L} \cdot \underline{S} = \lambda [L_x S_x + L_y S_y + L_z S_z] . \qquad (11)$$

This term must be added to the Zeeman terms in the Hamiltonian i.e.

$$H = H_{SH} + H_{LS} = \beta \underline{H} \cdot (\underline{L} + g_e \underline{S}) + \lambda \underline{L} \cdot \underline{S} . \qquad (12)$$

For a Σ molecule, the ground state represented by $|G,M_S\rangle$ is orbitally nondegenerate. The energy (to the first order) is given by the diagonal matrix element (6)

$$W_G^{(1)} = \langle G,M_S|g_e\beta H_z S_z|G,M_S\rangle + \langle G,M_S|(\beta H_z + \lambda S_z)L_z|G,M_S\rangle . \quad (13)$$

The first term represents the "spin-only" electron Zeeman energy. The second term may be expanded as

$$\langle M_S|\beta H_z + \lambda S_z|M_S\rangle \langle G|L_z|G\rangle .$$

For an orbitally non-degenerate state, $\langle G|L_z|G\rangle$ equals zero. The second-order correction to each element in the Hamiltonian matrix is given by (6)

$$H_{M_S,M'_S} = \frac{-\sum_n' |\langle G,M_S|(\beta\underline{H} + \lambda\underline{S})\cdot\underline{L} + g_e\beta\underline{H}\cdot\underline{S}|n,M'_S\rangle|^2}{W_n^{(o)} - W_G^{(o)}} . \quad (14)$$

The prime designates summation over all states except the ground state. Neglecting all zero terms and expanding this, it is seen that the quantity Λ may be factored out where

$$\underline{\Lambda} = \frac{-\sum_n' \langle G|\underline{L}|n\rangle\langle n|\underline{L}|G\rangle}{W_n^{(o)} - W_G^{(o)}} \quad (15)$$

and is a second-rank tensor. The ijth element of this tensor is given by

$$\Lambda_{ij} = \frac{-\sum_n' \langle G|L_i|n\rangle\langle n|L_j|G\rangle}{W_n^{(o)} - W_G^{(o)}} \tag{16}$$

where L_i and L_j are orbital angular momentum operators appropriate to the x, y, or z directions. Substitution of this tensor into the term H_{M_S,M'_S} yields

$$H_{M_S,M'_S} = \langle M_S|\beta^2 \underline{H}\cdot\underline{\Lambda}\cdot\underline{H} + 2\lambda\beta\underline{H}\cdot\underline{\Lambda}\cdot\underline{S} + \lambda^2\underline{S}\cdot\underline{\Lambda}\cdot\underline{S}|M'_S\rangle . \tag{17}$$

The first operator represents a constant contribution to the paramagnetism and need not be considered further. The second and third terms constitute a Hamiltonian which operates only on spin variables. When combined with the operator $g_e\beta\underline{H}\cdot\underline{S}$, the result is called the spin Hamiltonian H_{spin} which may be written

$$H_{spin} = \beta\underline{H}\cdot(g_e\underline{1} + 2\lambda\underline{\Lambda})\cdot\underline{S} + \lambda^2\underline{S}\cdot\underline{\Lambda}\cdot\underline{S} = \beta\underline{H}\cdot\underline{g}\cdot\underline{S} + \underline{S}\cdot\underline{D}\cdot\underline{S} \tag{18}$$

where

$$\underline{g} = g_e\underline{1} + 2\lambda\underline{\Lambda} \tag{19}$$

and

$$\underline{D} = \lambda^2\underline{\Lambda} . \tag{20}$$

The $\underline{S}\cdot\underline{D}\cdot\underline{S}$ term is effective only in systems with $S \geq 1$ and will be considered later, but for $^2\Sigma$ molecules it may be deleted. The first term then is the spin Hamiltonian given in the beginning of this discussion. It is evident from this derivation that the anisotropy of the g-tensor arises from the spin-orbit interaction due to the orbital angular momentum of the electron.

If the angular momentum of a system is solely due to spin angular momentum, the g-tensor should be isotropic with a value of 2.0023. That is, the principal components of the g tensor are $g_{xx} = g_{yy} = g_{zz} = g_e = 2.0023$. Any anisotropy or deviation from this value results from the $\underline{\Lambda}$ tensor which involves only contribution of the orbital angular momentum from excited states. For a completely isotropic system, H_{spin} may be written

$$H_{spin} = \begin{bmatrix} S_x S_y S_z \end{bmatrix} \begin{bmatrix} g_e & 0 & 0 \\ 0 & g_e & 0 \\ 0 & 0 & g_e \end{bmatrix} \begin{bmatrix} H_x \\ H_y \\ H_z \end{bmatrix} \tag{21}$$

$$= g_e \beta \left[S_x H_x + S_y H_y + S_z H_z \right] .$$

For a system with orthorhombic symmetry, i.e., for a system in which none of the x, y, and z axes are equivalent, the spin Hamiltonian must be written

$$H_{spin} = \beta (g_{xx} S_x H_x + g_{yy} S_y H_y + g_{zz} S_z H_z) . \tag{22}$$

Here $g_{xx} \neq g_{yy} \neq g_{zz}$.

Some systems may have an n-fold axis of symmetry ($n \geq 3$). These systems are described as having axial symmetry for which two axes are equivalent. The unique axis is usually designated as z and the value of g for $H||z$ will be called $g_{||}$. If $H\perp z$, then the g value will be termed $g_{\perp}$. The spin Hamiltonian is then

$$H_{spin} = \beta(g_{\perp}S_xH_x + g_{\perp}S_yH_y + g_{||}S_zH_z) . \qquad (23)$$

From the equation given for the g tensor (i.e. $\underline{g} = g_e\underline{1} + 2\lambda\underline{\Lambda}$) the various components of the g-tensor can be determined. The general formula, widely used in the interpretation of ESR spectra, for the ijth term is then (see 15-22).

$$g_{ij} = g_e\delta_{ij} - 2\lambda\Sigma_n'\langle 0|L_i|n\rangle\langle n|L_j|0\rangle/E_n . \qquad (24)$$

In this notation δ_{ij} is the Kronecker symbol and E_n is the energy separation of the state $|n, SM_n\rangle$ from the ground state. As shown, this result is obtained by calculation of the second-order shift in energy of the ground-state levels due to a combination of spin-orbit coupling and Zeeman energies. In a similar fashion Tippins (22) has extended these calculations to the third-order for the energy shift of the ground state and has determined to the second-order similar correction terms for the g tensor components. Only the result of these calculations will be given. It was found, letting

X_{jk} represent $\langle j|L_x|K\rangle$, that

$$\Delta g_{zz}^{(2)} = \lambda^2[\Sigma'_{jk}(i/E_jE_k)(Z_{oj}X_{jk}Y_{ko} + X_{oj}Y_{jk}Z_{ko} + X_{oj}Z_{jk}Y_{ko}) - \Sigma'_j(1/E_j^2)(|X_{oj}|^2 + |Y_{oj}|^2)], \quad (25a)$$

$$\Delta g_{xx}^{(2)} = \lambda^2[\Sigma'_{jk}(i/E_jE_k)(Y_{oj}X_{jk}Z_{ko} + X_{oj}Y_{jk}Z_{ko} + Y_{oj}Z_{jk}X_{ko}) - \Sigma'_j(1/E_j^2)(|Y_{oj}|^2 + |Z_{oj}|^2)], \quad (25b)$$

and

$$\Delta g_{yy}^{(2)} = \lambda^2[\Sigma'_{jk}(i/E_jE_k)(Z_{oj}X_{jk}Y_{ko} + Z_{oj}Y_{jk}X_{ko} + Y_{oj}Z_{jk}X_{ko}) - \Sigma'_j(1/E_j^2)(|X_{oj}|^2 + |Z_{oj}|^2)]. \quad (25c)$$

For the special case of axial symmetry, it is evident that $\Delta g_{||}^{(2)} = \Delta g_{zz}^{(2)}$ and $\Delta g_{\perp}^{(2)} = \Delta g_{xx}^{(2)} = \Delta g_{yy}^{(2)}$.

A Tensors

As shown in the equation for H_{SI}, the hyperfine tensor $\underline{A}$ will be comprised of three types of interactions. The first term which is dependent on $\underline{L}\cdot\underline{I}$ involves the interaction between the magnetic field produced by the orbital momentum and the nuclear moment. This term

will necessarily be zero for $^2\Sigma$ molecules since L = 0, except for any small orbital angular momentum entering through the $\underline{L}\cdot\underline{S}$ interaction. The other interactions are due to the amount of s-character of the wavefunction (the Fermi contact term) and to the non-s-character of the wavefunction.

The interaction due to the s-character is called A_{iso} since the interaction is isotropic. Fermi (23) has shown that for systems with one electron the isotropic interaction energy is given approximately by

$$W_{iso} = - \frac{8\pi}{3} |\Psi(0)|^2 \mu_e \mu_N \qquad (26)$$

where $\Psi(0)$ represents the wave function evaluated at the nucleus (i.e. the s-character). Here μ_e and μ_N are the electron and nuclear magnetic moments, respectively.

The interaction due to the non-s-character of the wavefunction is called A_{dip} since it arises from the dipole-dipole interaction of the electron and nucleus. In a rigid system such as we have in matrix isolation, this dipolar interaction gives rise to the anisotropic component of hyperfine coupling. The expression for the dipolar interaction energy between a fixed electron and nucleus separated by a distance r is

$$W_{dipolar} = \frac{\mu_e \cdot \mu_n}{r^3} - \frac{3(\mu_e \cdot r)(\mu_n \cdot r)}{r^5} \quad . \qquad (27)$$

H_{SI} can be written then

$$H_{SI} = H_{iso} + H_{dip}$$

$$= [A_{iso} + A_{dip}]\underline{I}\cdot\underline{S} \qquad (28)$$

where

$$A_{iso} = \frac{8\pi}{3} g_N\beta_N g_e\beta_o |\Psi(0)|^2 \qquad (29)$$

and

$$A_{dip} = g_N\beta_N g_e\beta_o \left\langle \frac{3\cos^2\theta - 1}{2r^3} \right\rangle . \qquad (30)$$

The brackets indicate the average of the expressed operator over the wave function Ψ. In tensor notation (it can be seen that the dipolar component involves a tensor interaction by expanding the vector notation term for H_{dip}) then

$$H_{SI} = \underline{I}\cdot\underline{A}\cdot\underline{S} \qquad (31)$$

where $\underline{A} = A_{iso}\underline{1} + \underline{T}$.

Here $\underline{1}$ is the unit tensor and $\underline{T}$ is the tensor representing the dipolar interactions. Thus the components of the A tensor may be given

$$A_{ij} = A_{iso}\underline{1} + T_{ij} . \qquad (32)$$

By a method similar to that used for the g tensor, the components of the A tensor for a completely isotropic system may be written

$$A_{xx} = A_{yy} = A_{zz} = A_{iso} . \tag{33}$$

For a system with axial symmetry, we find

$$A_{xx} = A_{yy} = A_{\perp} = A_{iso} + T_{xx} \tag{34}$$

and

$$A_{zz} = A_{\parallel} = A_{iso} + T_{zz} . \tag{35}$$

If the system exhibits a completely anisotropic A tensor then

$$A_{xx} \neq A_{yy} \neq A_{zz} . \tag{36}$$

Spin Hamiltonian for $^3\Sigma$ Molecules

Until now, we have considered only systems with $S = 1/2$. In the absence of a magnetic field, the spin states for these systems are degenerate.

For a system with two noninteracting electrons, four electronic configurations may be constructed.

$$\alpha(1)\alpha(2) \qquad \alpha(1)\beta(2) \qquad \beta(1)\alpha(2) \qquad \beta(1)\beta(2)$$

Where interactions occur, these configurations are combined into states which are either symmetric or antisymmetric with respect to exchange of the electrons. These states are (11)

$$\alpha(1)\alpha(2)$$

$$\frac{1}{\sqrt{2}}[\alpha(1)\beta(2) + \beta(1)\alpha(2)] \qquad \frac{1}{\sqrt{2}}[\alpha(1)\beta(2) - \beta(1)\alpha(2)].$$

$$\beta(1)\beta(2)$$

Symmetric Antisymmetric

The multiplicity of the state with $S = 1$ is $(2S + 1) = 3$. This is called a triplet state. Similarly the state with $S = 0$ is called a singlet state. If the two electrons occupy the same spatial orbital, only the singlet state is possible. However, if the two electrons occupy different spatial orbitals then both the singlet and triplet states exist.

For systems with two or more unpaired electrons, the degeneracy of these spin states may be removed even in the absence of a magnetic field. This is called zero-field splitting. If this separation is larger than the energy of the microwave quantum, it may not be possible to observe an ESR spectrum. If the splitting is less than the energy of the microwave quantum, the resulting ESR spectra will show considerable anisotropy.

At small distances, two unpaired electrons will experience a strong dipole-dipole interaction. The electron spin-electron spin interaction is given by a spin-spin Hamiltonian (H_{SS}). Written in terms of the spin operators

$$H_{SS} = g^2\beta^2 \left[\frac{S_1 \cdot S_2}{r^3} - \frac{3(S_1 \cdot r)(S_2 \cdot r)}{r^5} \right] . \qquad (37)$$

Substitution of the scalar products and the total spin operator $\underline{S} = \underline{S}_1 + \underline{S}_2$ in the above equation leads to the following form of the spin-spin Hamiltonian (4, 6, 8, 11)

$$H_{SS} = \underline{S} \cdot \underline{D} \cdot \underline{S} \qquad (38)$$

where $\underline{D}$ is a second-rank tensor with a trace of zero. The individual components of the D tensor may be written as

$$D_{ij} = (g^2\beta^2/2) < (r_{ij}^2 - 3Z_{ij}^2)/r_{ij}^5 > \qquad (39)$$

where i and j represent x, y, and z in the equation $r^2 = x^2 + y^2 + z^2$, with r representing the distance between the electrons. This tensor can be diagonalized with the principal components equal to D_{xx}, D_{yy}, and D_{zz}. For this axis system then

$$H_{SS} = D_{xx}S_x^2 + D_{yy}S_y^2 + D_{zz}S_z^2 \qquad (40)$$

where $D_{xx} + D_{yy} + D_{zz} = 0$. This is customarily written

$$H_{SS} = -XS_x^2 - YS_y^2 - ZS_z^2 \tag{41}$$

where $X = -D_{xx}$, etc. X, Y, and Z are the respective energies of this system in zero magnetic field. Since the tensor is traceless, the zero-field splitting can be written in terms of just two independent constants called D and E where $D = -3Z/2$ and $E = -1/2(X - Y)$. Therefore, the correct spin Hamiltonian for $S \geq 1$ must now be written

$$H_{spin} = \beta \underline{S} \cdot \underline{g} \cdot \underline{H} + \underline{S} \cdot \underline{D} \cdot \underline{S} \tag{18}$$

or

$$H_{spin} = \beta \underline{S} \cdot \underline{g} \cdot \underline{H} + D[S_z^2 - 1/3\ S(S + 1)] + E[S_x^2 - S_y^2] \tag{42}$$

where hyperfine interactions and nuclear Zeeman interactions have been ignored.

For a linear molecule where z is the axis of symmetry of the molecule, the x and y directions are equivalent and the term involving E is zero. Then for $S = 1$ in a linear case, H_{spin} reduces to

$$H_{spin} = g_{||}\beta H_z S_z + g_{\perp}\beta(H_x S_x + H_y S_y) + D(S_z^2 - 2/3). \tag{43}$$

Hyperfine Interaction for $^3\Sigma$ Molecules

The difficulties in observing hyperfine splittings in randomly-oriented triplet molecules are usually caused by the large line-widths; however, ^{13}C, H, and F hyperfine splittings have been observed (24-27). Generally, the hyperfine interaction is small compared to the fine structure (D term) and the electronic Zeeman energy, so that first-order perturbation is sufficient to account for the hfs. In linear molecules the tensors $\underline{g}$, $\underline{D}$, and $\underline{A}$ must all be coaxial which simplifies interpretation of the hfs. Then for one magnetic nucleus in a linear molecule, the complete spin Hamiltonian can be written

$$H_{spin} = g_{||}\beta H_z S_z + g_{\perp}\beta(H_x S_x + H_y S_y) + D(S_z^2 - 2/3) + A_{||} S_z I_z + A_{\perp}(S_x I_x + S_y I_x) \quad (44)$$

neglecting any nuclear Zeeman interactions.

Solution to the Spin Hamiltonian for $^2\Sigma$ Molecules and the Observed Spectrum

As shown previously, if nuclear effects are ignored, the spin Hamiltonian reduces to

$$H_{spin} = \beta \underline{S} \cdot \underline{g} \cdot \underline{H} \ . \quad (9)$$

When g is diagonalized then

$$H_{spin} = \beta(g_1 S_x H_x + g_2 S_y H_y + g_3 S_z H_z) \ . \quad (45)$$

The energy of the levels (obtained from the eigenvalve equation $H|S,M_S> = E_{M_S}|S,M_S>$) will then be given by (28)

$$E = \beta S_H H(g_1^2 \sin^2\theta\cos^2\phi + g_2^2 \sin^2\theta\sin^2\phi + g_3^2\cos^2\theta)^{1/2} = \beta g_H S_H H \qquad (46)$$

where S_H represents the component of spin vector S along H, g_H is the g-value in the direction of H, θ is the angle between the z-axis of the molecule and the field direction and ϕ is the angle from the x-axis to the line of the projection of the field vector in the xy plane.

In the case of axial symmetry, $g_1 = g_2 = g_\perp$ and $g_3 = g_{||}$, g_H reduces to

$$g_H = (g_\perp^2 \sin^2\theta + g_{||}^2\cos^2\theta)^{1/2} \qquad (47)$$

and the energy of the levels is given by

$$E = \beta S_H H(g_\perp^2 \sin^2\theta + g_{||}^2\cos^2\theta)^{1/2} . \qquad (48)$$

For the allowed transitions, what type of a spectrum will be observed if the molecules are randomly-oriented but rigidly held, as in a solid matrix? (See 29-40.) The spectrum will be independent of the angle that the magnetic field makes with the solid sample.

Consider first the case of axial symmetry. If N_o molecules are randomly oriented with respect to the applied magnetic field, then the number within an increment of angle $d\theta$, where θ is the angle measured from the field direction, is

$$dN = \frac{N_o}{2} \sin\theta d\theta \ . \tag{49}$$

That is, dN is proportional to the area of the surface of a sphere included within an angle variation of $d\theta$; the factor two enters because it is only necessary to cover a hemisphere. The absorption intensity as a function of angle is proportional to the number dN of molecules lying between θ and $\theta + d\theta$, assuming the transition probability is independent of orientation. Since g is a function of θ for a fixed frequency ν, the resonant magnetic field is

$$H = \frac{h\nu}{\beta} \left(g_{||}^{\ 2}\cos^2\theta + g_{\perp}^{\ 2}\sin^2\theta\right)^{-1/2} \tag{50}$$

and from this

$$\sin^2\theta = \frac{(g_o H_o/H)^2 - g_{||}^{\ 2}}{g_{\perp}^{\ 2} - g_{||}^{\ 2}} \tag{51}$$

where $g_o = (g_{||} + 2g_{\perp})/3$

and

$$H_o = h\nu/g_o\beta. \tag{52}$$

Therefore

$$\sin\theta d\theta = \frac{-g_o^2 H_o^2}{H^3} \{(g_{||}^2 - g_\perp^2)(g_o H_o/H)^2 - g_\perp^2\}^{-1/2} dH. \tag{53}$$

The intensity of absorption in a range of magnetic field dH is proportional to

$$|dN/dH| = |dN/d\theta| \cdot |d\theta/dH| \tag{54}$$

where $dN/d\theta = \frac{N_o}{2} \sin\theta$ and $d\theta/dH$ is obtained from the equation for $\sin\theta d\theta$. From the above equations

$$H = h\nu/g_{||}\beta = g_o H_o/g_{||} \text{ at } \theta = 0^o \tag{55a}$$

and

$$H = h\nu/g_\perp\beta = g_o H_o/g_\perp \text{ at } \theta = 90^o. \tag{55b}$$

At these two extremes, the intensity of absorption varies from

$$|dN/dH| = N_o g_{||}^3/2g_o H_o (g_{||}^2 - g_\perp^2) \text{ at } \theta = 0^o \tag{56a}$$

to

$$|dN/dH| = \infty \text{ at } \theta = 90^{o} . \qquad (56b)$$

If the resonant field is plotted versus the magnetic field the absorption will have the following shape (for $g_{||} > g_{\perp}$), Figure 6. If the natural width of the lines of the individual molecules contributing to this absorption is considered then the sharp angles in the above curve become rounded (33), and it takes the appearance shown in Figure 7 (a). Since in ESR the first derivative of the absorption curve is usually observed the spectrum would then appear as in Figure 7 (b).

In the case of an orthorhombic system in randomly-oriented and rigidly held sample, instead of the two turning points in the spectrum corresponding to $g_{\perp}$ and $g_{||}$, there will be three turning points corresponding to g_1, g_2, and g_3. The shapes of the absorption line and to its derivative are given in Figure 8 (a) and (b).

If now there is also hyperfine interaction in the randomly oriented molecules the previously discussed pattern will be split into 2I + 1 patterns, if one nucleus of spin I is involved. The spin Hamiltonian for an axially symmetric molecule is given

$$H_{spin} = \beta[g_{||}S_zH_z + g_{\perp}(S_xH_x + S_yH_y)] + A_{||}S_zI_z + A_{\perp}(S_xI_x + S_yI_y) . \qquad (57)$$

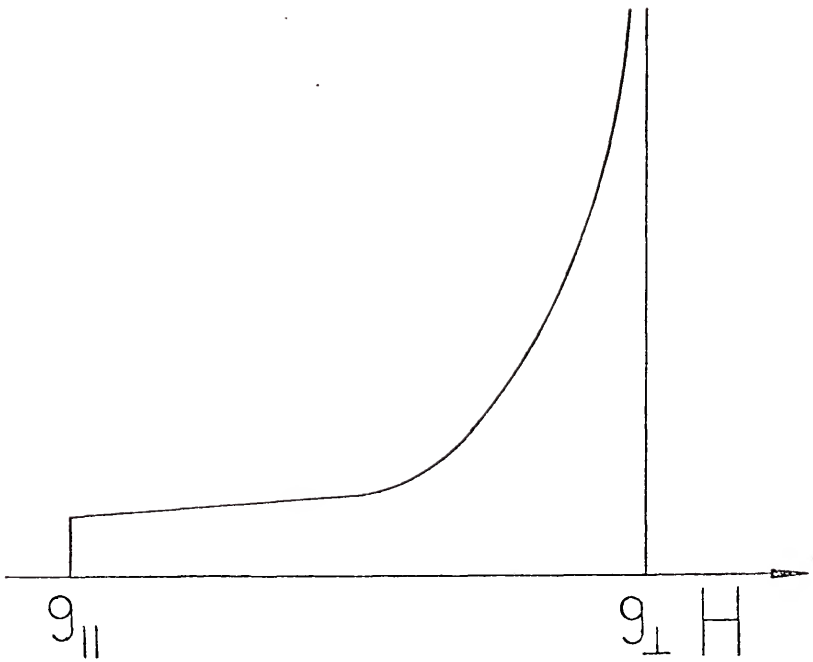

Figure 6: Idealized absorption line shape for a randomly oriented system having an axis of symmetry and no hyperfine interaction ($g_{\perp} < g_{\parallel}$).

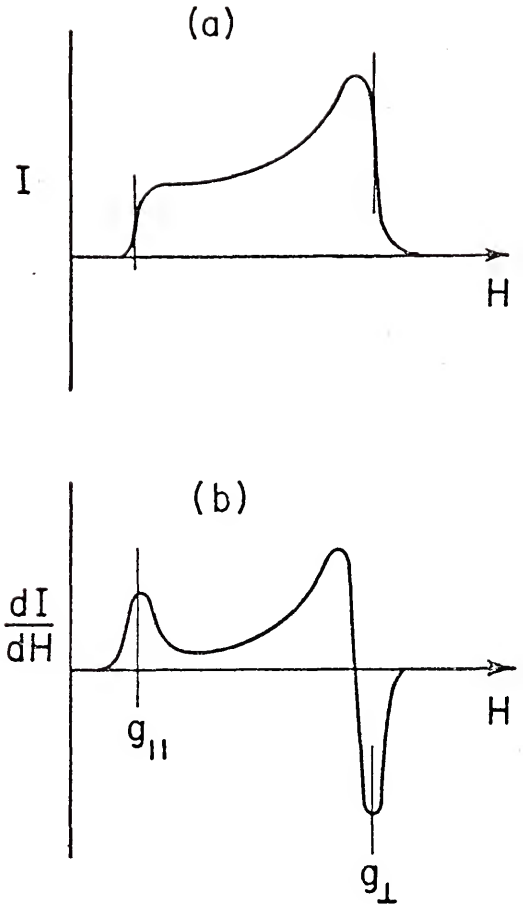

Figure 7: (a) Theoretical absorption and (b) first derivative spectra for randomly-oriented system having an axis of symmetry and no hyperfine interaction ($g_{\perp} < g_{||}$).

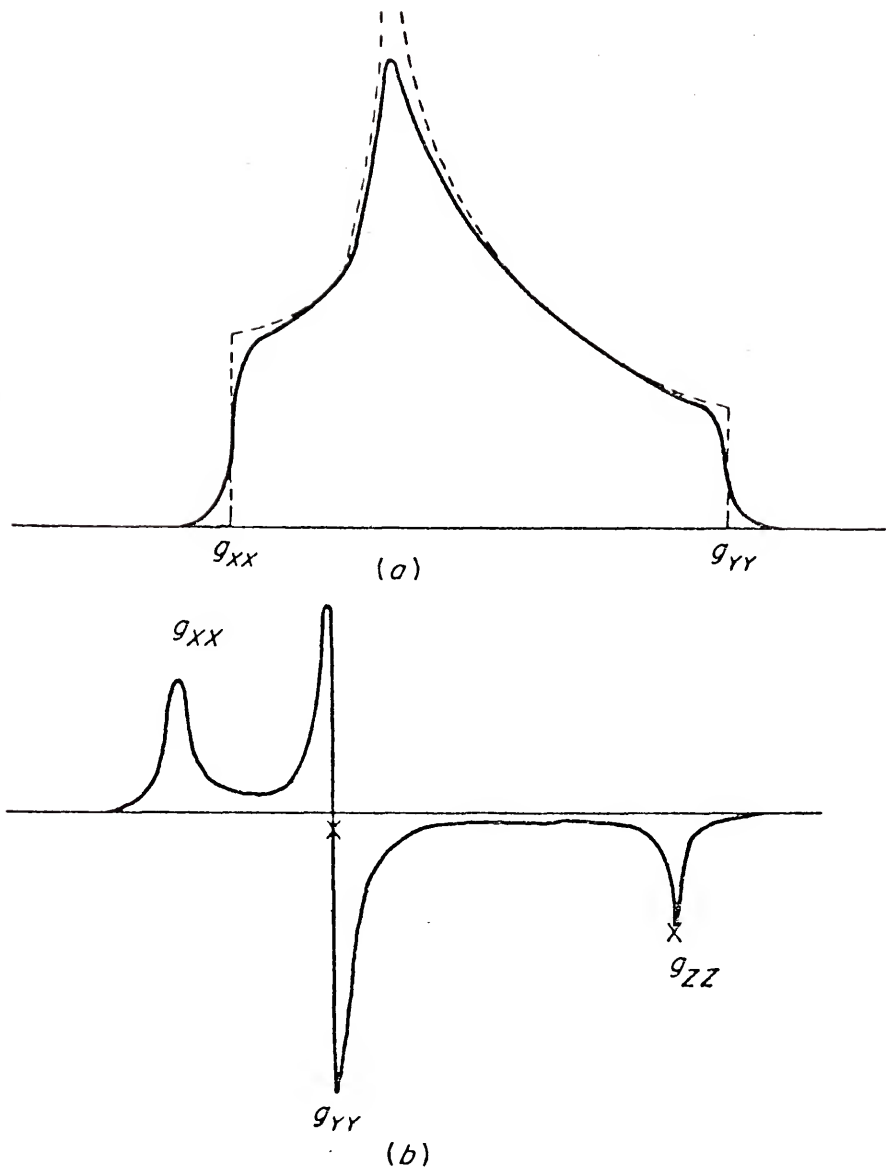

Figure 8: (a) Absorption line shape for a system with orthorhombic symmetry, (b) first derivative of the curve in (a). ($g_{xx} > g_{yy} > g_{zz}$)

When g is given by equation (47), the nuclear hyperfine splitting can be included in the equation for the resonant magnetic field to a first-order approximation by (9)

$$H = \frac{h\nu}{g\beta} - \frac{K}{g\beta} m_I \tag{58}$$

where $K^2g^2 = A_{||}{}^2 g_{||}{}^2 \cos^2\Theta + A_{\perp}{}^2 g_{\perp}{}^2 \sin^2\Theta$. The intensity of absorption $|dN/dH|$, can again be derived and is found to be

$$\frac{dN}{dH} = \frac{N_o}{2}\left(\frac{2\cos\Theta}{g^2}\left[\frac{(g_{||}{}^2 - g_{\perp}{}^2)g_o H_o}{2g} + \frac{m_I}{\beta}\,\frac{(g_{||}{}^2 A_{||}{}^2 - g_{\perp}{}^2 A_{\perp}{}^2}{2K} - \frac{K(g_{||}{}^2 - g_{\perp}{}^2)}{g^2}\right]\right)^{-1}. \tag{59}$$

Here $\sin\Theta d\Theta$ cannot be solved explicitly so that dN/dH cannot be written as a function of only the magnetic parameters. Equations 58 and 59 must be solved for a series of values Θ to obtain the resonant fields and intensities as a function of orientation. However

$$H = (g_o H_o / g_{||}) - (m_I A_{||}/\beta g_{||}) \quad \text{at } \Theta = 0^o, \tag{60a}$$

$$H = (g_o H_o / g_{\perp}) - (m_I A_{\perp}/\beta g_{\perp}) \quad \text{at } \Theta = 90^o, \tag{60b}$$

and again $|dN/dH| \to \infty$ at $\Theta = 90^o$. The absorption pattern for a randomly-oriented molecule in which there is also

hf interaction is then a superposition of 2I + 1 pattern of the type shown in Figure 6. The first derivative of that pattern is the observed spectrum. Figure 9 shows a typical case in which $g_{||} > g_{\perp}$ and $A_{||} > A_{\perp}$. Here the patterns do not overlap so that the spectrum is relatively simple. If overlap does occur, the total absorption curve and its first derivative will be more complicated. The best approach is to solve the given euqations (58 and 59) by computer for a trial set of magnetic parameters g and A for $\Theta = 0$ to 90^{o}, and have the absorption and its first derivative plotted as a function of H. (For example, see ESR discussion concerning C_2H.)

It should be noted here that second order perturbation theory applied to the spin Hamiltonian for axial symmetry including hyperfine interaction yields results similar to equation (58) for the allowed ESR transitions. This is derived in Low (9) and given as

$$\Delta E = h\nu = g\beta H + Km + \frac{A_{\perp}^{2}}{4g\beta H_{o}}\left(\frac{A_{||}^{2} + K^{2}}{K^{2}}\right)\left[I(I+1) - m^{2}\right]$$

$$+ \frac{1}{2g\beta H_{o}}\left(\frac{A_{||}^{2} - A_{\perp}^{2}}{K^{2}}\right)\left(\frac{g_{||}g_{\perp}^{2}}{g^{2}}\right)\sin^{2}\Theta\cos^{2}\Theta m^{2} \quad (61)$$

where K and H_{o} are the same terms as given previously.

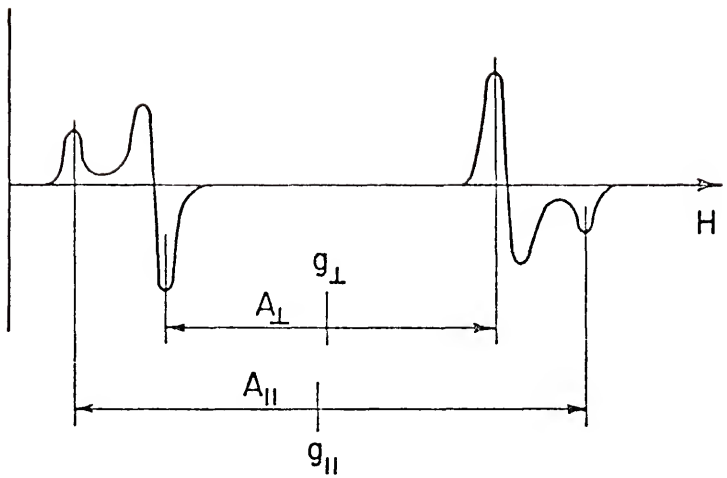

Figure 9: First derivation absorption pattern for randomly-oriented molecules with hyperfine splitting from one nucleus with I = 1/2 ($g_{||} > g_\perp$, $A_{||} > A_\perp$).

The same general techniques can be used to solve for the spin Hamiltonian of various cases and then the expected powder spectrum plotted. Several typical situations have been illustrated by Atkins and Symons (41). These cases cover examples of powder spectra of radicals with one spin-1/2 nucleus, where g and A are varied from isotropic to completely anisotropic forms, and one spin-1 nucleus.

Solution to the Spin Hamiltonian for $^3\Sigma$ Molecules and the Observed Spectrum

The solution to the general Hamiltonian is given by Wasserman, Snyder, and Yager (42) for the triplet states of randomly oriented molecules. Here, the special case for linear molecules will be briefly discussed.

Neglecting hyperfine and other spin-orbit interactions, a linear triplet molecule in a magnetic field will have the spin Hamiltonian:

$$H_{spin} = g_{||}\beta H_z S_z + g_{\perp}\beta(H_x S_x + H_y S_y) + D(S_z^2 - 2/3) \qquad (43)$$

where z is the molecular axis.

The basis functions are the orthonormal spin wavefunctions

$$|+1\rangle = |\alpha_1\alpha_2\rangle \qquad (62a)$$

$$|0\rangle = \frac{1}{\sqrt{2}}|\alpha_1\beta_2 + \beta_1\alpha_2\rangle \tag{62b}$$

$$|-1\rangle = |\beta_1\beta_2\rangle . \tag{62c}$$

If y is chosen arbitrarily to be perpendicular to the fixed magnetic field H, then $H_y = 0$ and the spin Hamiltonian reduces to

$$H_{spin} = g_{||}\beta H_z S_z = g_{\perp}\beta H_x S_x + D(S_z^2 - 2/3) . \tag{63}$$

Consider the cases now where (1) H is parallel to the z axis and (2) when H is perpendicular to the z axis.

For case (1) with $H||z$, $H_z = H$ and $H_x = 0$ the matrix of the Hamiltonian with respect to the basis functions can be determined, the eigenvalues of which are

$$W_{+1} = \frac{D}{3} + g_{||}\beta H \tag{64a}$$

$$W_o = -\frac{2}{3} D \tag{64b}$$

$$W_{+1} = \frac{D}{3} - g_{||}\beta H \tag{64c}$$

with the corresponding eigenvectors $|+1\rangle$, $|0\rangle$, and $|-1\rangle$, respectively. At zero field the +1 and -1 states are degenerate and the appropriate wavefunctions are

$$\phi_1 = \frac{1}{\sqrt{2}} (|+1\rangle - |-1\rangle) = T_x \tag{65a}$$

$$\phi_2 = \frac{1}{|\overline{2}} (|+1\rangle + |-1\rangle) = T_y \tag{65b}$$

$$\phi_3 = |0\rangle = T_z . \tag{65c}$$

The eigenvalues for $H||z$ are plotted versus H in Figure 10.

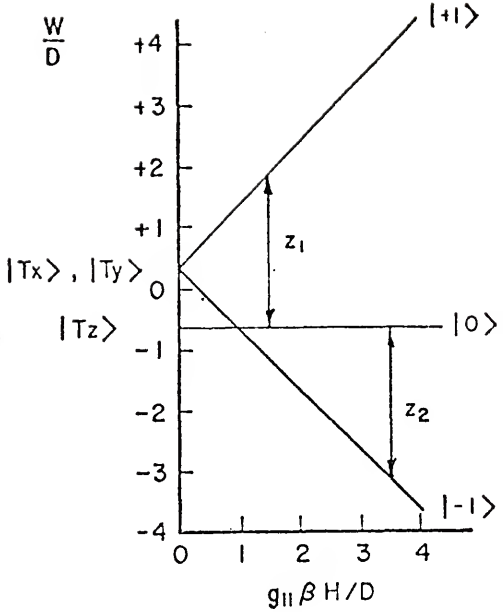

Figure 10: Energies of the triplet state in a magnetic field for a molecule with axial symmetry.

For case (2) $H \perp z$, $H = H_x$, $H_z = 0$ and the roots of the secular determinant are

$$W_1 = D/3 \tag{66a}$$

$$W_2 = [-D/3 + (D^2 + 4g_\perp^2\beta^2H^2)^{1/2}]/2 \tag{66b}$$

$$W_3 = [-D/3 - (D^2 + 4g_\perp^2\beta^2H^2)^{1/2}]/2 . \tag{66c}$$

Substitution of each of these eigenvalues into the secular equation and solving for the eigenvectors, with normalization, yields

$$\Phi_1 = \frac{1}{\sqrt{2}} [|+1\rangle - |-1\rangle] = \Psi_x \tag{67a}$$

$$\Phi_2 = \cos\alpha \frac{1}{\sqrt{2}} [|+1\rangle + |-1\rangle] + \sin\alpha|o\rangle = \Psi_y \tag{67b}$$

$$\Phi_3 = -\sin\alpha \frac{1}{\sqrt{2}} [|+1\rangle + |-1\rangle] + \cos\alpha|o\rangle = \Psi_z \tag{67c}$$

where $\tan 2\alpha = 2g_\perp\beta H/D$. As H approaches zero where $\alpha = 0$, the Φ_i reduce to

$$\Phi_1 = T_x \tag{65a}$$

$$\Phi_2 = T_y \tag{65b}$$

$$\Phi_3 = T_z \tag{65c}$$

where T_j are the same as for case (1). The eigenvalues for $H \perp z$ are plotted versus H in Figure 11. Only at high fields, where $\alpha \to \Pi/4$ do the lines become straight. In the intermediate region, Ψ_y and Ψ_x are mixed and lead to a curvature of the energy with H.

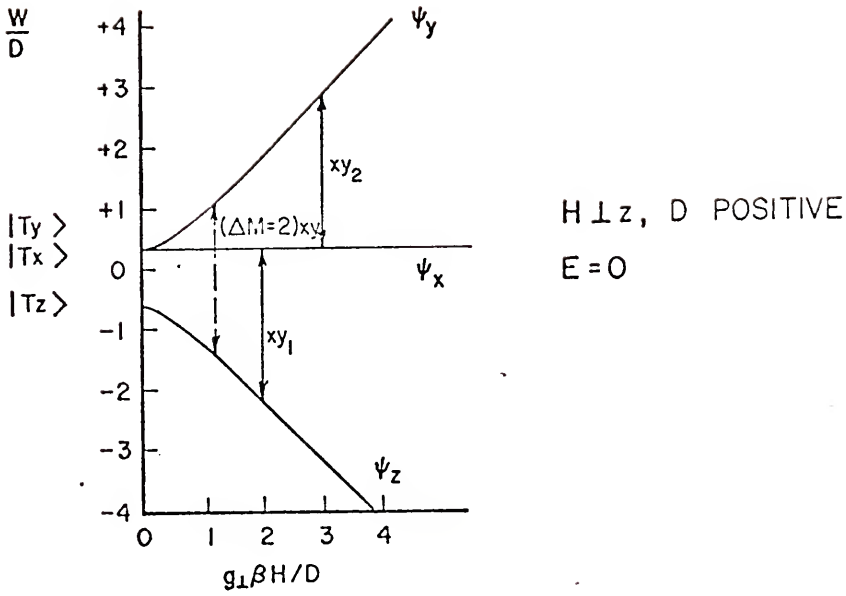

Figure 11: Energies of the triplet state in a magnetic field for a molecule with axial symmetry.

It is evident that the energy levels and the fields at which transitions occur are dependent upon the orientation of the axis of the molecule relative to magnetic field, i.e. the spectra of randomly-oriented molecules will be broad and more difficult to observe.

If transition probabilities are considered, it can be shown that with the oscillating magnetic field $H_{osc} \perp H$, transitions are allowed between energy levels characterized by the following wavefunctions: (1) $T_x \leftrightarrow T_z$, designated z_1, (2) $T_y \leftrightarrow T_z$, z_2, (3) $\Psi_y \leftrightarrow \Psi_x$, xy_2, and (4) $\Psi_z \leftrightarrow \Psi_x$, xy_1. These transitions are indicated in Figures 10 and 11 and all correspond to $\Delta M = \pm 1$ transitions. When $H_{osc} \| H$, another type of transition is allowed ($\Psi_y \leftrightarrow \Psi_z$), referred to as a "forbidden" transition because it connects the two outermost energy levels and corresponds to a $\Delta M = \pm 2$ transition. The $\Delta M = 2$ transition usually has a finite transition probability when H is not parallel to any of the x, y, or z axes, even if $H_{osc} \perp H$ (11). Therefore for our experimental apparatus with $H_{osc} \perp H$, the $\Delta M = 2$ will be observable if D is not too large.

Employing the exact solution of the matrix of the spin Hamiltonian, the resonant field positions for the transitions can be determined (42). Then

$$H_{xy_1}^{\ 2} = (g_e/g_\perp)^2 H_o(H_o - D') \qquad (68a)$$

$$H_{xy_2}^{\ 2} = (g_e/g_{\perp})^2 H_o(H_o + D') \tag{68b}$$

$$H_{z_1} = (g_e/g_{||})|H_o - D'| \tag{68c}$$

$$H_{z_2} = (g_e/g_{||})(H_o + D') \tag{68d}$$

where $D' = D/g_e\beta$. For the $\Delta M = \pm 2$ transition (6)

$$H_{\Delta M = \pm 2} = \frac{1}{g\beta}\left(\frac{h^2\nu^2}{4} - \frac{D^2}{3}\right)^{1/2}. \tag{69}$$

For a fixed cavity frequency of 9.39 GHz, $h\nu \simeq 0.3\ cm^{-1}$. Using this $h\nu$ and $g = g_e$, Figure 12 shows a plot of H_r for the above energy levels as D is varied from 0 to 1.0. As D increases from zero and approaches $h\nu$, it is seen that the transition z_1 approaches H = 0 and for $D>h\nu$ the z_1 and z_2 transitions appear but at increasingly higher values of H. Both the xy_1 and $\Delta M = 2$ transitions will not be able to be observed for $D>h\nu$ and only the xy_2 transition can possibly be seen.

For linear molecules, it was shown (see previous section) that the transition probability was proportional to $\sin\theta/dH/d\theta$ or for the unnormalized absorption

$$\text{Intensity} = \sin\theta/(\partial H_r/\partial\theta) \tag{70}$$

where $H_r = H_o \pm [(D'/2)\sin^2\theta - D'\cos^2\theta]$ in polar coordinates. Thus

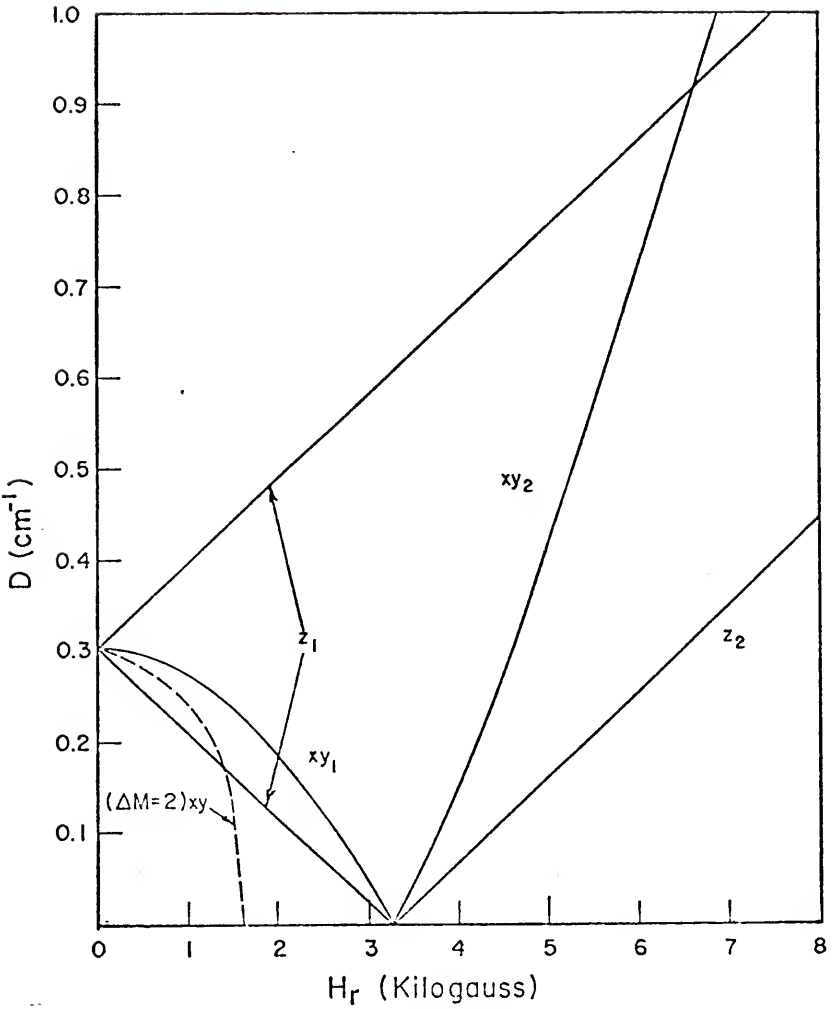

Figure 12: Axial resonant fields with E = 0 for varying D from equations 68 and 69.

$$\text{Intensity} \propto [(D'/2) \pm (H - H_o)]^{-1/2} . \qquad (71)$$

The upper sign refers to the region about H_o of $-D'$ to $+D'/2$ and the lower sign to the region $-D'/2$ to $+D'$. The total absorption is the sum of these terms. As indicated in Figure 13 (a), there is a step in the curve at $\pm D'$. At these fields absorption is due to molecules when $H||z$. The absorption rises without limit at $\pm D'/2$ due to those triplets where H lies in the x,y plane or $H\perp z$. In Figure 13 (b), the first derivative curve of the theoretical absorption spectrum is shown. This contains only the region corresponding to $\Delta M_s = \pm 1$ transitions. Due to the small anisotropy of the $\Delta M = 2$ transitions, i.e. a small value of $dH/d\theta$, these transitions exhibit relatively large amplitude.

As previously stated, generally the hyperfine interaction is small compared to the fine structure and the electronic Zeeman energy so that first order perturbation is sufficient to account for the hfs. For one magnetic nucleus in the molecule the hf contributions to the energy levels is found to be (for $H||z$)

$$W_{+1} = A_{||} m \qquad (72a)$$

$$W_o = 0 \qquad (72b)$$

$$W_{-1} = -A_{||} m . \qquad (72c)$$

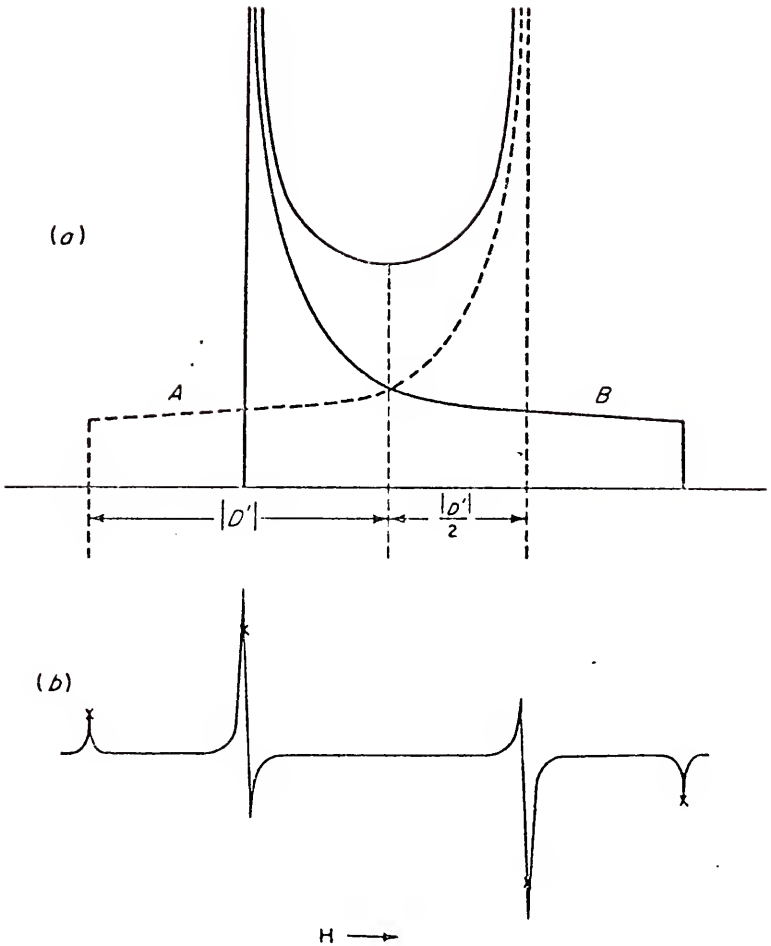

Figure 13: (a) Theoretical ESR absorption spectrum for a randomly oriented triplet system for a given value of D' and ν (E = 0).

(b) Derivative curve computed from (a) (Only the field region corresponding to $\Delta M_s = \pm 1$ is shown).

For a $\Delta M = \pm 1$ transition of $h\nu$ then

$$h\nu = -D + g_{||}\beta H + A_{||}m \tag{73}$$

so that the resonant field is

$$H = [h\nu + D - A_{||}m]/g_{||}\beta. \tag{74}$$

For hf interaction with a nucleus of spin I = 1/2, the hfs is then

$$\Delta H = A_{||}/g_{||}\beta . \tag{75}$$

In the same way, it can be shown that the $\Delta M = \pm 2$ transition will have the same hfs.

For $H \perp z$, it is found that

$$W_1' = W_1 \tag{76a}$$

$$W_2' = W_2 \pm \frac{A_\perp \sin 2\alpha}{2} \tag{76b}$$

$$W_3' = W_3 \pm \frac{A_\perp \sin 2\alpha}{2} \tag{76c}$$

where W_1, W_2 and W_3 are the same as given before and $\sin 2\alpha = [1 - (D/h\nu)^2]^{1/2}$. Then in the limit of small D relative to $h\nu$, H approaches $A_\perp/g_\perp\beta$. When D and $h\nu$ are comparable

$$\Delta H \simeq \left(\frac{A_\perp}{g_\perp \beta} \right) (h\nu + D/2) \left[h\nu (h\nu + D) \right]^{-1/2}. \tag{77}$$

Derived Molecular Parameters

Coefficients of the Wave Functions

It is easily shown, using the relations developed for the A tensor of a linear molecule, that the observed ESR parameters $A_{||}$ and $A_{\perp}$ can be related to the fundamental molecular parameters in terms of A_{iso} and A_{dip} by the relations

$$A_{iso} = \frac{(A_{||} + 2A_{\perp})}{3} = \frac{8\pi}{3} g_N \beta_N g_e \beta_o |\psi(0)|^2 \qquad (78)$$

$$A_{dip} = \frac{(A_{||} - A_{\perp})}{3} = g_e \beta_o g_N \beta_N \left\langle \frac{3\cos^2\theta - 1}{2r^3} \right\rangle . \qquad (79)$$

In order to describe the odd-electron distribution, an approximate wavefunction can be constructed using a simple linear combination of the essential atomic orbitals for a given species (41). A procedure which is sometimes used to determine the coefficients in the ground state wavefunction depends upon a comparison of molecular hfs constants with those in the free atoms. The s or p character of the odd-electron at a particular nucleus is then obtained by taking the ratio of A_{iso} (molecule)/A_{iso} (atom) or A_{dip} (molecule)/A_{dip} (atom). As an example of this, consider C_2H. The ground state wavefunction could then be written:

$$\Psi_{C_2H} = a_1\chi(2s_{C_\alpha}) + a_2\chi(2p_{C_\alpha}) + a_3\chi(2s_{C_\beta}) + a_4\chi(2p_{C_\beta}) + a_5\chi(1s_H). \quad (80)$$

In this approximation,

$$a_1^2 = \frac{A_{iso}(C_\alpha \text{ in } C_2H)}{A_{iso}(C \text{ atom})}, \quad a_2^2 = \frac{A_{dip}(C_\alpha \text{ in } C_2H)}{A_{dip}(c \text{ atom})}, \text{ etc.,}$$

where A_{iso} (molecule) and A_{dip} (molecules) values are obtained from the hfs of $^{13,13}C_2H$. If this were correct, then $\sum_i a_i^2 = 1$. A_{iso} (atom) and A_{dip} (atom) values are obtained from experiment and/or theory and a list has been compiled in Ayscough (1). [Note: in reference (1), A_{dip} is designated as B_o.] This procedure depends upon the doubtful supposition that the atomic properties are unchanged in the molecule.

A more general statement of this method is, that if we know what splitting an entire electron will give with a nucleus when it is in either an ns or an np-orbital on that nucleus we can estimate the actual occupancy of those orbitals and compare these with the calculated values of the coefficients of the molecular orbitals.

Spin densities

From the experimentally determined values of A_{iso} and A_{dip} for a particular nucleus, the basic quantities $|\Psi(0)|^2$ and $\langle(3\cos^2\Theta - 1)/r^3\rangle$ may be determined. As

shown previously, the relation may be written

$$A_{iso}^{N} = \frac{8}{3}\pi g_e g_N \beta_o \beta_N |\Psi(0)_N|^2 \qquad (78)$$

and

$$A_{dip}^{N} = g_e g_N \beta_o \beta_N \langle (3\cos^2\theta - 1)/2r_N^3 \rangle . \qquad (79)$$

Where N stands for a particular nucleus. It would be helpful to compare these values with calculated values. Morikawa and Kikuchi (43) have presented an SCF-MO-INDO method for predicting the values for A_{iso} and A_{dip} which have been used in a comparison with the observed values, for example in C_2H.

Δg and the Spin-Doubling Constant

It was shown that perturbation theory gives corrections to the various components of the g-tensor and the equations for these shifts were given (see section on g-tensor). For linear molecules with axial symmetry it can be seen that $g_{||}$ and $g_{\perp}$ involved summations of terms which depend upon spin-orbit coupling with excited Π states to the ground state. Also the g-shifts were dependent upon the energy separation of these states from the ground state. It is evident that

$$\Delta g_{\perp} = g_{\perp} - g_e = -2\lambda \Sigma_n' \frac{\langle n|L_x|0\rangle\langle 0|L_x|n\rangle}{E_n - E_o} . \qquad (81)$$

Therefore, the lower-lying the Π state and the larger the value of λ, the more effective the coupling. $g_{||}$ should always be close to g_e, however, since the matrix elements are zero, and it is normally found that $g_{||} \simeq g_e$. However, $\Delta g_\perp$ is more affected by the coupling, and it can be positive or negative depending upon the character of the Π state involved. In general the lowest-lying Π state will dominate the summation so that higher states can be neglected, and the sign of $\Delta g_\perp$ will depend upon whether that excited state has the properties of an electron in a π orbital or of a "hole" in a π orbital. In molecular orbital notation, the excited state would be obtained by excitation of a ground $^2\Sigma$ state with a configuration $\ldots\pi_1^4\sigma^1$ to $\ldots\pi_1^4\pi_2^1$, $^2\Pi_r$(r for regular) or to $\ldots\pi_1^3\sigma^2$, $^2\Pi_i$(i for inverted). Mixing of the $^2\Pi_r$ state with the ground state will cause $\Delta g_\perp$ to be negative whereas a $^2\Pi_i$ state will cause $\Delta g_\perp$ to be positive. In the simplest case, it can be said that if the experimental value of $\Delta g_\perp$ is negative, usually a $^2\Pi_r$ excited state lies lowest and if $\Delta g_\perp$ is positive, a $^2\Pi_i$ state is lowest. In this way qualitative information about the excited state of a $^2\Sigma$ molecule is immediately obtained from the value of $\Delta g_\perp$.

$^2\Sigma$ molecules in the gas phase also exhibit a splitting of their rotational levels given by $\gamma(K + 1/2)$,

where γ is very small compared with the rotational constant, B, and K is the rotational quantum number. γ is called the spin-doubling constant and has been shown by Van Vleck (44) to be given by

$$\gamma = 4\sum_n \langle 0|\lambda L_x|n\rangle\langle n|BL_x|0\rangle/E_n - E_o \qquad (82)$$

when $|n\rangle$ includes all excited $^2\Pi$ states, B is the rotational operator $h^2/(8\pi^2\mu r^2)$ and all other terms have been defined previously. If B is assumed to be constant then γ reduces to

$$\gamma = 4B\sum_n \langle 0|\lambda L_x|n\rangle\langle n|L_x|0\rangle/E_n - E_o \ , \qquad (83)$$

Then

$$\gamma = -2B\Delta g_{\perp} \qquad (84)$$

for a molecule in a $^2\Sigma$ state [derived by Knight and Weltner, (45)]. Thus from $\Delta g_{\perp}$ values, the sign and magnitude of γ can be predicted. Since γ can often be determined with good accuracy by gas-phase spectroscopists from analysis of the rotational structure of high-dispersion optical spectra, a check of the experimental data from two quite different sources is allowed. For an example, see the discussion of C_2H.

References - Chapter III

1. P. B. Ayscough, Electron Spin Resonance in Chemistry, London: Methuen, 1967.

2. R. S. Alger, Electron Paramagnetic Resonance: Techniques and Applications, New York: Wiley-Interscience, 1968.

3. C. P. Poole, Jr., Electron Spin Resonance, New York: Wiley-Interscience, 1967.

4. A. Carrington and A. D. McLachlan, Introduction to Magnetic Resonance, New York: Harper and Row, 1967.

5. C. P. Slichter, Principles of Magnetic Resonance, New York: Harper and Row, 1963.

6. J. C. Wertz and J. R. Bolton, Electron Spin Resonance, New York: McGraw-Hill, 1972.

7. H. M. Assenheim, Introduction to Electron Spin Resonance, New York: Plenum, 1966.

8. A. Abragam and B. Bleaney, Electron Paramagnetic Resonance of Transition Ions, London: Oxford University, 1970.

9. W. Low, Paramagnetic Resonance in Solids, New York: Academic, 1960.

10. I. N. Levine, Quantum Chemistry, Volume II, Boston: Allyn and Bacon, 1970.

11. S. P. McGlynn, T. Azumi, and M. Kinoshita, Molecular Spectroscopy of the Triplet State, Englewood Cliffs, New Jersey: Prentice Hall, 1969.

12. Hyperfine Interactions, edited by A. J. Freeman and R. B. Frankel, New York: Academic, 1967.

13. G. E. Pake, Paramagnetic Resonance, New York: Benjamin, 1962.

14. B. Taylor, W. Parker, and D. Langenberg, Rev. Mod. Phys. 41, 375 (1969).

15. P. H. Kasai, J. Chem. Phys. 49, 4979 (1968).

16. L. B. Knight, Jr. and W. Weltner, Jr., J. Chem. Phys. 54, 3875 (1971).

17. L. B. Knight, Jr. and W. Weltner, Jr., J. Chem. Phys. 55, 2061 (1971).

18. J. M. Brom, Jr. and W. Weltner, Jr., J. Chem. Phys. 57, 3379 (1972).

19. J. M. Brom, Jr., W. R. M. Graham, and W. Weltner, Jr., J. Chem. Phys. 57, 4116 (1972).

20. W. C. Easley and W. Weltner, Jr., J. Chem. Phys. 52, 197 (1970).

21. A. J. Stone, Proc. Roy. Soc. 271, 424 (1963).

22. H. H. Tippins, Phys. Rev. 160, 343 (1967).

23. E. Fermi, Z. Physik 60, 320 (1930).

24. The Triplet State, Proceedings of the International Symposium held at The American University of Beirut, Lebanon, February 14-19, 1967. Cambridge University Press, London, 1967.

25. J. Mispelter, J. P. Grivet, and J. M. Lhoste, Mol. Phys. 21, 999 (1971).

26. R. A. Bernheim, H. W. Bernard, P. S. Wang, L. S. Wood, and P. S. Skell, J. Chem. Phys. 54, 3223 (1971).

27. E. Wasserman, V. J. Kuck, R. S. Hutton, E. D. Anderson, and W. A. Yager, J. Chem. Phys. 54, 4120 (1971).

28. J. A. McMillan, Electron Paramagnetism, New York: Reinhold, 1968.

29. B. Bleaney, Proc. Roy. Soc. 63, 407 (1950).

30. B. Bleaney, Phil. Mag. 42, 441 (1951).

31. R. H. Sands, Phys. Rev. 99, 1222 (1955).

32. D. E. O'Reilly, J. Chem. Phys. 29, 1188 (1958).

33. J. W. Searl, R. C. Smith, and S. J. Wyard, Proc. Phys. Soc. 74, 491 (1959).

34. B. Bleaney, Proc. Phys. Soc. 75, 621 (1960).

35. E. M. Roberts and W. S. Koski, J. Amer. Chem. Soc. 82, 3006 (1960).

36. F. K. Kneubuhl, J. Chem. Phys. 33, 1074 (1960).

37. J. A. Ibers and J. P. Swalen, Phys. Rev. 127, 1914 (1962).

38. T. S. Johnston and H. G. Hecht, J. Mol. Spec. 17, 98 (1965).

39. M. M. Malley, J. Mol. Spec. 17, 210 (1965).

40. L. D. Rollman and S. I. Chan, J. Chem. Phys. 50, 3416 (1969).

41. P. W. Atkins and M. C. R. Symons, The Structure of Inorganic Radicals, New York: Elsevier Publishing Company, 1967.

42. E. Wasserman, L. C. Snyder, and W. A. Yager, J. Chem. Phys. 41, 1763 (1964).

43. T. Morikawa and O. Kikuchi, Bull. Chem. Soc. Japan 45, 3715 (1972).

44. J. A. Van Vleck, Phys. Rev. 33, 467 (1929).

45. L. B. Knight, Jr. and W. Weltner, Jr., J. Chem. Phys. 53, 4111 (1970).

CHAPTER IV
C_2H RADICAL

Introduction

A study of ethynyl (C_2H) is of importance for three reasons: (1) because of its interest as a σ-electron free radical, (2) because of its possible relevance to astrophysical phenomena, and (3) because this work was done in conjunction with a study of the C_2^- radical (also included in this dissertation) in which ^{13}C substitution was required for the ESR identification of that radical. In the production of $^{13}C_2^-$, $^{13}C_2H$ was simultaneously produced as an impurity, therefore its ESR spectrum needed to be characterized.

Tsuji (1) and Morris and Wyler (2) have predicted from theoretical studies of molecular distribution in stellar atmospheres that C_2H is one of the most abundant polyatomic species in the atmospheres of carbon-rich stars, especially below 2800°K. The electronic properties were expected to be similar to CN, its isoelectronic diatomic counterpart, which is indeed a ubiquitous stellar molecule. C_2H, prior to this study however, had not been observed spectroscopically in the gas phase.

C_2H had been investigated previously by two groups of researchers. Cochran, Adrian, and Bowers (3) had observed

the hydrogen and deuterium hyperfine splittings in an electron spin resonance experiment. Milligan, Jacox, and Abouaf-Marguin (4,5) observed the C≡C stretching frequency of C_2H in argon matrix at 1848 cm^{-1}. This identification was confirmed by the effects of isotopic substitution however, no electronic transitions were observed in their work. In both of the above cases, C_2H was prepared by the ultraviolet photolysis of acetylene and then trapped in argon matrices at liquid helium temperatures.

The object of this research was to investigate further the properties of the C_2H radical by means of ESR and optical spectroscopy. As a result of the ESR study, complete spin density data have been obtained for C_2H such that a detailed comparison can be made with theoretically derived spin distributions.

As mentioned previously, C_2H is isoelectronic with CN, therefore it is expected that there should be optical absorptions corresponding to the red and violet systems of CN. As a result of these optical studies, two weak absorption systems of C_2H have been found in the general regions of the CN bands.

Experimental

Acetylene (99.5% pure) was obtained from Airco and 90% ^{13}C-enriched acetylene was obtained from Merck, Sharpe and Dohme of Canada, Ltd. Both were used without further

purification. Monoiodoacetylene (C_2HI) which was also used as a parent molecule for C_2H was prepared after the method described by Carpenter et al. (6) by the reaction of acetylene with iodine in an alkaline solution. The purity of the product was established by comparison with the published infrared spectrum (6).

These gases were mixed with argon prior to deposition. Samples of mole ratio (argon: acetylene or monoiodoacetylene) between 100 and 1000 were prepared using standard manometric procedures. For maximum production of C_2H gas mixtures were deposited at the rate of $\simeq$ 0.1 l-atm/h. During deposition of acetylene mixtures the incoming gas was subjected to direct irradiation produced by the electrodeless flowing hydrogen discharge lamp through a lithium fluoride window. Similarly, monoiodoacetylene mixtures were irradiated with a high pressure mercury lamp through a quartz window.

ESR Spectra

The linear C_2H molecule in its $^2\Sigma$ ground state should have an ESR spectrum which is a doublet due to the interaction of the one odd electron with the single proton. Since the C_2H was trapped in argon matrices at liquid helium temperatures, the molecules are randomly-oriented and rigidly held. Therefore, each line of the C_2H doublet should exhibit both perpendicular and parallel components. Figure 14 shows the ESR spectrum which was obtained after

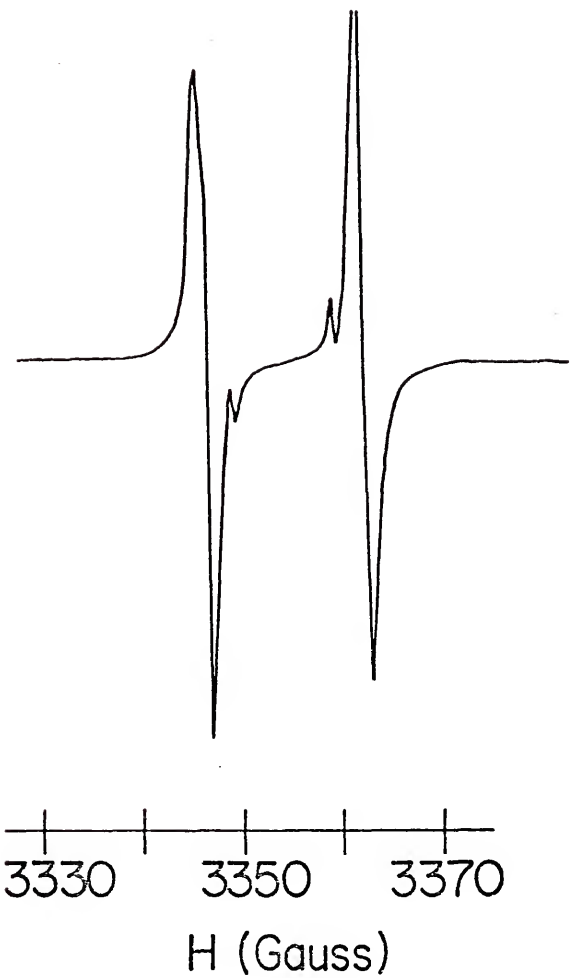

Figure 14: ESR spectrum of $^{12}C_2H$ isolated in argon at $4^{o}K$. The weaker inner doublet arises from the forbidden transitions (ν = 9398 MHz).

photolysis of 0.1% C_2H_2:Ar samples. It is consistent with an isotropic g tensor which was verified when ^{13}C substitution was made. The proton hyperfine splitting is 14.5 G for the large perpendicular components observed. Analysis of the H hfs observed in the spectrum with ^{13}C-substituted C_2H yields values of $A_{\perp}(H)$ = 14.5 G and $A_{\parallel}(H)$ = 18.2 G. Since there is an isotropic g tensor and $A_{\perp}(H)$ is approximately equal to $A_{\parallel}(H)$, the two components are overlapped, which effectively leads to broadening of the perpendicular lines on the outside by the smaller parallel line, also making the lines appear slightly asymmetric. This is similar to the spectrum reported by Cochran, Adrian, and Bowers (3). They observed a line to line splitting of 16.1 G which is an average of our A values.

Also shown in Figure 14 is an additional, weaker doublet with a splitting of 9.7 G. These lines had not been previously observed and they only appeared for high yields of the C_2H radical in this work. They have been attributed to forbidden transitions in which $\Delta M_s = 1$ and $\Delta M_I = 1$. The small hydrogen hfs is of the same order as the nuclear Zeeman energy so that the forbidden transition becomes observable.

When the concentration of C_2H_2 in argon was increased to 1% or more, other species not seen in Figure 14 were enhanced. These species were identified as vinyl radicals (C_2H_3) (3, 7, 8) and methyl radicals (CH_3) (8). It was

also found that C_2H spectrum was observed only when the matrix material was irradiated with the H_2:He lamp during deposition and that irradiation after deposition was ineffective.

If instead of $^{12}C_2H$, ^{13}C-substituted C_2H is formed, additional hfs should be observed due to interaction of the magnetic moment of the unpaired electron with the magnetic moments of these nuclei. Since the two carbon nuclei are inequivalent, the hfs will also be inequivalent. Here the carbon nucleus interacting strongly with the unpaired electron will be designated C_α and the more weakly interacting nucleus C_β. The complete hfs pattern that is expected for a 50% ^{13}C enrichment of C_2H is shown in Figure 15. The original line in C_2H should actually be a doublet due to H hfs but this hyperfine interaction has been initially neglected for the sake of simplicity. Due to strong interaction with the $^{13}C_\alpha$ (I = 1/2) nucleus, the original line is split in two. Each of these lines will then be split to a less amount due to interaction with the $^{13}C_\beta$ (I = 1/2) nucleus and split again by the hydrogen hfs. Therefore, in a sample of C_2H containing 50% of ^{13}C and ^{12}C, there should be a total of eighteen perpendicular and eighteen parallel lines with all perpendicular lines of equal intensity and all parallel lines of equal intensity.

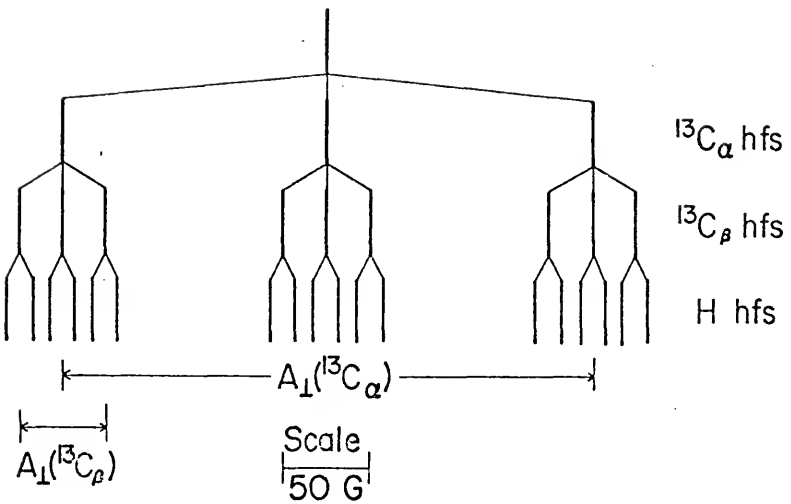

Figure 15: Predicted hyperfine splittings for a mixture of C_2H molecules containing all possible combinations of ^{12}C and ^{13}C isotopes.

If ^{13}C enrichment were increased to 90%, then the most abundant species would be $^{13}C^{13}CH$ (31%), least abundant $^{12}C^{12}CH$ (1%) and $^{12}C^{13}CH$ equal to $^{13}C^{12}CH$ (9%). Figure 16 shows experimental results when the ^{13}C enrichment was 90%. (The parent compound was 90% ^{13}C enriched C_2H_2.) The perpendicular components of the hfs are clearly observed for both ^{13}C nuclei, however, due to overlap by the perpendicular lines of the $^{12}C^{13}CH$ and $^{13}C^{12}CH$ species the parallel lines are obscured even at high gain. These parallel lines are also overlapped by weak lines attributable to C_2H_3 and CH_3 radicals.

A new route was sought by which to prepare C_2H in an effort to find a new parent compound which (1) could be enriched to a larger extent with ^{13}C and (2) would not produce the CH_3 and C_2H_3 impurities present in the C_2H_2 method of preparation. An alternate method was found in which C_2H was prepared from the photolytic decomposition of C_2HI. In this preparation C_2HI was deposited with argon in a 1:1000 ratio while being irradiated with light from the previously described high pressure mercury lamp. The resulting ESR spectrum was much simplified, consisting at low gain of a very intense C_2H doublet and very weak H lines. The absence of intense H lines indicated that the principal effect of the photolysis was detachment of the halogen. Due to this, there were only very small amounts of background impurities and it was possible at high gains

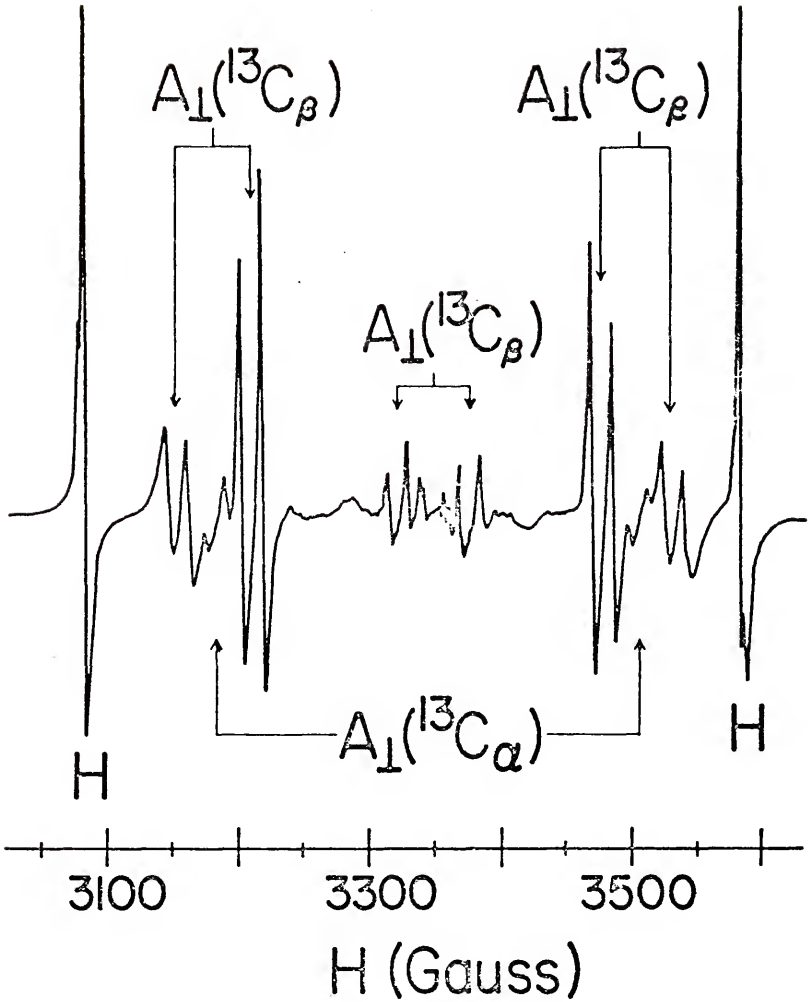

Figure 16: ESR spectrum observed for C_2H:Ar at 4°K produced by the photolysis of 90% ^{13}C-substituted C_2H_2 (ν = 9398 MHz).

to see lines attributable to $^{12}C^{13}CH$ and $^{13}C^{12}CH$ species due to the 1% natural abundance of ^{13}C in the parent molecule. Figure 17 shows the lines that are observable due to the $^{12,13}C_2H$ species. The outer doublets around 3500 and 3200 G are attributable to species in which ^{13}C is substituted for the C_α nucleus. Only one parallel and two perpendicular lines are visible. The second parallel line is overlapped by the perpendicular lines. The inner doublets around 3380 and 3320 G arise from species in which ^{13}C is substituted for the C_β nucleus.

It should be noted that these inner doublets occur on the background of the steeply rising limbs of the $^{12}C_2H$ doublet. Both parallel and perpendicular components are observed for these inner doublets although one perpendicular line of each doublet is slightly overlapped by weak lines due to the CH_3 impurity. The clearly resolved perpendicular and parallel components of the lines split by the hf interactions establish that C_2H is indeed linear and has a $^2\Sigma$ ground state.

ESR Analysis

g Tensor

By substituting the line positions that were obtained from the ESR spectrum shown in Figure 17 into the second-order solution of the axially symmetric spin Hamiltonian, the values of $|A_{||}|$, $|A_{\perp}|$, $g_{\perp}$ and $g_{||}$ can be obtained.

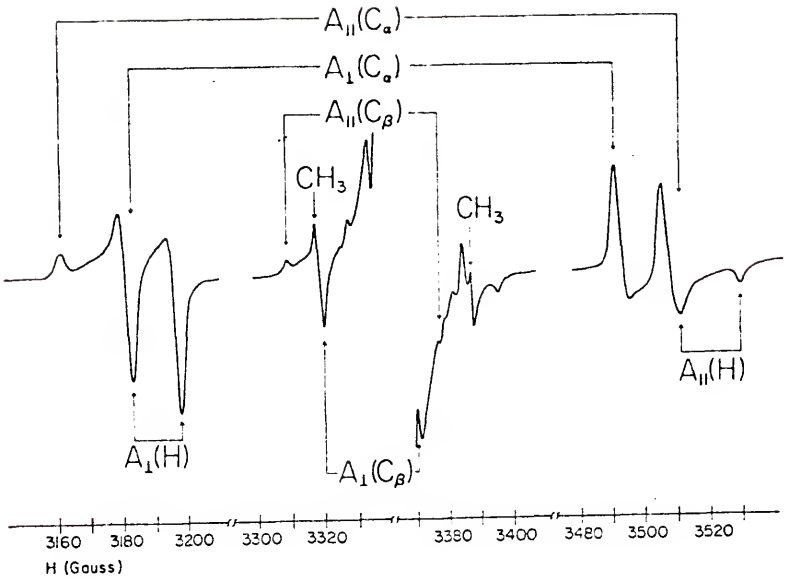

Figure 17: ESR spectrum of $^{12,13}C_2H$ species at $4^{\circ}K$ arising from the natural abundance of ^{13}C in the photolysis products of $^{12}C_2HI$. The intense $^{12}C_2H$ lines have been omitted from the central portion of the spectrum (ν = 9398 MHz).

From the ESR theory recall that the second-order solution of the axially symmetric spin Hamiltonian is given by

$$H = g_{||}\beta H_z S_z + g_{\perp}\beta(H_x S_x + H_y S_y) + \sum_N [A_{||}(N) I_z S_z + A_{\perp}(N)(I_x S_x + I_y S_y)]. \quad (57)$$

Table I shows the values of $|A_{||}|$ and $|A_{\perp}|$ for each nucleus found in this analysis. It was found that the g tensor was isotropic with $g_{||} = g_{\perp} = 2.0025$ (5). Table II lists the ESR lines observed in solid argon. The four values in parentheses refer to parallel lines which underlie perpendicular lines and were calculated from the observed values of $A_{||}(H)$. By using $g_{\perp}$ and $g_{||}$ values calculated from line positions and hfs for the $^{13}C_{\beta}$-substituted molecule, with $A_{\perp}(^{13}C_{\alpha})$ and $A_{||}(^{13}C_{\alpha})$, line positions for $^{13}C_{\alpha}$-substituted molecule were generated. The agreement of the generated line positions with the observed positions is within $\pm$ 0.1 G. Figure 18 shows a comparison between the observed and simulated spectra for $^{13}C_{\alpha}$-substituted C_2H. The calculations used the parameters given in Table I and assumed randomly oriented molecules.

A Tensors

As shown in the section on ESR theory, the hfs for a particular nucleus can be expressed in terms of isotropic (A_{iso}) and dipolar (A_{dip}) components.

Table I

Hyperfine splitting parameters[a] for $^{13}C_2H$ in the $^2\Sigma$ ground state in an Ar matrix.

Nucleus	$\|A_\perp\|$ (MHz)	$\|A_{\|\|}\|$ (MHz)
H	41(1)	51(1)
$^{13}C_\alpha$	863(1)	980(1)
$^{13}C_\beta$	139(1)	191(1)

[a] $g_{\|\|} = g_\perp = 2.0025(5)$

Table II

Observed ESR lines in gauss[a] for $^{12,13}C_2H$ isolated in solid argon at 4°K.

$M_I(^{13}C_\alpha)$	$M_I(^{13}C_\beta)$	$M_I(H)$	$\|\|$ lines[b]	$\perp$ lines
—	—	+ 1/2	(3343.7)	3346.6
—	—	- 1/2	(3361.9)	3361.1
+ 1/2	—	+ 1/2	3161.6	3183.5
+ 1/2	—	- 1/2	(3179.9)	3198.1
- 1/2	—	+ 1/2	(3511.5)	3491.5
- 1/2	—	- 1/2	3529.7	3506.0
—	+ 1/2	+ 1/2	3309.4	3320.6
—	+ 1/2	- 1/2	3327.7	3335.1
—	- 1/2	+ 1/2	3377.5	3370.2
—	- 1/2	- 1/2	3395.8	3384.7

[a] ν = 9398 MHz.

[b] Entries in brackets are positions of parallel lines overlapped by perpendicular lines; the values shown are calculated from the parameters in Table I.

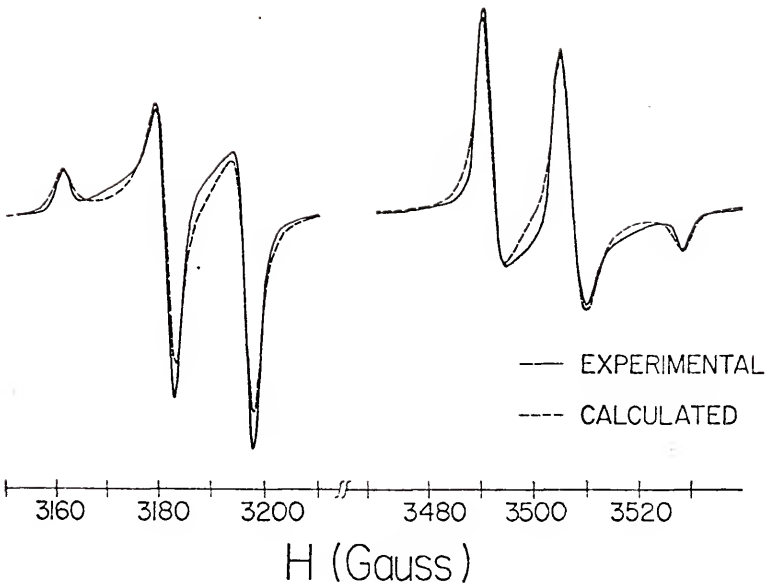

Figure 18: A comparison of the calculated ESR spectrum with the observed for the outer doublet in which the C_α nucleus of C_2H is ^{13}C substituted (ν = 9398 MHz).

$$A_{iso}(N) = 1/3(A_{||} + 2A_{\perp}) \quad (78)$$

$$= (8\pi/3)g_e g_n \beta\beta_n \rho(0)_N$$

$$A_{dip}(N) = 1/3(A_{||} - A_{\perp})$$

$$= g_e g_n \beta\beta_n \langle(3\cos^2\theta - 1)/2r^3\rangle_N. \quad (79)$$

These derived parameters are shown in Table III for each of the three nuclei (N). From these values of $A_{iso}(N)$ and $A_{dip}(N)$, the fundamental quantities $|\Psi(0)|^2$ and $\langle 3\cos^2\theta - 1/r^3\rangle$ for interaction with that nucleus can be derived. These values are also given in Table III. The signs of $A_{||}$ and $A_{\perp}$ are assumed to be positive for interaction with all nuclei since variation of signs indicate that this is the only condition for which physically reasonable spin densities are obtained.

Forbidden Transitions

The appearance of the weak inner doublet in Figure 14 can be accounted for by the methods of McConnell et al.(9,7) and are attributed to the appearance of forbidden transitions. It has been shown using second-order perturbation theory that transitions of the type $\Delta M_S = \pm 1$, $\Delta M_I = \pm 1$, are weakly allowed, whereas to the first-order, the transitions are strictly forbidden. The theory of these transitions has been discussed and treated mathematically by Miyagawa and Gordy (10), McConnell et al. (9), Poole and Farach (11), and others. Analysis shows that for

Table III

Isotropic and anisotropic hfs of
$^{13}C_2H$ and derived matrix elements.[a]

Nucleus	A_{iso}(MHz)	A_{dip}(MHz)	$\rho(0)_N$(a.u.)	$\langle(3\cos^2\theta-1)/r^3\rangle_N$(a.u.)
$^{13}C_\alpha$	902(1)	39(1)	0.803(1)	0.58(1)
$^{13}C_\beta$	156(1)	17(1)	0.139(1)	0.26(1)
H	44(1)	4(1)	0.0098(1)	0.013(2)

[a] $g_{||} = g_{\perp} = 2.0025(5)$.

radicals containing one proton, such as C_2H, four ESR transitions are possible and they are classified as an outer doublet ($\Delta M_S = \pm 1$, $\Delta M_I = 0$) and an inner doublet ($\Delta M_S = \pm 1$, $\Delta M_I = \pm 1$). Assuming that the anisotropy of the g tensor is negligibly small in comparison to that of the hyperfine coupling tensor, McConnell et al. (9) developed the following expressions for the resonance positions, $H^{\pm}_{out}$ and $H^{\pm}_{inn}$.

$$H^{\pm}_{out} = H_o \pm 1/2(A_+ + A_-) \tag{85a}$$

$$H^{\pm}_{inn} = H_o \pm 1/2(A_+ - A_-) \tag{85b}$$

where

$$H_o = h\nu/g_e\beta_e \ , \tag{1}$$

$$H_p = (g_p\beta_n/\beta_e g_e)H_o \ , \tag{86}$$

and

$$(A\pm)^2 = (H_p \pm 1/2A)^2\cos^2\Theta + (H_p \pm 1/2B)^2\sin^2\Theta\cos^2\phi + (H_p \pm 1/2C)^2\sin^2\Theta\sin^2\phi. \tag{87}$$

A, B, and C are the diagonal elements of the principle hyperfine coupling tensor and the angles Θ and ϕ define the direction of the magnetic field relative to the principle axes. It can be shown that the effect of the forbidden transitions is significant when the magnitude of hydrogen hfs is of the same order as the nuclear

Zeeman energy. Using the values obtained from the experiments for the magnetic constants, the hfs for the inner and outer doublets is calculated to be 10.1 and 14.5 G compared with the observed values of 9.7(2) and 14.5(1) G, respectively. The agreement between the calculated and experimental hfs for the inner doublet is better than it appears because the measured peak positions are superimposed on the steep wings of the outer doublet which tends to push them together.

Spin-doubling Constant

It has been shown (12) that $g_{\perp}$ is related to the spin-doubling constant γ, for $^2\Sigma$ molecules. γ can be determined by gas-phase spectroscopy from analysis of the rotational structure in high-dispersion optical spectra. The relationship is

$$\gamma = -2B\Delta g_{\perp} \tag{84}$$

where $B = h/8\pi^2cI$ is an average rotational constant (I = moment of inertia). For C_2H, $\Delta g_{\perp} = g_{\perp} - g_e$ is estimated to be small and positive (+0.0002), therefore one would predict γ to be approximately -20 ± 50 MHz for $B \simeq 44.2$ GHz. C_2H was recently identified using astronomical observations by Tucker, Kutner, and Thaddeus (13). These observations yielded a precise value for γ of -62.57 MHz.

Optical Spectra

An extensive search was made for the optical spectrum of C_2H from the vacuum ultraviolet into the infrared. Since C_2H is isoelectronic with CN, it is reasonable to expect C_2H to have "red" and "violet" band system which would correspond to the red and violet system of CN. For CN, these systems occur around 11,000 Å for the $A^2\Pi \leftarrow X^2\Sigma$ transition and 3800 Å for the $B^2\Sigma \leftarrow X^2\Sigma$ transition (14). However, it is known that for HCN and C_2H_2 bent ← linear transitions occur in the violet (15), so it is also possible that C_2H will have similar transitions.

As previously stated, C_2H is isoelectronic with CN, having a ground state electronic configuration written as $\sigma_1{}^2\pi^4\sigma_2$ where the inner closed shells are not indicated. σ_1 is presumably an orbital binding the H and C . It is assumed to be formed from an $C_\beta 2sp\sigma$ hybrid valency and a H 1s orbital. π is a $p\pi$ bonding orbital between C_α and C_β. It is formed by the in-phase overlap of p orbitals on C_α and C_β. σ_2 is essentially a non-bonding $2sp\sigma$ orbital localized largely on C_α. The transition A ← X, written

$$\sigma_1{}^2\pi^3\sigma_2{}^2, A^2\Pi_i \leftarrow \sigma_1{}^2\pi^4\sigma_2, X^2\Sigma$$

corresponds to the red transition ($^2\Pi_i \leftarrow {}^2\Sigma^+$) of CN. The transition B ← X, written

$$\sigma_1\pi^4\sigma_2{}^2, B^2\Sigma \leftarrow \sigma_1{}^2\pi^4\sigma_2, X^2\Sigma$$

corresponds to the violet transition ($^2\Sigma^+ \leftarrow {}^2\Sigma^+$) of CN. C_2H differs from CN in this transition because the electron is being transferred from a C-H bonding σ orbital to a non-bonding σ orbital, whereas in CN the electron is being transferred from a slightly antibonding σ orbital to a bonding σ orbital (14).

Excitation occurring to the next higher π^* level will result in a bent excited state because the π^* orbital is strongly angle dependent as indicated by the Walsh diagram (16) for the HAB molecules. That is to say when an electron is excited into a π^* orbital, the binding energy of the orbital is increased as the H-C-C angle goes from 180° to 90°, thus the resulting transition should be from a linear ground state to a bent excited state. The possible excited state configurations that can arise from transfer of any of the seven valence electrons to this π^* state are listed along with their linear counterpart.

non linear		linear	
$(a')^2(a")^2(a')^2(a')$	$^2A'$	$\sigma_1{}^2\pi^4\pi^*$	$^2\Pi_r$
$(a')^2(a")\ (a')^2(a')(a')$	$^2A'(2), {}^2A"(1)$	$\sigma_1{}^2\pi^3\sigma_2\pi$	$^2\Sigma^+(2), {}^2\Sigma^-(2), {}^2\Delta(2)$
$(a')^2(a")^2(a')\ (a')(a')$	$^2A'(3)$		
$(a')\ (a")^2(a')^2(a')(a')$	$^2A'$	$\sigma_1\pi^4\sigma_2\pi^*$	$^2\Pi_r$

The numbers in parentheses after the electronic state indicate the number of such states. It should be noted that for HCN, the transitions to non-linear excited states lie in the 2000-1600 Å region (for A-X and B-X transitions) and in the 1500-1300 Å region (for C-X) and that the longer wavelength bands are much weaker in intensity.

Much effort was directed toward finding the proper conditions for maximum production of C_2H for optical studies. Production was followed by observing the intensity of the 1848 cm^{-1} C≡C vibrational frequency in the infrared which was identified previously by Milligan, Jacox, and Abouaf-Marquin (4). It was found that the best production of C_2H resulted from very slow, long deposition (rate equal to 0.03 l atm/h) of 1% C_2H_2 in argon being photolyzed during deposition with the H_2:He discharge lamp. For these conditions, two very weak band systems were observed, one around 10,000 Å and the other around 3400 Å. The ultraviolet system ranged from 3400 Å down to 2500 Å. No other bands were observed between 2500 Å and 1500 Å. Since these band systems were so broad, many experiments were carried out in an attempt to determine the wavelengths as accurately as possible. The observed transitions and the uncertainties in their positions for both systems are listed in Tables IV and V.

As mentioned in ESR Spectra and Analysis, impurities such as C_2H_3 and CH_3 were also formed during the production of C_2H. These optical transitions do not appear to belong

Table IV

Bands[a] of $^2\Pi_i \leftarrow X^2\Sigma$ transition of C_2H in Ar at ~ 4^oK.

(ν_1,ν_2,ν_3)	λ(Å)	Intensity	$\nu(cm^{-1})$	$\Delta\nu$
(0,0,0)	10,080	strong	9,920(20)	
				1,560
(0,0,1)	8,708	medium	11,480(20)	

[a]Two very weak bands were also observed at 9,688 and 9,430 Å.

Table V

Bands observed in the 3000 Å region for C_2H:Ar at 4°K.

(Relevant frequencies differences are also indicated)

λ(Å)	Relative[a] Intensity	ν(cm^{-1})	Δν(cm^{-1})			
3405(3)	w	29360				
3336(3)	w	29967	---	----	----	
			860			
3243(3)	w	30827	---	1323		
3195(3)	w	31290	---	----	2703	----
			844			
3111(2)	m	32134	---	1380		
						2679
3060(4)	m	32670		----	----	
				1299		
2943(2)	w	33969		----	2556	----
				1257		
2838(4)	w	35226	---	----	---	
			864			2477
2770(2)	w	36090	---	1220		
2743(2)	s	36446		----		----
			799			
2710(3)	w	36889	---			2212
2586(2)	w	38658				----

[a]Estimated relative intensities; strong, s; medium, m; weak, w.

to these impurities or other impurities. The optical bands listed appear only when a strong absorption occurs at 1848 cm^{-1} in the infrared. Furthermore, these transitions occur independent of the appearance of C_2H_3 as monitored by the ESR. When C_2H_3 signals are strong in the ESR at the expense of C_2H, these electronic transitions have not been observed.

10,000 Å Bands, $A^2\Pi_i \leftarrow X^2\Sigma$

Two broad bands were observed in this region at 10,080 and 8708 Å. Other bands in this progression were not observed but these bands did exhibit the expected decreasing relative intensities. It is expected that this is the band system of C_2H which corresponds to the red system of CN. The vibrational frequency observed is 1560 cm^{-1} due to a C≡C stretching vibration. In the ground state, the C≡C stretching frequency is 1848 cm^{-1}. In the corresponding transition for CN the ground state vibrational frequency is 2060 cm^{-1} which decreases to 1814 cm^{-1} in the excited state therefore, it is reasonable to expect such a decrease in C_2H. In this transition which is written

$$\sigma_1^2\pi^3\sigma_2^2, A^2\Pi_i \leftarrow \sigma_1^2\pi^4\sigma_2, X^2\Sigma$$

the electron is being transferred from essentially a π bonding orbital to a σ non-bonding orbital localized at C_α.

Since this excited state is a $^2\Pi_i$, each band should be split into two bands via spin-orbit coupling. In CN, the spin-orbit coupling constant is -52 cm^{-1}. Due to the fact that these bands are very broad (approximately 100 cm^{-1} wide at half-height) a splitting of that magnitude would not be observed. In order to improve the resolution, an attempt was made to produce C_2H in neon; however, these experiments were not successful.

The corresponding band system in CN is relatively weak, and it is not surprising that in C_2H only weak transitions are also observed.

3000 Å Bands, $B^2\Sigma \leftarrow X^2\Sigma$ or $B^2A' \leftarrow X^2\Sigma$

Two possible assignments for this band system will be discussed here however the assignments of the bands in this region are less definite.

The first possibility is the linear-linear $^2\Sigma \leftarrow {}^2\Sigma$ transition in which a bonding σ electron from the C-H bonding (or perhaps C≡C) orbital is excited into the corresponding non-bonding σ orbital localized at C_α. If this transition were to occur the C-H (or C≡C) bond, would be weakened, i.e. the C-H bond length might increase, and in the excited state the C-H vibrational frequency would be expected to decrease. For this case it might be expected to observe C-H vibrations much less than 3300 cm^{-1} (estimated C-H stretch of C_2H from C_2H_2 ground state). (If instead, the electron from the C≡C orbital

is excited, C≡C vibrations less than 1848 cm^{-1} might be expected to be observed.) Although several differences between bands give frequencies of this magnitude, no obvious progressions appear.

It is likely that the $B^2\Sigma \leftarrow X^2\Sigma$ transitions should occur in this region since no other absorptions are observed below 2500 Å to 1500 Å.

A second possibility for the assignment of these transitions might be a $B^2A' \leftarrow X^2\Sigma$ transition, i.e. a bent ← linear transition. The lowest bent excited state would be expected to be produced by excitation of the σ_2 nonbonding electron into a π^* or more correctly a' orbital to produce a $^2A'$ electronic state. The transition would be written

$$(a')^2(a")^2(a')^2(a'),B^2A' \leftarrow \sigma_1{}^2\pi^4\sigma_2,X^2\Sigma.$$

This transition would be expected to be of relatively low intensity and to exhibit progression in the H-C≡C bending frequency in the excited state. In HCN, excitation from the ground state to the C state corresponds to such a transition in which there is a $\pi^* \leftarrow \sigma$ transition. The ground state bending frequency is 713 cm^{-1} and the excited C state frequency is 869 cm^{-1}. Therefore for C_2H the ground state bending frequency might occur around 700 cm^{-1} and be expected to increase in the upper state.

Either of the cases are possibilities. Table IV suggests that vibrational frequencies of 840 and 1300 cm^{-1} may appear in progressions in the spectrum which would tend to favor either the latter case or a possible overlap of both cases presented.

Discussion

Hyperfine Tensors and Spin Density

The isotropic and dipolar components of the hyperfine coupling constants observed for C_2H are compared in Table VI with several theoretical calculations. The first listed in an INDO calculation performed by Pople and Beveridge (17). They used bond distances for C≡C = 1.40 Å and for C-H = 1.08 Å. These calculations are in poor agreement with the observed values. The second INDO calculation was performed using acetylenic bond distances, but the agreement is still rather poor. The last calculation by Morikawa and Kikuchi (18) was carried out using a more extended basis SCF MO INDO procedure. The agreement is much better, however, there are still discrepancies. The A_{iso} (H) is estimated to be much too large, and A_{iso} (C_β) is considerably underestimated.

In a procedure sometimes used (see Chapter III) to obtain an approximate description of the odd-electron distribution, the ground state wavefunction is expressed as a simple linear combination of atomic orbitals including

Table VI

Comparison between observed hfs parameters for C_2H and values obtained from INDO calculations.

		Observed	Calculated (MHz)		
		(MHz)	INDO[a]	INDO[b]	M & K[c]
H	A_{iso}	44	93	101	151
	A_{dip}	4			2
$^{13}C_{\alpha}$	A_{iso}	902	970	826	978
	A_{dip}	39		36	44
$^{13}C_{\beta}$	A_{iso}	156	-7	12	54
	A_{dip}	17		8	13

[a]From reference (17) page 131. Bond distances used, C≡C = 1.40 Å, C-H = 1.08 Å.

[b]Same computation as in footnote [a] but with C≡C = 1.208 Å, C-H = 1.058 Å (as in acetylene). Values for A_{dip} were calculated using the equations of Beveridge and McIver (19).

[c]Reference (18).

only the essential atomic orbitals. The wavefunction for C_2H can then be written

$$\Psi(C_2H) = a_1\chi(1s_H) + a_2\chi(2s_{C_\beta}) + a_3\chi(2p_{C_\beta}) + a_4\chi(2s_{C_\alpha}) + a_5\chi(2p_{C_\alpha}) \quad (80)$$

where $\chi(1s_H)$ represents the 1s atomic orbital of H and $\chi(2s_{C_i})$ and $\chi(2p_{C_i})$ (I = α,β) are the 2s and 2p orbitals of the C nucleus. The coefficients ($a_{1\to5}$) are estimated by a comparison of the molecular hfs constants with those in the free atom. The s or p character of the odd electron at a particular nucleus is then estimated by taking the ratio of A_{iso} (molecule)/A_{iso} (atom) or A_{dip} (molecule)/A_{dip} (atom). In this approximation

$$a_1^2 = \frac{A_{iso}\ H(\text{molecule})}{A_{iso}\ H(\text{atom})} ,$$

$$a_2^2 = \frac{A_{iso}\ C\ (\text{molecule})}{A_{iso}\ C(\text{atom})} , \text{ etc.}$$

Values for atomic hfs constants are taken from Asycough (20). They are A_{iso} = 3110 MHz and A_{dip} = 90.8 MHz for the ^{13}C nuclei and A_{iso} = 1420 MHz for the H nucleus. The results are given in Table VII and indicate that the odd-electron spin density resides predominantly on C_α with substantial sp hybridization of the σ orbital. Table VII lists for comparison the values taken from Easley and

Table VII

Approximate coefficients of $\Psi(X^2\Sigma)$ derived from A tensors for C_2H[a], and comparison with CN[b].

C_2H		CN	
$a_1^2(1s_H)$	0.03		
		$a^2(2s_N)$	-0.008
$a_2^2(2s_{C_\beta})$	0.05		
$a_3^2(2p_{C_\beta})$	0.19	$a^2(2p_N)$	0.32
$a_4^2(2s_{C_\alpha})$	0.29	$a\ (2s_C)$	0.19
$a_5^2(2p_{C_\alpha})$	0.43	$a\ (2p_C)$	0.48

[a]Derived from the isotropic and dipolar hf constants using the approximate atomic values, $A_{iso}(^{13}C)$ = 3110 MHz, $A_{dip}(^{13}C)$ = 91 MHz, and $A_{iso}(H)$ = 1420 MHz. From reference (20).

[b]Taken from reference (21) for comparison purposes the C atom in CN is considered equivalent to C_α in C_2H, and the N atom as equivalent to CH in C_2H.

Weltner (21) for CN. In this comparison, the C atom in CN is considered as the C_α in C_2H, it is seen that the spin distributions are similar.

g Tensor

The g values obtained for C_2H were $g_\perp = g_{||} = 2.0025(5)$. The $\Delta g_\perp$ value ($g_\perp - g_e$) indicates that there is little mixing of orbital angular momentum into the ground state wavefunction of C_2H from the higher-lying Π states. Recall that the CN molecule exhibited a small negative shift of $g_\perp$ ($\Delta g_\perp = -0.002$) which was attributed to mixing with the $^2\Pi_r$ excited state. This state was approximately 55,000 cm^{-1} above the $^2\Sigma$ ground state. It was thought and supported by approximate calculation, however, that the lower lying $^2\Pi_i$ excited state did not couple appreciably. This state was 9200 cm^{-1} above the $^2\Sigma$ ground state.

This difference in g for C_2H and CN is interesting because the excited states in the same configurations are expected to couple to the ground state. In C_2H the lowest-lying $^2\Pi_i$ excited state is approximately 10,000 cm^{-1} above the ground state and could possibly give a positive g shift. But as in CN, it appears to exhibit only very small coupling.

The $^2\Pi_r$ state of CN, at about 55,000 cm^{-1}, has its counterpart in C_2H in a bent excited state, presumably at about the same energy above the ground state, or perhaps lower if it is contained in the observed violet

system. In this bent state of C_2H, the outer orbital is an a' orbital which corresponds largely to an s orbital on C_α (16). There would be only a small coupling expected between this excited state and the ground state, so it is again not surprising that $g_\perp$ in C_2H is not negatively shifted.

Optical Transitions

The observation of the spectrum of gas phase C_2H would be very helpful. It appears that the C_2H red system should be no more difficult to observe than CN. The observation of the violet system would be of great interest because of the anomalous nature of the spectral bands observed in solid argon. This would also give more insight into the treatment of the $\Delta g_\perp$ data.

Summary

It should be noted that these ESR measurements formed the essential foundation for the identification of C_2H in the interstellar medium by Tucker, Kutner, and Thaddeus (13) using the methods of radio astronomy. These observations have shown that C_2H, as expected and predicted, is an extremely common constituent of the interstellar medium.

Table VIII shows a comparison of the observed results of Tucker *et al.* (13) with the observed results from these ESR experiments. In Table VIII, $A_{iso} = b + c/3$

Table VIII

Hyperfine Structure and Spin-Doubling Constants of C_2H from Matrices and Interstellar Gas Measurements (in MHz).

	ESR in Matrix	Interstellar Gas[a]
b(^{1}H)	+41 ± 1	+40.24 ± 0.68
c(^{1}H)	+11 ± 2	+12.23 ± 0.43
γ	-20 ± 50	-62.57 ± 0.15

[a]Reference (13).

and $A_{dip} = c/3$. The agreement of the hyperfine constants from two quite different experimental techniques is excellent.

References - Chapter IV

1. T. Tsuji, Ann. Tokyo Astron. Obs., Ser. 2 9, 1 (1964).

2. S. Morris and A. A. Wyler, Astrophys. J. 150, 877 (1967).

3. E. L. Cochran, F. J. Adrian, and V. A. Bowers, J. Chem. Phys. 40, 213 (1964).

4. D. E. Milligan, M. E. Jacox, and Abouaf-Marguin, J. Chem. Phys. 46, 4562 (1967).

5. D. E. Milligan and M. E. Jacox, J. Chem. Phys. 51, 1952 (1969).

6. J. H. Carpenter, D. F. Rimmer, and D. H. Whiffen, J. Chem. Soc. Faraday Trans. II 68, 1914 (1972).

7. P. H. Kasai, J. Am. Chem. Soc. 94, 5950 (1972).

8. R. W. Fessenden and R. H. Shuler, J. Chem. Phys. 39, 2147 (1963).

9. H. M. McConnell, C. Heller, T. Cole, and R. W. Fessenden, J. Am. Chem. Soc. 82, 766 (1960).

10. J. Miyagawa and W. Gordy, J. Chem. Phys. 32, 255 (1960).

11. C. P. Poole and H. A. Farach, J. Mag. Res. 4, 312 (1971).

12. L. B. Knight, Jr., and W. Weltner, Jr., J. Chem. Phys. 53, 4111 (1970).

13. K. D. Tucker, M. L. Kutner, and P. Thaddeus, "The Ethynyl Radical, C_2H--A New Interstellar Molecule", privately communicated by Dr. P. Thaddeus.

14. G. Herzberg, Spectra of Diatomic Molecules, Princeton, New Jersey: Van Nostrand, 1950.

15. G. Herzberg, Electronic Spectra and Electronic Structure of Polyatomic Molecules, New York: Van Nostrand-Reinhold, 1966.

16. A. D. Walsh, J. Chem. Soc. 468, 2288 (1953).

17. J. A. Pople and D. L. Beveridge, Approximate Molecular Orbital Theory, New York: McGraw-Hill, 1970, p. 11.

18. T. Morikawa and O. Kikuchi, Bull. Chem. Soc. Japan 45, 3715 (1972).

19. D. L. Beveridge and J. W. McIver, Jr., J. Chem. Phys. 54, 4681 (1971).

20. P. B. Ayscough, Electron Spin Resonance in Chemistry, London: Methuen, 1967, p. 438.

21. W. C. Easley and W. Weltner, Jr., J. Chem. Phys. 52, 197 (1970).

CHAPTER V
$M^+C_2^-$ AND C_2^- RADICALS

Introduction

This work was begun as an attempt to observe the ESR spectrum of C_2^-, which was reported to have a $^2\Sigma$ ground state, thereby making it observable in ESR. The historical background leading to this research will first be presented in a very brief form and then the actual results obtained in this work.

The spectrum of C_2 has been the subject of intensive study. It was believed that the lower state ($^3\Pi_u$) of the Swan band transition, which appears between 6700 and 4300 Å in emission spectra, was the ground state of C_2. However, the gas phase analysis of Ballik and Ramsey (1) demonstrated that the $x^1\Sigma_g^+$ state of C_2 was approximately 600 cm^{-1} lower than the $X'^3\Pi_u$ state.

Several workers observed features attributed to the Swan system of C_2 in matrices at 4°K. This presented a problem in that at these low temperatures all molecules should be deactivated to their ground state, i.e. from what did this band system actually arise?

Later, Herzberg and Lagerqvist (2) provisionally identified a band system appearing at 5416 Å in a flash

discharge through gaseous methane as a $^2\Sigma_u^+ \leftarrow {}^2\Sigma_g^+$ transition of C_2^-. A progression at 5208 Å observed by Milligan, Jacox, and Abouaf-Marguin (3,4) in the spectrum of the photolysis products of acetylene isolated in argon at 4^oK was identified as the same spectrum. This was the spectrum that had previously been assigned to the Swan system of C_2 in the matrix. The vibrational frequency of the excited state in the matrix was found to be 1955 cm^{-1}. This corresponded to $\Delta G'_{1/2}$ = 1939 cm^{-1} for the gas phase as observed by Herzberg and Lagerqvist. This system was also observed by Frosch (5) by X irradiation of acetylene trapped in argon, krypton, and xenon matrices. This emission results indicated that the vibrational frequency of the ground state was 1771 cm^{-1} in matrices which corresponded to 1758 cm^{-1} in the gas phase observed by Herzberg and Lagerqvist. The assignments to C_2^- in both matrix studies are supported by the observation that the transitions are unaffected by deuteration. Bondybey and Nibler (6) have observed the fluorescence of the C_2^- system in argon and nitrogen matrices. The vibrational frequencies in argon agreed with those of Frosch and were extended to v" = 4. Emission from the v' = 1 level indicated that this level was populated by secondary excitation of a substantial v" = 1 population. The conclusion reached was that relaxation for C_2^- in argon is quite

slow in both ground and excited electronic states. Further proof established definitely the fact that the Herzberg-Lagerqvist band system belonged to C_2^- and that the ground state was $^2\Sigma_g^+$. Further proof was added by Lineberger and Patterson (7) in a two photon-photodetachment experiment.

With this background, it is evident that the ESR spectrum of C_2^- should consist of one absorption near g = 2.00. If ^{13}C were substituted then this line would be split in a triplet due to the hyperfine interaction with the two equivalent ^{13}C nuclei. The intensity ratio for $^{13}C_2^-$ would appear as 1:2:1.

It is possible, if there are low lying $^2\Pi$ states, that $g_\perp$ can be shifted away from the free-electron value. This occurs by coupling of some orbital angular momentum into the ground state, i.e. spin-orbit coupling. To the first order, $\Delta g_\perp = g_\perp - g_e = -2\lambda \sum'_k \langle o|L_i|k\rangle\langle k|L_i|o\rangle / E_k$ where λ is the spin-orbit coupling constant, L_i are the components of the angular momentum L, E_k is the energy separation of the o and k states, and the prime means that the ground state is omitted from the summation. However, the lowest excited state of C_2^- is expected to be $^2\Pi_u$ which cannot mix with the ground state since $\underline{L}$ does not couple g and u states. The ESR spectra of CN (8) and C_2H (9), $^2\Sigma$ molecules isoelectronic with C_2^-, yield

$g_\perp$ values of 2.0003 and 2.0025 respectively. The $^2\Pi_i$ excited state of CN (corresponding to the unobserved $^2\Pi_u$ of C_2^-) lies only 9200 cm^{-1} above the $X^2\Sigma$ state, yet its contribution is so small that the much higher-lying $^2\Pi_r$ state determines the sign of $\Delta g_\perp$. Since the next higher excited $^2\Pi$ state of C_2^- is expected to lie above the $^2\Sigma_g^+$ state at 20,000 cm^{-1}, one can predict with a high degree of confidence that the ESR spectrum of "free" C_2^- should consist of one line at $g_\perp \simeq g_{||} \simeq g_e$.

In the matrix a counter-cation for C_2^- must exist although such an ion has not been identified when C_2^- is prepared by the photolysis of acetylene in the absence of alkali atoms. Thus C_2^- is not strictly a "free" radical as in the cases of matrix-isolated CN and C_2H, i.e. there will always be a perturbing positive ion in the vicinity of C_2^-. Although the ESR and optical spectra of ion pairs involving the alkali metal ions are observed, it was found that an ESR spectrum could not be observed when C_2^- was prepared without the addition of the metal atoms.

Experimental

Acetylene (99.5% pure) was obtained from Airco and 90% ^{13}C-enriched acetylene was obtained from Merck, Sharpe and Dohme of Canada, Ltd. Both were used without further

purification. These gases were mixed with argon prior to deposition in mole ratios (argon:acetylene) between 20 and 1000.

High purity alkali metals (~99.9%) were obtained from various commercial sources (sodium from J. T. Baker Chemical Co., lithium from Matheson, Coleman and Bell, and potassium from Mallinckrodt). Cesium chromate (Cs_2CrO_4) was obtained from Matheson, Coleman and Bell and silicon was obtained from Alfa Inorganics.

In experiments in which C_2^- was to be investigated, the acetylene in argon gas mixture was photolyzed during deposition with a H_2/He discharge lamp through a LiF optical window. Deposits lasted from one to two hours with the flow rate varying from 0.2 to 0.06 l atm/h with the best production of C_2^- resulting from the slowest rate.

In experiments in which the $M^+C_2^-$ ion pairs were to be investigated, the alkali metals were codeposited with the acetylene in argon gas mixtures and then photolyzed *in situ* from one to one and a half hours. Deposits lasted approximately one hour with a gas flow rate of about 0.2 l atm/h. The alkali metals (Na, K, Li) were heated in tantalum cells to temperatures suitable to produce a vapor pressure of approximately 0.001 torr in the furnace section. For sodium, this temperature

is about 510°K, for potassium 434°K and for lithium 740°K (10). An atomic beam of cesium is produced using the technique of Scheer and Fine (11) involving the reduction of Cs_2CrO_4 by silicon at a temperature of 650 to 600°C. All the alkali metals effuse from a pinhole leak in the resistively heated tantalum cells.

It should be mentioned that experiments in which acetylene in argon was deposited and photolyzed in situ no C_2^- signals were observed. Only when the alkali metal was codeposited could the C_2^- signals be produced, i.e. the metal functioned as an electron donor.

Optical Spectra

The optical spectrum of C_2^- was used primarily as a test of the efficiency of the production of C_2^- for ESR studies. As reported by Milligan and Jacox (4), the intensity of C_2^- was enhanced considerably when alkali metals were codeposited and used as a photoelectron source. No new absorptions due to species produced by the reaction of alkali metals with the sample was detected when the alkali metal concentration was kept at approximately 0.5 to 1% of the total matrix. However, if the metal vapor pressure was increased such that the final metal concentration was approximately 5 to 10% of the matrix then a second series of bands was observed for all alkali metals deposited. Figure 19 shows the observed spectra when the second series of bands was produced. Other bands

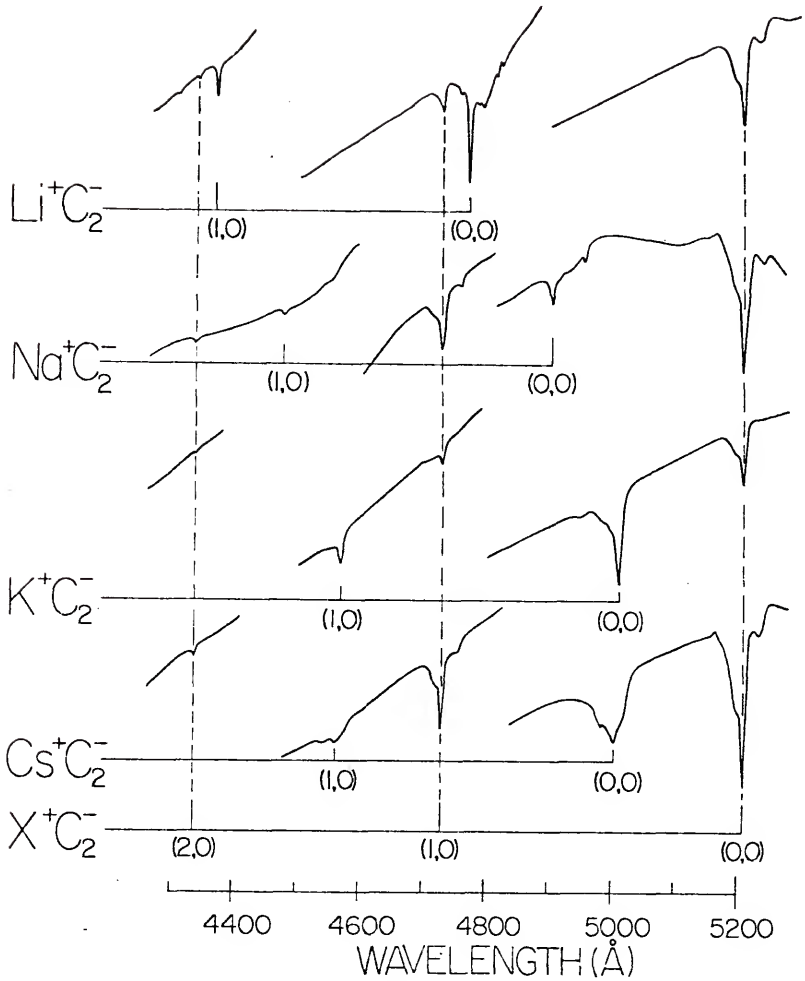

Figure 19: Optical spectra of $M^+C_2^-$ (M = Li, Na, K and Cs) isolated in argon matrices at 4°K. The C_2^- bands (designated as $X^+C_2^-$) of MJA (3,4) in each spectrum are indicated by the vertical dashed lines.

that were observed but not shown were attributed to the alkali metal atomic resonance transitions and also weaker bands due to their dimers. Due to these species the resulting matrices were colored, but both the color and the atomic resonance lines disappeared upon photolysis. It was also observed that when the light from a tungsten filament lamp was focused on the matrices for optical studies, the color was bleached. However, bleaching of the matrix had no effect on the progressions shown in Figure 19.

As can be readily seen in Figure 19 the new progressions observed for higher concentrations of alkali metals are shifted to the blue in comparison with C_2^-. This shift to higher energy is largest for Li, decreases for Na and is least for K with a slight increase for Cs. The vibrational spacing in the excited state ($\Delta G_{1/2}'$) also varies depending upon the alkali metal used. $\Delta G_{1/2}'$ is approximately 1930 cm^{-1} for the alkali metal with C_2^- ($M^+C_2^-$) spectra whereas for C_2^- without the alkali, $\Delta G_{1/2}'$ is 1949 cm^{-1}. For $^{13}C_2^-$, the corresponding figures are 1850 cm^{-1} and 1862 cm^{-1}. Tables IX and X list the wavelength of transitions and $\Delta G'$ for all the species studied. The C≡C stretching frequency for the $M^+C_2^-$ clearly exhibits a trend with $\Delta G_{1/2}'$ increasing from Li to Na to K and then decreasing to Cs. This trend is observed for both $^{12}C_2^-$ and $^{13}C_2^-$ however there is

Table IX

Transitions observed for $X^+C_2^-$[a] and the ion pairs $M^+C_2^-$ (M = Li, Na, K, Cs) trapped in Ar at ~4°K.

Molecule	(v',v")	λ(Å)	ν(cm^{-1})	ΔG'(cm^{-1})
$X^+C_2^-$	(0,0)	5208	19196	1949
	(1,0)	4728	21145	
	(2,0)	4335	23062	1917
$Li^+C_2^-$	(0,0)	4771	20954	
	(1,0)	4368	22887	1933
$Na^+C_2^-$	(0,0)(I)[b]	4956	20172	
	(0,0)(II)	4905	20382	
	(1,0)	4479	22320	1938
$K^+C_2^-$	(0,0)	5011	19949	
	(1,0)	4569	21879	1930
$Cs^+C_2^-$	(0,0)	5002	19986	
	(1,0)	4562	21912	1926

[a] Designation of ion pair produced by photolysis of C_2H_2 in the absence of metal atoms.

[b] Evidence of multiple trapping sites appears in the spectra. Although normally one site predominates, two appear for $Na^+C_2^-$, of which (II) predominates for $Na^+{}^{12}C_2^-$, and (I) for $Na^+{}^{13}C_2^-$.

Table X

Transitions observed for $X^{+}{}^{13}C_2^{-}$[a] and ion pairs $M^{+}{}^{13}C_2^{-}$ (M = Li, Na, K, Cs) trapped in Ar at ~4°K.

Molecule	(v',v")	λ(Å)	ν(cm^{-1})	ΔG'(cm^{-1})
$X^{+}{}^{13}C_2^{-}$	(0,0)	5210	19189	1862
	(1,0)	4749	21051	
$Li^{+}{}^{13}C_2^{-}$	(0,0)	4773	20948	1851
	(1,0)	4385	22799	
$Na^{+}{}^{13}C_2^{-}$	(0,0)(I)[a]	4956	20170	1858
	(1,0)	4539	22028	
	(0,0)(II)	4905	20382	
$K^{+}{}^{13}C_2^{-}$	(0,0)	5012	19949	1851
	(1,0)	4586	21799	
$Cs^{+}{}^{13}C_2^{-}$	(0,0)	5004	19978	1852
	(1,0)	4580	21830	

[a]See footnote Table IX.

more uncertainty in the ^{13}C data (wavelength measured within ~1 Å) than in the ^{12}C data (wavelength measured within 0.5 Å).

An extensive search was made in the infrared region for the C≡C stretching frequency and the possible M-C vibrational frequency for the ground state $M^+C_2^-$. The C≡C stretching frequency would be expected to be in the 1800 to 1750 cm^{-1} region since the ground state for C_2^- has $\Delta G_{1/2}$" of 1771 cm^{-1} in Ar at 4°K. Apparently any infrared transitions are too weak and no absorptions were observed which could be attributed to the $M^+C_2^-$ species.

Optical Analysis

These new optical transitions observed for the increased alkali metal concentrations, compared to the known C_2^- spectrum, clearly indicate the formation of ion pairs between the alkali metal ions and the C_2^- ion ($M^+C_2^-$) in which the stretching frequency due to the C≡C stretch exhibits a small dependence on the alkali metal cation. In a Raman and infared study reported by Andrews and Smardzewski (12), a similar dependence has been observed for the $M^+(O_2^-)$ ion pair. The trend in $M^+O_2^-$ could not be explained by mass dependence on the alkali metal cations or by an interaction with the $M^+ \leftrightarrow O_2^-$ stretching frequency. The O=O stretching frequency was found to be dependent on the polarizability

of both cation and anion with O_2^- being treated as a monatomic anion based on the method of Rittner (13) for determining dipole moments of alkali halide molecules. These polarizabilities govern the induced dipoles on both the M^+ and O_2^- and thereby the dipole moment of the species. The dipole moment was regarded as a measure of the charge transfer between the ions and the removal of electron density from the highest lying antibonding σ_u orbital of O_2^-. The removal of electron density from an antibonding orbital strengthened the 0=0 bond therefore increasing the vibrational frequency. It was also possible to account quantitatively for the variation in the C≡C stretching frequency by a similar argument.

The electronic transition being observed for C_2^- is $\sigma_u\pi_u^4\sigma_g^2, B^2\Sigma_u \leftarrow \sigma_u^2\pi_u^4\sigma_g, X^2\Sigma_g^+$. The highest filled molecular orbital of the excited state is a bonding orbital. For the $M^+C_2^-$ ion pair the unpaired electron is not completely transferred from the alkali metal but instead, some small amount of the electron density is retained in the s-orbital of the alkali metals. The C≡C stretching frequency in the $M^+C_2^-$ ion pair should show a dependence on the completeness of charge transfer from the alkali metal since the additional electron is in a bonding orbital. As the effective electron density is removed from this bonding orbital in the C_2^- ion,

the bond will be weakened and the force constant will decrease evidenced by a decrease in the vibrational stretching frequency.

The Rittner ionic model for polarizable ion pairs was used to get approximate values for the dipole moments of the $M^+C_2^-$ species. The dipole moment was then compared with the ion dipole in each case to indicate the approximate fractional ionic character (ionicity).

To calculate the dipole moment, it is assumed that the C_2^- ion can be treated as a monatomic anion. The dipole moment is then given by the equation

$$\mu = exr - \frac{\alpha_c e}{r^2} - \frac{\alpha_a e}{r^2} \qquad (88)$$

where α_c and α_a ($\alpha_\perp$ for C_2^-) are polarizabilities of the cation and anion, e is the charge and r is the interionic distance from M^+ along the perpendicular bisector to the C-C internuclear axis. The ionicity is the calculated dipole moment divided by the ion dipole (μ/exr).

Polarizabilities of the alkali metal ions were taken from Rittner (13). Two assumptions were made to calculate α_a($\alpha_\perp$ for C_2^-). It was assumed that

$$1 \qquad \frac{\alpha(C_2^-)}{\alpha(O_2^-)} = \frac{\alpha(C\equiv C)}{\alpha(O_2)} \qquad (89a)$$

and

$$2 \qquad \frac{\alpha_{\perp}(C_2^-)}{\alpha(C_2^-)} = \frac{\alpha_{\perp}(C{\equiv}C)}{\alpha(C{\equiv}C)} . \qquad (89b)$$

A value of $\alpha_a = 2.10$ Å was obtained from these calculations (14).

A crude estimation of the radii for the $M^+C_2^-$ ion pairs was made by assuming r to be the sum of the radius of the metal ion (r_{M^+}) and the perpendicular radius of the C_2^- ion ($r_{C_2^-}$). Various values of r_{M^+} and $r_{C_2^-}$ were tested with r varying over a wide and reasonable range for each ion pair. Table XI lists one such calculation in which r_{M^+} was taken from Rittner (13) and $r_{C_2^-}$ is based on a calculation from the CaC_2 crystal structure (15).

Because of the various assumptions used in these calculations, the results cannot be taken quantitatively but the trend is of importance. All the calculations indicate that the ionic character should increase from Li to Na or K then decrease from K to Cs. As the ionic character increases, the vibrational spacings ($\Delta G_{1/2}'$) should approach more closely that of C_2^-. Table XII lists the calculated ionicities as well as the $\Delta G_{1/2}'$ for C_2^- and the $M^+C_2^-$ species. From a comparison of these values it is apparent that the vibrational frequency follows the general predicted trend for the $M^+C_2^-$ ion pairs.

Table XI

Dipole moment calculations for $M^+C_2^-$

Ion Pair	α_a (Å^3)	r(A)	exr	$(\alpha_a+\alpha_c)e/r^2$	$\mu_{calc.}$	μ_{calc}/exr (ionicity)
$Li^+C_2^-$	0.0298	2.13	10.2	2.24	7.9	0.77
$Na^+C_2^-$	0.185	2.64	12.7	1.57	11.1	0.874
$K^+C_2^-$	0.831	2.92	14.0	1.65	12.3	0.879
$Cs^+C_2^-$	2.460	3.18	15.3	2.16	13.1	0.856

Table XII

Calculated ionicities and $\Delta G_{1/2}'$ for C_2^- and $M^+C_2^-$.

Species	$\Delta G_{1/2}'(cm^{-1})$ $^{12}C/^{13}C$	Calculated Ionicities
C_2^-	1949/1862	1.000
$Li^+C_2^-$	1933/1851	0.77
$Na^+C_2^-$	1938/1858	0.874
$K^+C_2^-$	1930/1851	0.879
$Cs^+C_2^-$	1926/1852	0.856

ESR Spectra and Analysis

$X^+C_2^-$

As mentioned previously, optimum conditions for the intensity of the optical transition for C_2^- were found to occur for slow depositions. The intensity could be improved by the addition of a low concentration of Cs atoms (~0.5%) as reported by Milligan, Jacox, and Abouaf-Marguin (3,4). In no sample was an ESR absorption due to C_2^- found even for optical absorption at 5208 Å of 80%. The possibility that the C_2^- signal might be obscured by the C_2H doublet or CH_3 quartet was dismissed because of the lack of any distortion in the line shapes of these species and because of the absence of any additional hyperfine lines when ^{13}C was substituted in the parent acetylene molecule. It was thought at one time that possibly C_2H was causing the absorption at 5208 Å, however this is not the case as proven by the absence of the 5208 Å absorption when strong C_2H ESR signals are produced in photolyzed samples of C_2HI in argon (9).

$M^+C_2^-$

The ESR spectra obtained when the alkali metals (Li, Na, K) were codeposited in such a manner as to form the ion pairs $M^+C_2^-$ are shown in Figure 20. Each spectrum consists of three groups of four lines with overlap occurring with the C_2H doublet at g = 2.0025 (9) and the

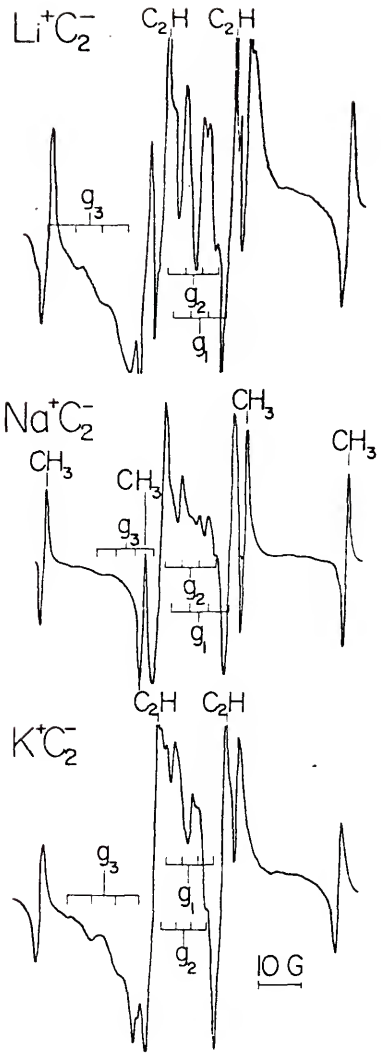

Figure 20: ESR spectra of $M^+C_2^-$ (M = Li, Na, K) isolated in argon matrices at 4°K. The symbols g_1, g_2, and g_3 denote the three principal components of the g tensor. Quartet structure is due to the hfs on the metallic cation (I = 3/2). Also shown are the C_2H doublet and CH_3 quartet appearing in the same region.

two inner members of the CH_3 quartet (16). $M^+C_2^-$ ion pairs possess orthorhombic symmetry rather than axial symmetry as in C_2^-. Thus we see three groups of lines for g_1, g_2, and g_3 rather than two groups for $g_\perp$ and $g_{||}$. The g tensor is only slightly anisotropic since the two components, g_1 and g_2, which would correspond to $g_\perp$ for axial symmetry, are approximately equal. Because of the hyperfine interaction of the unpaired electron with the nuclear spin of the alkali metal cations, each group of lines has a quartet structure (I = 3/2 for Li, Na, and K). Similar spectra have been observed for $M^+O_2^-$ showing hfs due to the M^+ ions, although in that case there was no complication of analysis from overlapping impurity lines (17,18). The ESR spectrum for $Cs^+C_2^-$ was also observed but because of overlap of the extensive hfs of Cs^+ (I = 7/2) no analysis was carried out.

All of the g and A tensors derived from these spectra are listed in Table XIII. In order to confirm the g and hfs assignments, a spectrum for $Na^+C_2^-$ was simulated by computer for randomly oriented molecules with orthorhombic symmetry possessing the assigned values. The programs used in this calculation are modified versions of MAGNSPEC and SPREAD, programmed by M. Kopp and supplied by the Quantum Chemistry Program Exchange. Figure 21 shows a comparison between the observed ESR spectrum of $Na^+C_2^-$ (a) and the computer simulated spectrum (b) based on the magnetic parameters shown in Table XIII. In the

Table XIII

Components of the g and cation A tensors[a] for the $M^+C_2^-$ species. Cavity frequencies are ν = 9366, 9375, and 9378 MHz for the Li^+, Na^+, and K^+ experiments, respectively.

Alkali cation	g_1	g_2	g_3	$\|A_1\|$	$\|A_2\|$ (Gauss)	$\|A_3\|$
Li^+	2.0021(6)	2.0030(6)	2.0135(40)	4.5(2)	4.4(2)	7.2(5)
Na^+	2.0015(6)	2.0036(6)	2.0124(30)	4.3(2)	3.9(2)	4.4(2)
K^+	2.0025(6)	2.0037(6)	2.0147(30)	3.9(2)	3.9(2)	5.5(2)

[a]Axes 1, 2, and 3 refer to the x-, y-, and z-axes in Figure 22.

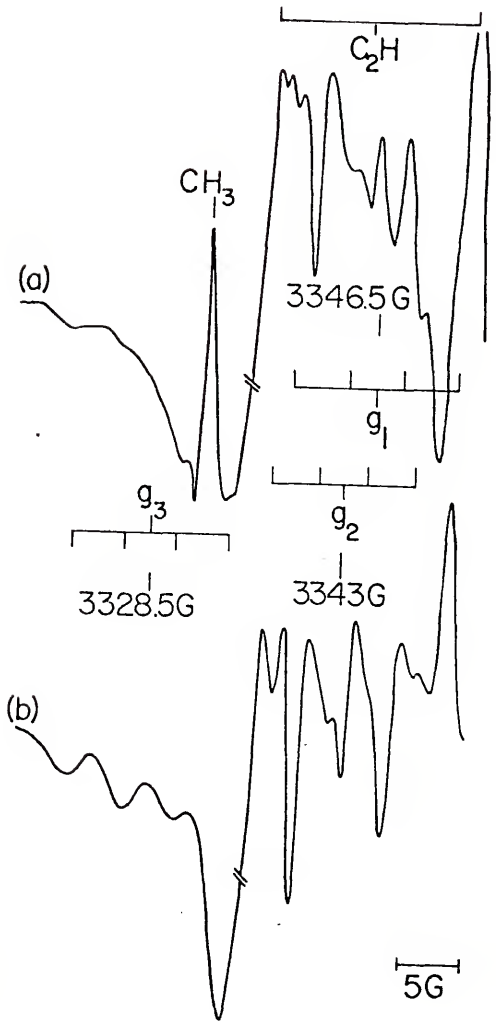

Figure 21: A comparison between (a) the observed ESR spectrum and (b) the powder pattern spectrum calculated from an exact solution of the spin Hamiltonian using the observed magnetic parameters for $Na^{+}C_2^{-}$. g_3 tensor components are smeared out by overlap with strong lines of C_2H and CH_3.

observed spectrum there is overlap, with the ESR signals of C_2H and CH_3 which tends to distort and smear the $Na^+C_2^-$ signals. However, the spectra are in very good agreement. The overlap with the CH_3 signal is particularly bothersome for the g_3 quarter; however, shifts in g_3 beyond the given parameter significantly alter the shape of the theoretical powder pattern. Computer simulations were not performed for the other $M^+C_2^-$ species.

It will be shown later in the discussion of the g tensor that axis 3 is along the C-C internuclear axis, axis 2 is perpendicular to the $M^+C_2^-$ plane, and axis 1 is co-linear with the bisector of the C-C internuclear axis. It was determined that the components of the hfs for the metal cation are those along the principal axes of the g tensor which are not necessarily the principal axes of the cation A tensors. This may be clarified by determining whether or not the two carbon nuclei are equivalent or not. If the nuclei are equivalent, then the basic symmetry of the ion pair can be determined. This can be determined by the results obtained when ^{13}C is substituted in the parent C_2H_2 molecule.

If ^{13}C were substituted and the carbon nuclei were equivalent it would be expected that each group of lines (corresponding to each of the three g tensors) would be split into a triplet pattern. The intensity ratio would be 1:2:1. The center of the spectrum (at $g \simeq 2.0$) should remain unchanged from the ^{12}C case, but the other

two components of the ^{13}C hfs would appear at higher and lower fields. INDO calculations performed for C_2^- yield spin densities which should not be far removed from the hfs expected for $M^+C_2^-$. From these calculations it is predicted for C_2^- that $A_\perp\ ^{13}(C) \simeq 89$ G and $A_{||}\ ^{13}(C) \simeq$ 124 G. As stated previously, $A_\perp$ would correspond to A_1 and A_2 for $M^+C_2^-$ and $A_{||}$ would correspond to A_3.

If ^{13}C were substituted and the carbon nuclei were not equivalent, the center region of the spectrum would be changed appreciably. Each group of lines would be split into two separate sets of doublets with an intensity ratio of 1:1.

Experimentally, it was found that the center region of the spectrum for ^{13}C substitution was essentially unaltered. However, due to the reduced intensity and the smearing of the high and low field components, individual members of the quartets corresponding to A_1 and A_2 could not be resolved. From the overall shape of the spectrum however, a value of $A_1 \simeq A_2 \simeq 83(8)$ G was obtained. The weaker A_3 component is overlapped by $^{13}C_2H$ lines. The overall pattern indicates that the C nuclei are equivalent which implies a triangular conformation for $M^+C_2^-$. Then the ion pair has C_{2v} symmetry. In view of this geometry, it is clear that the g tensor and A tensors for the metal cations are coaxial.

Discussion

g Tensor

In the case of "free" C_2^-, it is expected that there will be little mixing of orbital angular momentum into the $(\sigma_u)^2(\pi_u)^4(\sigma_g)$, $^2\Sigma_g^+$ ground state. The lowest excited states are $(\sigma_u)^2(\pi_u)^3(\sigma_g)^2$, $^2\Pi_u$ and $(\sigma_u)(\pi_u)^4(\sigma_g)^2$, $^2\Sigma_u^+$. As stated in the introduction, g shifts depend on mixing of excited states with the ground state and can be expressed in terms of the components of the angular momentum operator $\underline{L}$. Since $\underline{L}$ does not couple g and u states, there will be no mixing from these excited states with the ground state. Consequently, g values for C_2^- would be expected to be essentially unshifted from the free-electron value of $g_e = 2.0023$. However, this is not the case for the ion-pair complexes $M^+C_2^-$ with C_{2v} symmetry.

In the presence of the metal cation the molecular orbitals containing the carbon p-orbitals become

Linear C_2^-	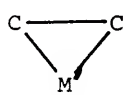
σ_g	a_1
π_u	b_1, a_1
σ_u	b_2

The geometry of the complex and a general molecular orbital scheme are given in Figure 22. The coordinate system at each nuclei is taken with +x, +y and +z in the

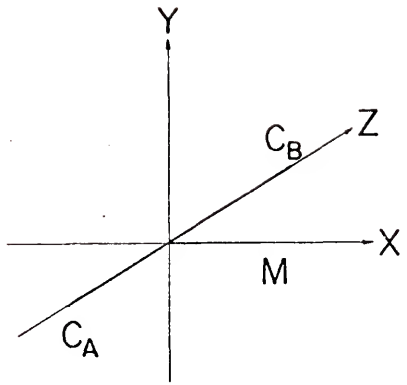

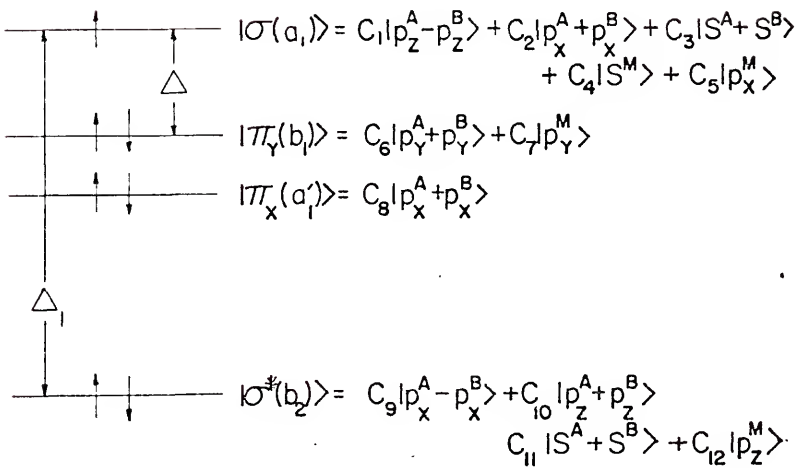

Figure 22: The geometry and molecular orbital scheme for $M^+C_2^-$.

same direction. The bonding is predominantly ionic with the small overlap between the ions causing the hfs on the metal. Then in the ground state, where the odd electron is in the a_1-orbital, contributions from other than $C_1|p_z^A - p_z^B>$ should be small. In an ionic model it is expected that as a result of distortion of the anion by the M^+ cation, the π_u orbitals of C_2^- will be split into an in-plane component $\pi_x(a_1')$ and an out-of-plane component $\pi_y(b_1)$. The cation interacts more strongly with the in-plane orbital which is largely $C_8|p_x^A + p_x^B>$ causing it to lie lower in energy than the out-of-plane orbital which is principally $C_6|p_y^A + p_y^B>$. The carbon p-orbitals in the molecular orbitals are also mixed with the symmetry-allowed combinations of alkali metal s- and p-orbitals, but this contribution is small.

The ground state for $M^+C_2^-$ ion-pair is then $(b_2)^2(a_1')^2(b_1)^2(a_1)$, $^2A_1$. The lowest excited state contributing largely to the g-tensor shift by spin-orbit coupling is then $(b_2)^2(a_1')^2(b_1)(a_1)^2$, $^2B_1$. An additional, but small, contribution arises from the much higher lying $(b_2)(a_1')^2(b_1)^2(a_1)^2$, $^2B_2$ state. The excited $(b_2)^2(a_1')(b_1)^2(a_1)^2$, $^2A'_1$ state will have no effect on g. These statements can be verified by calculating the terms Δg_{ij} for all of these states with the ground state.

For the energy levels corresponding to the above scheme, the g tensor shifts have been calculated to the second order from the relations given by Tippins (19).

The shifts from the free-electron value $\Delta g_{ij} = g_{ij} - g_e$ are then found to be:

$$\Delta g_{xx} = -4\frac{\lambda^2}{\Delta^2}C_2^2C_6^2 \tag{90a}$$

$$\Delta g_{yy} = 8\frac{\lambda}{\Delta_1}(C_1C_9 - C_2C_{10})^2 - 4\frac{\lambda^2}{\Delta^2}C_2^2C_6^2 \tag{90b}$$

$$\Delta g_{zz} = 8\frac{\lambda}{\Delta}C_2^2C_6^2 \tag{90c}$$

when it is assumed the spin-orbit coupling constant $\lambda << \Delta << \Delta_1$ and terms contributing less than a few percent to Δg_{ij} have been omitted. The largest shift is Δg_{zz} which is positive, and thus corresponds to the g_3 component of the observed g tensor. A small negative shift occurs for g_{xx} as a result of a second order contribution. This corresponds to the g_1 component for the observed g tensor. Coupling with the $^2B_2$ state causes a small, but positive, shift for g_{yy}. The situation with respect to Δg_{xx} and Δg_{yy} is at least qualitatively in agreement with the observations, which show, to within experimental error, $\Delta g_1 \simeq 0$ for K^+ and Li^+, and a very small negative shift for Na^+; while, on the other hand, Δg_2 exhibits a small, but consistently positive shift.

Substituting the measured $\Delta g_{zz} \simeq 0.011$, $\lambda_c = 26\ cm^{-1}$, and $C_6^2 = 0.5$ in the equation for Δg_{zz} gives a relationship between Δ, the excitation energy of the $^2B_1$ state and the coefficient C_2, when it is expected that $C_2 < C_1$. Results obtained for reasonable values of C_2 imply that the $^2B_1$ state is very low-lying, probably less than

than 4000 cm^{-1} above the ground state. (For example, $C_2^2 \simeq 0.21$ for $\Delta = 2000\ cm^{-1}$). The gas phase observations have indicated that the $^2\Pi_u$ state for C_2^- lies below 10,000 cm^{-1}. Using these values in the equation for Δg_{xx}, a rough estimate for $\Delta g_{xx} \simeq -0.0001$ is obtained, which is in agreement with g_1 values that show only slight negative shifts. Assuming $(C_1C_9 - C_2C_{10})^2 \simeq 0.1$ and the excitation energy of the $^2B_2$ state $\Delta_1 \simeq 20{,}000\ cm^{-1}$ (from the optical spectra described earlier), then the equation of Δg_{yy} yields a value of $\simeq +0.001$. The experimental values found for Δg_{yy} range from 0.0007 to 0.0014 which compares favorably with this predicted value.

There is a less likely possibility that, if the distortion by the metal ion were particularly severe, the σ_g level in C_2^- could be effectively lowered to such an extent that the a_1-orbital was below the b_1-orbital, or even approaching the a_1' orbital. Then the odd electron would reside in the b_1-orbital resulting in a $^2B_1$ ground state for the ion-pair. A similar construction of molecular orbitals indicates that such a scheme would also yield Δg_{ij}'s in reasonably good agreement with observations. However, the close similarity between the $^2\Sigma_u^+ \leftarrow {}^2\Sigma_g^+$ transition of gas phase C_2^- and the $M^+C_2^-$ spectra indicates that the effect of the metal ion on the electronic states is small and a $^2B_1$ ground state (corresponding to $^2\Pi_u$ for C_2^-) is considered unlikely.

Expressions for the effect of the metal orbitals on the g tensor components can also be derived. They are generally of the same form as those in the previous equations for $\Delta g_{xx,yy \ \& \ zz}$ but they involve the metal spin-orbit parameter, λ_M, and the coefficients C_5, C_7 and C_{12} in Figure 22. λ_M for the alkali atoms is not large and in view of the small cation hfs observed and the lack of correlation of the g shifts with λ_M, the effect of the metal cations on the value of Δg was considered negligible.

The important low-lying $^2B_1$ state, estimated from the g tensor data to be below 4000 cm^{-1}, has not been observed optically although a search of this region was carried out. It is expected, in analogy with the isoelectronic CN molecule, that the $^2\Sigma_u \leftarrow X^2\Sigma_g^+$ transition for C_2^- will be much weaker than the $^2\Sigma_u^+ \leftarrow {}^2\Sigma_g^+$ transition (2), and this is supported by recent approximate theoretical calculations (20). Thus the corresponding $^2B_1 \leftarrow X^2A_1$ transition of $M^+C_2^-$ is also expected to be much weaker than the $^2B_2 \leftarrow X^2A_1$ transition near 5000 Å, so that it is unfortunate but not unexpected that it could not be found in the matrix spectra.

A Tensors

The A tensor for ^{13}C is only approximately determined as $A_1 \simeq A_2 \simeq 83(8)$ G because hf lines are overlapped as well as decreased in intensity. The weaker A_3 component is completely obscured by $^{13}C_2H$ lines also. INDO

calculations showing $A_{\perp} \simeq 89$ G and $A_{||} \simeq 124$ G are at least in reasonable agreement.

The alkali metal cation A tensors are determined as shown in Table XIV. Since these small values are typical of hfs from ion pairs it is assumed that, as in other cases, they arise largely from spin polarization of the metal ion and are negative in sign. Then the isotropic constant (A_{iso}) and the dipolar components (T_i) of the hfs are derived and shown in Table XIV. The trend in the A_{iso} values indicates that the effect is least for Na^+ (A_{iso} for Na atom is 886 MHz, 231 MHz for K atom, and 109 MHz for the Li atom).

Absence of the ESR Spectrum of $X^+C_2^-$

Although it was originally thought that the gas phase work (2,7) might not have provided proof of a $^2\Sigma_g^+$ ground state for C_2^-, that state now seems quite certain from the emission work (5,6) and from recent theoretical calculations (21,22). Thus the absence of an ESR spectrum for the presumably least-perturbed C_2^- ion in an argon matrix exhibiting strong optical bands is perplexing.

If the matrix or ionic perturbations have effectively inverted the lower two electronic states and C_2^- (as $X^+C_2^-$) is in a $^2\Pi$ ground state, then its g values would lie near $g_{\perp} = 4$ and $g_{||} = 0$. Thus its ESR spectrum

Table XIV

The isotropic constants and dipolar tensor[a] components (in MHz) derived from the alkali cation hfs.

Alkali cation	A_{iso}	T_1	T_2	T_3
Li^+	-15.1	2.5	2.8	-5.2
Na^+	-11.8	-0.2	0.9	-0.6
K^+	-12.4	1.5	1.5	-3.1

[a]Axes 1, 2, and 3 refer to the x-, y-, and z-axis in Figure 22.

would be smeared out and unobservable. This might be imagined to occur by formation of a linear unsymmetrical ion pair $X^+C\text{-}C^-$, for example. The formation of triangular ion pairs with the alkali-metal atoms could then be considered to "quench" the $^2\Pi$ state (as occurs for the $^2\Pi_u$ state of O_2^-) (17,18). This could lead to the appearance of an ESR spectrum near g = 2. The magnitudes of the g shifts observed for $M^+C_2^-$ pairs are not in contradiction to such a proposal. This would mean that the optical spectrum for $X^+C_2^-$ would then be assigned to the forbidden $^2\Sigma_u^+ \leftarrow {}^2\Pi_u$ transition of C_2^- where the $u \not\leftarrow\!\!\rightarrow u$ selection rule has been negated by the formation of the unsymmetrical ion pair. The emission work of Frosch (5) and Bondybey and Nibler (6) does appear to exclude such a proposal unless reasons can be given to explain (1) why this presumed $^2\Pi$ state has approximately the same vibrational frequency (1771 cm^{-1} in argon) as the $^2\Sigma_g^+$ state in the gas (1758 cm^{-1}), and (2) the non-observance of emission to the lower $^2\Sigma$ state in the matrix (corresponding to the $^2\Sigma_g^+$ state in the gas). Although (1) can be rationalized, (2) cannot be. The emission spectra show only one electronic transition, but if the above were the case, they would necessarily show two transitions. Thus this emission spectra corresponding to the $^2\Sigma_u^+ \rightarrow {}^2\Sigma_g^+$ in the gas phase, indicates that the X^+ cation is not interacting strongly enough with C_2^-

to effectively remove the u ↔ g selection rule and this transition cannot be a $^2\Sigma \rightarrow {}^2\Pi$.

Another reason for not observing $X^+C_2^-$ could be a long spin-lattice relaxation time. In the case of the alkali metal ion pairs, it was observed that the spectra were broadened unless low power was used, necessitating the use of high gain. For this reason, in searching for $X^+C_2^-$, the microwave power was varied over a wide range and reduced to its lower limit. In order to reduce the spin-lattice relaxation time, spectra were also recorded with the argon matrix at 15, 20, and 30°K. None of these attempts proved successful.

Still another possible explanation may lie in an electron transfer process between C_2^- and a counterion or neutral species, which could result in substantial broadening of the spectrum. C_2^- isolated in the matrix differs from gas-phase C_2^- in that it is trapped in close proximity to its C_2H_2 parent, secondary species, and its own counterion. Fast electron transfer between neutral hydrocarbons and their radical anions in solution is well known (23). Since a strong (0,0) band of the Mulliken system indicates an abundance of C_2 in the C_2H_2 in argon matrix, an electron transfer process between C_2^- and C_2 may be possible. Similar transfers between the unidentified counterion and C_2^- is also feasible although candidates such as C_2^+, $C_2H_2^+$, and C_2H^+ appear to be

excluded because of their high ionization potentials (11.97, 12.45, and 11.40 eV, respectively) (24).

References - Chapter V

1. E. A. Ballik and D. A. Ramsey, Astrophys. J. 137, 61 (1963).

2. G. Herzberg and A. Lagerqvist, Can. J. Phys. 46, 2363 (1968).

3. D. E. Milligan and M. E. Jacox, and L. Abouaf-Marguin, J. Chem. Phys. 46, 4562 (1967).

4. D. E. Milligan and M. E. Jacox, J. Chem. Phys. 51, 1952 (1969).

5. R. P. Frosch, J. Chem. Phys. 54, 2660 (1971).

6. V. Bondybey and J. W. Nibler, J. Chem. Phys. 56, 4719 (1972).

7. W. C. Lineberger and T. A. Patterson, Chem. Phys Lett. 13, 40 (1972).

8. W. C. Easley and W. Weltner, Jr., J. Chem. Phys. 52, 197 (1970).

9. W. R. M. Graham, K. I. Dismuke and W. Weltner, Jr., J. Chem. Phys. 60, 3817 (1974).

10. R. E. Honig, RCA Review 23, 567 (1962).

11. M. D. Scheer and J. Fine, J. Chem. Phys. 37, 107 (1962).

12. L. Andrews and R. R. Smardzewski, J. Chem. Phys. 58, 2258 (1973).

13. E. S. Rittner, J. Chem. Phys. 10, 1030 (1951).

14. Values of $\alpha(C\equiv C)$ and $\alpha_{\perp}(C\equiv C)$ were obtained from E. R. Lippincott and J. M. Stutman, J. Phys. Chem. 68, 2926 (1964). Values of $\alpha(O_2^-)$ and $\alpha(O_2)$ were obtained from Andrews and Smardzewski (12).

15. M. Atoji, J. Chem. Phys. 35, 1950 (1961).

16. R. W. Fessenden and R. H. Shuler, J. Chem. Phys. 39, 2147 (1963).

17. F. J. Adrian, E. L. Cochran, and V. A. Bowers, J. Chem. Phys. 59, 56 (1973).

18. D. M. Lindsay, D. R. Herschbach, and A. L. Kwiram, Chem. Phys. Lett. 25, 175 (1974).

19. H. H. Tippins, Phys. Rev. 160, 343 (1967).

20. H. E. Popkie and W. H. Henneker, J. Chem. Phys. 55, 617 (1971).

21. J. Barshun, J. Phys. B 7, 155 (1974).

22. P. W. Thulstrup and E. W. Thulstrup, Chem. Phys. Lett. 26, 144 (1974).

23. T. Layloff, T. Miller, R. N. Adams, H. Fäh, A. Horsfield, and W. Proctor, Nature 205, 383 (1965).

24. W. A. Lathan, W. J. Hehre, and J. A. Pople, J. Am. Chem. Soc. 93, 808 (1971).

CHAPTER VI
C_4H RADICAL

Introduction

C_4H, a σ-electron free radical with one unpaired electron, had never been investigated prior to this work. However, calculations have been performed by Cowperthwaite and Bauer (1) concerning the standard heat of formation of C_4H. Using these computations, Tsuji (2) has predicted that C_4H may exist in relatively abundant quantities in carbon-rich stars below 2800°K. Also, Pontrelli (3) has predicted C_4H to be an intermediate by-product in the photolysis of C_4H_2 with radiation between 2000 and 3000 Å. However, C_4H was predicted to be formed by the reaction of C_2H with C_4H_2 and not directly by photolysis. The analysis was based on the detection of C_4HD by mass spectroscopy and no properties of C_4H were actually reported.

The object of this research was to investigate the unstable C_4H radical trapped in argon and neon at 4°K by means of ESR and optical spectroscopy. The electronic and infrared spectra of C_4H are presented, and the identification is confirmed by comparison with the spectrum of the isotopically substituted C_4D. The analysis is consistent with the known electronic and infrared spectra

of C_4H_2 (4) and C_4D_2 (5). In ESR, the hydrogen hyperfine splitting has been observed but due to the formation of deuterium atoms and C_2D as photolysis by-products of C_4D_2, the hyperfine splitting due to deuterated C_4D has not been observed. These results have been compared with INDO calculations for the C_4H.

Experimental

Diacetylene (C_4H_2) was prepared after the method described by Armitage *et al.*, (6) by the dehydrohalogenation of 1,4-dichloro-2-butyne. The purity of the product was established by comparison with the published infrared spectrum (4). Deuterated diacetylene (C_4D_2) was prepared from ordinary diacetylene after the method described by Callomon (5) by exchange in the liquid phase with heavy water in which a little sodium had been dissolved. The exchange was followed by observing the infrared spectra of successive samples in the region of the C-H and C-D stretching modes. The final sample contained about 95% C_4D_2. Hydrogen iodide (research grade) was obtained from Matheson Gas Product.

For the preparation of C_4H (or C_4D), a 1:100 mixture of C_4H_2 (or C_4D_2) and argon was deposited while being simultaneously photolyzed through a LiF optical window with radiation from the H_2/He discharge lamp. In order to produce the butatrienyl radical (C_4H_3), which had to be eliminated as an impurity, diacetylene was mixed with

hydrogen iodide and argon in a 1:1:100 ratio. Following deposition the mixtures were irradiated with the high pressure mercury lamp previously described equipped with a Corning 7-54 filter. Gas mixtures were deposited at a rate ≈ 0.2 l atm/h.

Optical Spectra and Analysis

Electronic Spectra

A thorough search for the electronic spectra of C_4H and C_4D was made from the ultraviolet to the infrared. Transitions to the first two excited states of C_4H_2 occur at 2970 Å (for the A ← X transition) and at 2650 Å (for the B ← X transition) in the gas phase (7). Figure 23 shows observed transitions for C_4H and C_4D which occur in the 3000 to 2500 Å region.

The possibility that these absorptions occur due to impurities or the parent compound is ruled out by comparison of the spectra of these compounds with Figure 23. The parent compounds C_4H_2 and C_4D_2 were identified in argon at $4^{\circ}K$ by deposition of the sample gas without photolysis. Very strong progressions originating at 2453 Å were observed for the unphotolyzed samples.

Because of these strong absorptions, analysis of the C_4H and C_4D spectra beyond 2453 Å was virtually impossible. C_4H_2 was found to produce broad, weak bands at 2897, 2725, and 2578 Å in solid argon, presumably the A ← X transition. The intensity of these bands was found to be

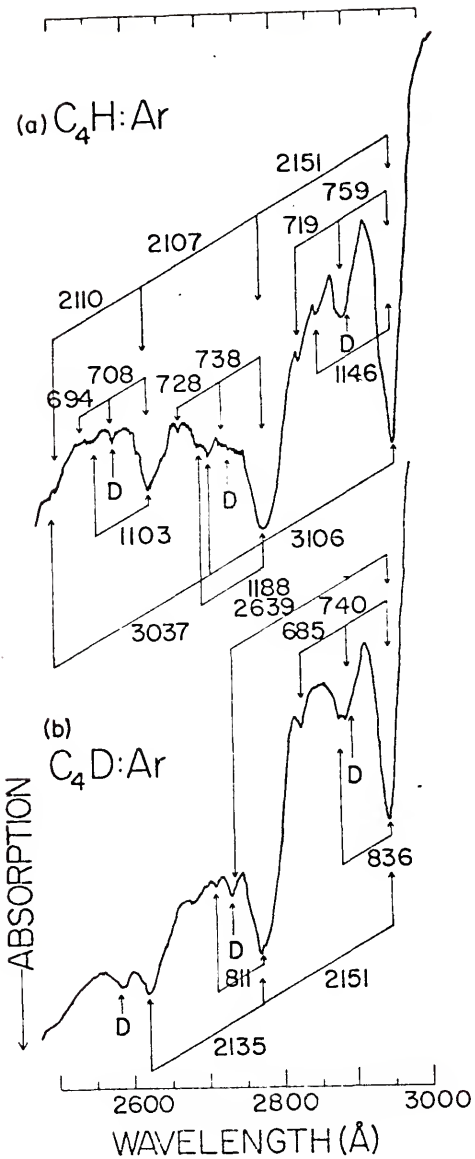

Figure 23: Optical spectra of C_4H and C_4D isolated in argon matrices at 4°K. Bands due to C_4H_2 and C_4D_2 are marked in the spectra by the letter D.

strongly dependent on the efficiency of the photolysis. These have been indicated in Figure 23 by the letter D. It was shown by ESR that the impurity C_4H_3 (butatrienyl radical) was present in the photolysis product. To eliminate the possibility that this species is the optical absorber, C_4H_3 was prepared by the method of Kasai *et al.* (8,9). The butatrienyl radicals were generated within the matrix by reacting hydrogen atoms (produced by the photolysis of HI) with diacetylene. None of the absorptions shown are due to C_4H_3.

Figure 23 shows very strong progressions in the spectra of C_4H and C_4D due to vibrational excitations of the two C≡C bonds. Since the frequencies of these vibrations are nearly equal, the bands appear very close to each other with large overlap. Figure 24 shows these transitions for C_4H at higher resolution so that both absorptions can be seen. In the presence of broader bands observed for C_4D, the two absorptions caused by these C≡C vibrations could not be resolved; however, the band shapes, as in the C_4H case, do indicate the presence of more than one absorption. (The vibrational spacings for these transitions, ν_2 and ν_3, are given in Tables XV and XVI with all the other observed bands and vibrational spacings.) It was found for C_4H that $\nu_2 = 2151\ cm^{-1}$ and $\nu_3 = 2060\ cm^{-1}$, with both progressions showing decreasing vibrational frequency for higher members of the progression (for C_4D, $\nu_2 = 2151\ cm^{-1}$).

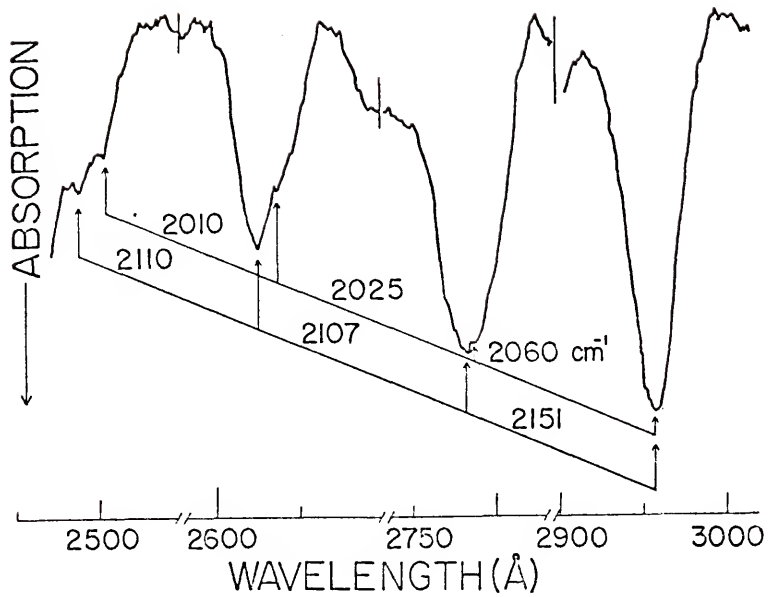

Figure 24: Optical spectrum of C_4H due to C≡C fundamental vibrations, ν_2 and ν_3, isolated in argon matrices at 4°K.

Table XV

Vibrational assignments for the 3000 Å transitions of C_4H:Ar at 4°K.

λ(Å)	ν(cm^{-1})	ΔG'(cm^{-1})					v'_1	v'_2	v'_3	v'_4	v'_5	a
2958	33797	----	----	----	---	----	0	0	0	0	0	
					759							
2893	34556				---	1146	0	0	0	1	0	
2861	34943			2060	719	----	0	0	0	0	2	
			2151									
2834	35275				---		0	0	0	2	0	
2788	35857	3106		----			0	0	1	0	0	
2781	35948		----		---	----	0	1	0	0	0	
2743	36446				738				C_4H_2			
2725	36686			2025	---	1188	0	1	0	1	0	
2709	36903	----			728		1	0	0	0	0	
			2107									
2692	37136					----	0	1	0	0	2	
2672	37414				---		0	1	0	2	0	
2639	37882			----			0	0	2	0	0	
2727	38055	3037	----		---	----	0	2	0	0	0	
					708							
2579	38763				---	1103	0	2	0	1	0	
				2010								
2553	39158				694	----	0	2	0	0	2	
2533	39467		2110		---		0	2	0	2	0	
2506	39892			----			0	0	3	0	0	
2503	39940	----					2	0	0	0	0	
2489	40165		----				0	3	0	0	0	

[a] v_1, v_2, v_3, v_4, and v_5 are the vibrational quantum numbers for the C-H stretching mode, 2 C≡C stretching modes, C-C stretching mode, and C-H bending mode, respectively.

Table XVI

Vibrational assignments for the 3000 Å transitions of C_4D:Ar at 4°K.

λ(Å)	ν(cm^{-1})	ΔG'(cm^{-1})				v_1'	v_2'	v_4'	v_5' [a]
2949	33900	----	----	---	---	0	0	0	0
				740					
2886	34640			---	836	0	0	1	0
2878	34736		2151	685	---	0	0	0	2
		2639							
2830	35325			---		0	0	2	0
2773	36051		----		---	0	1	0	0
2736	36539	----			811	1	0	0	0
2713	36862		2135		---	0	1	0	2
2676	37358								
2618	38186		----			0	2	0	0
2586	38658							C_4D_2	

[a] v_1, v_2, v_4, and v_5 are the vibrational quantum numbers for the C≡D stretching C≡C stretching mode, C-C stretching mode, and C-D bending mode, respectively.

The next most prominent progression is found to occur for the C-C vibration, ν_4, for both C_4H and C_4D. For C_4H, ν_4 was determined to be 759 cm^{-1}. In most cases, three members of each progression could be seen after which overlap would begin to occur with the strong ν_2 and ν_3 progressions. Upon isotopic substitution, ν_4 for C_4D = 740 cm^{-1} was found to be virtually unchanged.

ν_1, the C-H stretching frequency, was found to occur at 3106 cm^{-1}. The other members of the progression were too weak to be observed. Upon deuteration this frequency difference changed to 2639 cm^{-1}, due to the change in mass.

As shown in Figure 23, another transition was observed with a vibrational spacing of 1146 cm^{-1} for C_4H. This was attributed to a C≡C-H bending mode, ν_5. Upon deuteration, a similar transition was observed with a vibrational spacing of 836 cm^{-1} due to the C≡C-D bending mode, ν_5.

An attempt was made to produce C_4H trapped in neon at $4^{o}K$ in hopes of sharpening the vibrational structure of the bands observed in argon. Due to the difficulty of trapping H atoms from the photolysis in neon, the observed spectrum was weak and individual bands were broad. However, two progressions were observed due to the C≡C and C-C stretching modes. Table XVII lists the transitions and frequency differences observed for C_4H in neon.

Table XVII

Vibrational assignments for the 3000 Å transitions of C_4H:Ne at 4°K.

λ(Å)	ν(cm^{-1})	ΔG'		Vibrational Assignments[a] v_2'	v_4'
2963	33740	---	----	0	0
		804			
2894	34544	---	2028	0	1
2795	35768	---	----	1	0
		771			
2736	36539	---	2014	1	1
2646	37782	---	----	2	0
		712			
2597	38494	---		2	1

[a] v_2 and v_4 are the vibrational quantum numbers for the C≡C and C-C stretching modes, respectively.

Infrared Spectra

New transitions which occur in the infrared region when C_4H and C_4D are prepared in the matrix are shown in Figure 25. As before, the transitions due to C_4H_3, C_4H_2 and C_4D_2 are eliminated as the absorber by comparison with the infrared spectra of the parent molecules and with the infrared spectra of C_4H_3 produced by simultaneous deposition of C_4H_2 and H atoms. The infrared spectrum of the parent molecule, C_4H_2, is well characterized (4). The infrared spectrum of C_4D_2 was determined by deposition of C_4D_2 without photolysis for comparison with the photolyzed sample.

As shown in Figure 25, only two absorptions were seen for C_4H and C_4D in the infrared. C_4H has two bands, $\nu_2 = 2060\ cm^{-1}$ due to the C≡C vibration, and $\nu_5 = 735\ cm^{-1}$ due to the C≡C-H bending mode. These assignments are confirmed by isotopic substitution in C_4D in which $\nu_2 = 2050\ cm^{-1}$ and $\nu_5 = 585\ cm^{-1}$. As expected ν_2, the C≡C vibration, shows very little dependence upon the presence of the H or D while ν_5, the C≡C-H(D) bend, shows a large dependence upon the mass of the end nuclei. It would be expected that absorptions due to the stretching of the C-C bond should appear near 950-850 cm^{-1} by comparison with the C-C symmetric stretch of C_4H_2 (4), however no new absorptions were found to occur in this region. Similarly, it is expected C_4H would exhibit an

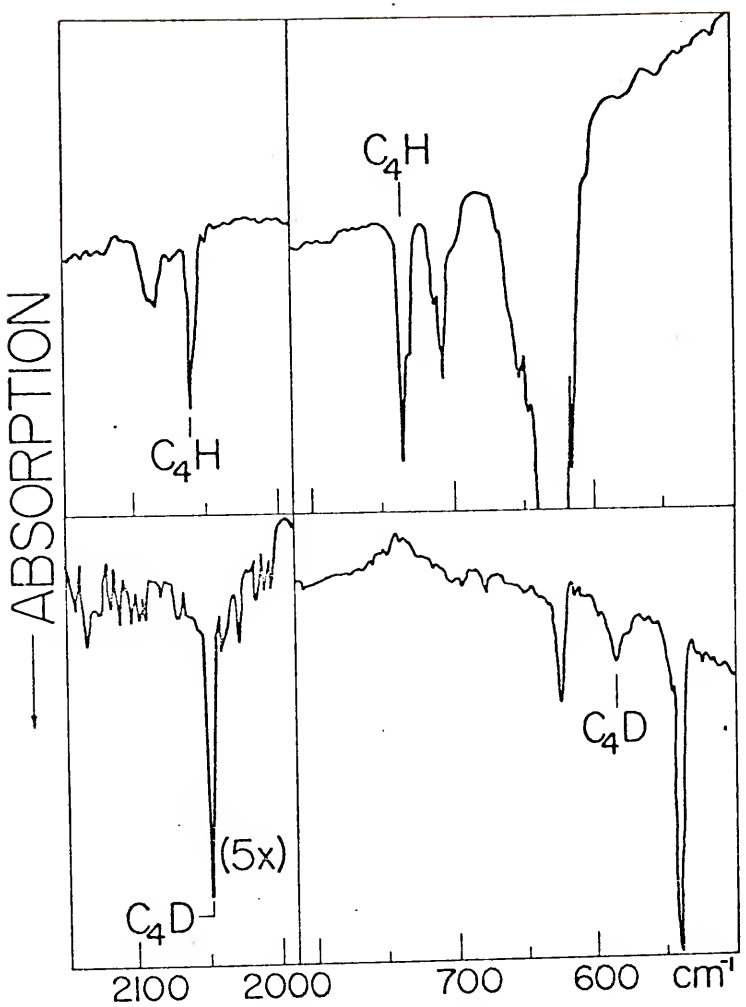

Figure 25: Infrared spectra of (a) C_4H and (b) C_4D isolated in argon matrices at 4°K. In the top spectrum, the strong bands at 636 and 709 cm^{-1} are due to the ν_8 and combination $\nu_7 + \nu_9$ modes, respectively, of the parent C_4H_2. In the lower spectrum, the strong band at approximately 530 cm^{-1} is due to the parent C_4D_2 molecule. The band at 636 cm^{-1} is due to a small C_4H_2 impurity in the C_4D_2 sample.

absorption near 3300 cm^{-1} caused by C-H stretching but due to the very strong bands of C_4H_2 in this region, it is probable that it would be overlapped and not observed.

ESR Spectra and Analysis

Figure 26 shows the observed ESR spectrum attributed to C_4H. In order to determine which lines were due to C_4H, various runs were made in which the concentration of C_4H_2 in argon was varied. It was found that lower concentrations of C_4H_2 resulted in the best observed spectrum since fewer by-products were formed. It can be seen in Figure 26 that in the production of C_4H, other species were observed such as C_2H, CH_3, and C_4H_3. (ESR spectra are given in references 10, 11 and 8 respectively.) Also hydrogen atoms and C_4 (see Chapter VII) were observed but cannot be seen in the Figure. In order to eliminate the C_4H_3 lines, C_4H_2 was deposited with H atoms to form large concentration of C_4H_3. It was found that C_4H_3 was indeed contributing to the ESR spectrum observed after the production of C_4H, but it was present in very small quantities.

Due to the overlap with these other species, only the hf lines due to the interaction of the unpaired electron with the hydrogen atom were observed. These lines are presumably perpendicular lines since the parallel

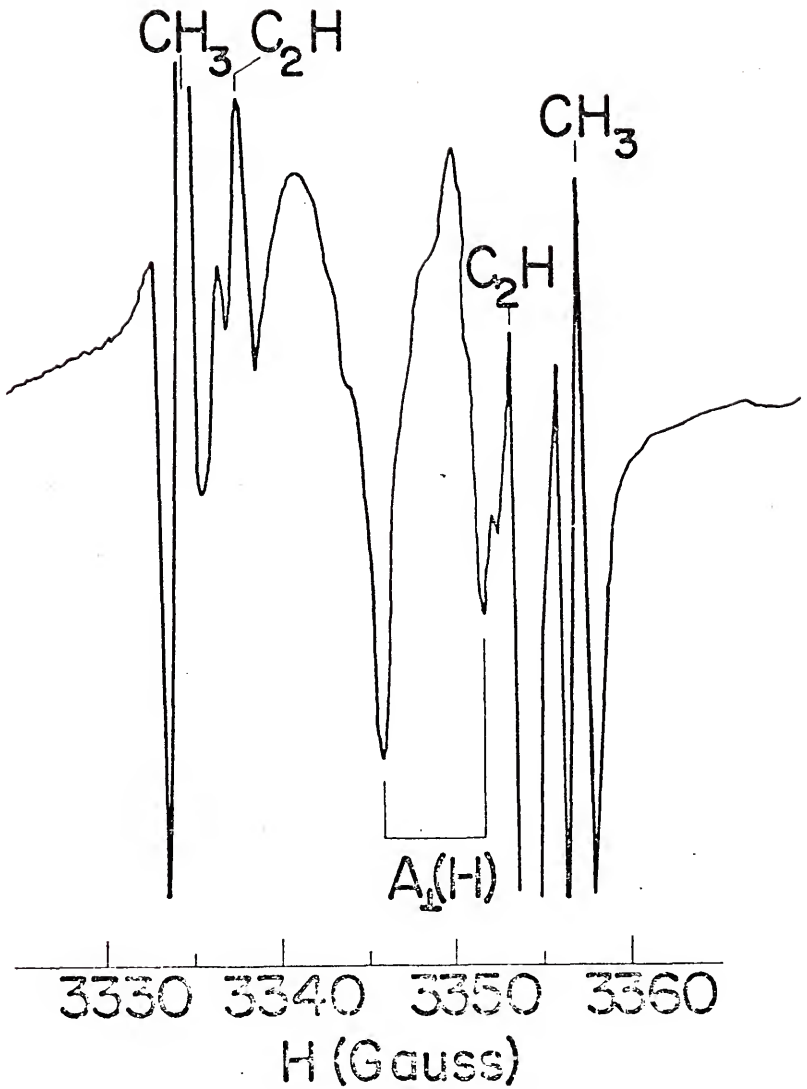

Figure 26: ESR spectrum of C_4H isolated in argon matrices at 4°K. Transitions due to the impurities CH_3 and C_2H are also indicated. The high field component of the C_4H doublet is overlapped with the high field component of the C_2H doublet. ν = 9380 MHz.

lines are expected to be weak or to overlap the perpendicular lines. The value of $A_{\perp}$(H) was determined to be 5.9 G.

An attempt was made to observe the ESR spectrum of C_4D. The ratio of the splitting of C_4H and C_4D would be A (H atom)/A (D atom) = 6.51 [values of A (H) and A (D) taken from reference 12]. The expected value of $A_{\perp}$(D) in C_4D would be ~ 1.0 G. However, in this case, the species C_2D and D atoms are also produced. The ESR spectrum of C_2D is known to consist of a triplet with a splitting of 2.58 G centered at g = 2.0025 (13) and that of the deuterium atoms consists of a triplet with a splitting of 78 G (11). Both of these species overlap the region in which the C_4D perpendicular lines are expected to occur making it impossible to observe the ESR spectrum of C_4D.

Analysis of Figure 26 yields a value of $A_{\perp}$(H) = 5.9 G and a $g_{\perp}$ value of 2.0004. The value of $A_{\perp}$(H) indicates little unpaired electron spin density on the H nuclei of C_4H. Since the odd electron is expected to be localized on the end carbon nuclei separated from the H nuclei by three other carbon nuclei, it is not unexpected that $A_{\perp}$(H) is of this magnitude.

The $g_{\perp}$ value of 2.0004 ($\Delta g_{\perp}$ = -0.0019) indicates a mixing of orbital angular momentum into the ground state wavefunction. As shown in Chapter III, a negative shift indicates mixing with a $^2\Pi_r$ excited state. It will be

shown in the discussion that a $^2\Pi_r$ excited state should exist possibly as low as 34,000 cm^{-1} above the ground state. It is probable that two $^2\Pi_i$ states lie lower in energy than the $^2\Pi_r$ state; however, as in C_2H (10) and CN (14), it is not expected, based on the value of $\Delta g_\perp$, that these states contribute very much to the g shift.

Discussion

Electronic Transitions

The ground state electronic configuration of C_4H_2, given by Callomon (5), is

$$(1s,\ 2sp,\ \sigma)^2(1s,\ 2sp,\ \sigma)^2_{C-H}(2sp,\ \sigma_g)^2_{C\equiv C}\ (2sp,\ \sigma_u)^2_{C\equiv C}$$
$$(2sp,\ \sigma_g)^2_{C-C}(2p,\ \pi_u)^4(2p,\ \pi_g)^4,\ X^1\Sigma_g^+.$$

This configuration may be viewed as the combination of two C_2H radicals through a $(2sp,\ \sigma_g)^2_{C-C}$ bond (5). Upon photolysis, a hydrogen atom is removed to give the C_4H radical. In a manner similar to that for C_2H (see Reference 10), the removal of the hydrogen atom effectively raised the $(1s,\ 2sp,\ \sigma)_{C-H}$ orbital in energy resulting in the ground state configuration for C_4H as

$$(1s,\ 2sp,\ \sigma)^2(2sp,\ \sigma_g)^2_{C\equiv C}(2sp,\ \sigma_u)^2_{C\equiv C}(2sp,\ \sigma_g)^2_{C-C}$$
$$(2p,\ \pi_u)^4(2p,\ \pi_g)^4(2sp,\ \sigma)^1,\ X^2\Sigma.$$

Several possible excited electronic states can then be found by the promotion of these electrons into higher orbitals. Two possible transitions of lowest energy might be expected by the promotion of either the π_u bonding electrons or π_g antibonding electrons into the outer σ non-bonding orbitals. These transitions are written as (neglecting other inner electrons)

$$\sigma_u^2\sigma_g^2\pi_u^4\pi_g^3\sigma^2,\ ^2\Pi_i \leftarrow \sigma_u^2\sigma_g^2\pi_u^4\pi_g^4\sigma^1,\ X^2\Sigma$$

or

$$\sigma_u^2\sigma_g^2\pi_u^3\pi_g^4\sigma^2,\ ^2\Pi_i \leftarrow \sigma_u^2\sigma_g^2\pi_u^4\pi_g^4\sigma^1,\ X^2\Sigma.$$

The resulting excited states are both $^2\Pi$ inverted states and it would be expected that the resulting spectra would show the strongest progressions in the C≡C stretching frequencies. These transitions correspond to the $A^2\Pi_i \leftarrow X^2\Sigma$ transition of C_2H (10).

If a $(2sp, \sigma_g)_{C-C}$ bonding electron is promoted into the outer σ-nonbonding orbital, the resulting state would be a $^2\Sigma$ state and the transition would be written

$$\sigma_u^2\sigma_g^1\pi_u^4\pi_g^4\sigma^2,\ \ ^2\Sigma \leftarrow \sigma_u^2\sigma_g^2\pi_u^4\pi_g^4\sigma^1,\ X^2\Sigma.$$

In the corresponding transition of the C_2H case (10), this is proposed as one of the possible states

giving rise to the electronic transitions observed in the 3000 Å region approximately 29,000 cm^{-1} above the ground state.

The final transition to be considered would arise from the promotion of the outer σ-nonbonding electron into a higher-lying π antibonding orbital forming a $^2\Pi_r$ excited state, written

$$\sigma_u{}^2\sigma_g{}^2\pi_u{}^4\pi_g{}^4\pi^*,\ ^2\Pi_r \leftarrow \sigma_u{}^2\sigma_g{}^2\pi_u{}^4\pi_g{}^4\sigma^2,\ X^2\Sigma.$$

The problem arises in trying to determine which of these excited states will give rise to the observed optical transition in the 3000 Å region. The observed spectra exhibit vibrational progressions involving most of the expected modes of the C_4H and C_4D radicals; however in both cases, the predominant bands involve a C≡C stretching frequency. Therefore it is expected to involve the π electrons. It is expected then that the excited state should be a $^2\Pi$ state. As observed for C_2H and CN, the $^2\Pi_i \leftarrow {}^2\Sigma$ transitions are weak and it is therefore likely that the upper state is $^2\Pi_r$. Also, a $^2\Pi_r$ state at this energy (~34,000 cm^{-1} above the ground state) could account for the $\Delta g_\perp$ value of -0.0019 observed in the ESR.

As stated previously concerning the optical spectra, the 1150 cm^{-1} progression was assigned to a C≡C-H bending frequency. In the isotopically substituted C_4D spectrum, this band shifts to give a frequency difference of

approximately 840 cm^{-1}. Due to the change in mass of the H nuclei to a D nuclei, such a decrease in the vibrational spacing is reasonable. Since all of the progressions are attributed to symmetrical stretches, with the exception of this transition, it seems unlikely that C_4H or C_4D is bent in the excited state. If the molecules are linear, then every other band of these bending progressions should be missing (7) (i.e. $\Delta v = 0, 2, 4 \ldots$). Therefore the 1146 cm^{-1} band is actually $2\nu_5$ for C_4H and similarly the 840 cm^{-1} band is $2\nu_5$ for C_4D. Thus ν_5 for C_4H should be approximately 570 cm^{-1} and for C_4D approximately 420 cm^{-1}. This represents a reasonable reduction as a result of deuteration on a bending mode. It should be noted that in the ground state ν_5 for C_4H is 735 cm^{-1} and 586 cm^{-1} for C_4D.

Infrared Transitions

The linear C_4H_2 molecule in its ground electronic state exhibits nine normal modes of vibration, four of which are doubly degenerate. All of these modes have been observed by infrared or Raman spectroscopic techniques (4,15).

In C_4H, there should be seven normal modes of vibration, three of which are doubly degenerate. There should be one C-H stretching mode ν_1 comparable to ν_1 and ν_4 of C_4H_2, two C≡C stretching modes, ν_2 and ν_3, comparable to ν_2 and ν_5 of C_4H_2, and one C-C stretching

mode, ν_4, comparable to ν_3 of C_4H_2. The three degenerate modes will be due to a C≡C-H bend, ν_5, and two skeletal bending modes, ν_6 and ν_7. These should be comparable to similar modes in C_4H_2.

The infrared analysis confirms one C≡C stretching mode and one C≡C-H bending mode, ν_5, verified by isotopic substitution. The non-observance of a C-H stretching frequency in C_4H is attributed to possible overlap with the large C-H stretching band of the C_4H_2 parent molecule. Much effort was taken to try to observe the C-C stretching frequency of C_4H which would be expected to appear near 850 cm^{-1} based on C_4H_2, however, this was never observed. No skeletal bendings were observed. Based on relative intensities and positions of similar transitions observed for C_4H_2, it is expected that these would be unobservable. In summary, Table XVIII lists the frequencies of the various vibrations observed in the $X^2\Sigma$ ground state and $^2\Pi_r$ excited state of C_4H and C_4D compared with the corresponding mode of C_4H_2 in $^1\Sigma_g^+$ ground state.

ESR Observations

The observance of an ESR spectrum which consists of a doublet due to the hfs of the H nuclei confirms that C_4H has a $^2\Sigma$ ground state. Since only two components were observed, it also indicates that C_4H is linear, i.e. has axial symmetry.

Table XVIII

The frequency of vibrational modes observed in $X^2\Sigma$ ground state and the $^2\Pi_r$ excited states of C_4H and C_4D compared with the corresponding modes of C_4H_2 in the $^2\Sigma_g^+$ ground state.

Mode		C_4H_2 (gas)[a] $X^1\Sigma_g^+$	C_4H:Ar $X^2\Sigma$	C_4H:Ar $^2\Pi_r$	C_4D:Ar $X^2\Sigma$	C_4D:Ar $^2\Pi_r$
C-H stretch	ν_1	3329	ν_1	3100		2640
C≡C symmetric stretch	ν_2	2184	ν_2[b]	2130		2140
C≡C antisymmetric stretch	ν_5	2020	ν_3[b] 2060	2060	2050	
C-C stretch	ν_3	874	ν_4	760		760
C-H bend	ν_6	627	ν_5 735	570	586	485

[a] See A. V. Jones, reference (4).

[b] Identification of ν_2 and ν_3 is somewhat arbitrary but may be rationalized on the basis of the behavior of similar C≡C stretching modes of C_4H_2.

Assuming that $A_{||}(H) \simeq A_{\perp}(H)$, as found for C_2H (10), then the value of A_{iso} (H) is found to be 16.5 MHz. INDO calculations have been performed on C_4H using the bond distances found for C_4H_2 by the electron diffraction work of Tanimoto (16). The predicted value of A_{iso} (H) obtained was 9.1 MHz. These values are in reasonable agreement.

The value of A_{iso} (H) = 16.5 MHz indicates that the unpaired electron has a spin density on the H nuclei of about 1%. As previously stated, the unpaired electron is presumably localized predominantly on the end carbon nuclei separated from the H nuclei by three other carbon nuclei, therefore a value of 1% is reasonable.

The negative g shift of 0.0019 indicates mixing of orbital angular momentum into the ground state wavefunction, caused predominantly by the excited $^2\Pi_r$ state approximately 34,000 cm^{-1} above the ground state. Although $^2\Pi_i$ states are expected to lie lower in energy than the $^2\Pi_r$ state, these states were not observed optically. As with C_2H, the $^2\Pi_i$ states evidently do not mix with the ground state wavefunction to any appreciable extent.

From the value of $\Delta g_{\perp} = -0.0019$, the value of the spin doubling constant, γ, may be estimated. From equation 84,

$$\gamma = -2B\Delta g_{\perp} \qquad (84)$$

where B is the average rotational constant. Using a calculated value of B = 0.1565 cm^{-1} [B for C_4H_2 was found to be 0.1464, see reference (17)], a value of $\gamma = + 6 \times 10^{-4}$ cm^{-1} is predicted.

References - Chapter VI

1. M. Cowperthwaite and S. H. Bauer, J. Chem. Phys. 36, 1743 (1962).

2. T. Tsuji, Proc. Japan Acad. 40, 99 (1964).

3. G. J. Pontrelli, The Formation and Properties of Certain Cometary Species, NASA publication, Contract number NASw707, Greenbelt, Maryland, (1965).

4. A. V. Jones, Proc. Roy. Soc. (London) 211A, 285 (1972).

5. J. H. Callomon, Can. J. Phys. 34, 1046 (1956).

6. J. B. Armitage, E. R. H. Jones, and M. C. Whiting, J. Chem. Soc., 44 (1951).

7. G. Herzberg, Electronic Spectra and Electronic Structure of Polyatomic Molecules, New York: Van Nostrand-Reinhold, 1966.

8. P. H. Kasai, J. Am. Chem. Soc. 94, 5950 (1972).

9. R. H. Kasai, L. Skattebol, and E. B. Whipple, J. Am. Chem. Soc. 90, 4509 (1968).

10. W. R. M. Graham, K. I. Dismuke, and W. Weltner, Jr., J. Chem. Phys. 60, 3817 (1974).

11. R. W. Fessenden and R. H. Shuler, J. Chem. Phys. 39, 2147 (1963).

12. P. B. Ayscough, Electron Spin Resonance in Chemistry, London; Methuen, 1967.

13. E. L. Cochran, F. J. Adrian, and V. A. Bowers, J. Chem. Phys. 40, 213 (1964).

14. W. C. Easley and W. Weltner, Jr., J. Chem. Phys. 52, 197 (1970).

15. F. A. Miller, D. H. Lemmon, and R. E. Witkowshi, Spectrochim. Acta. 21, 1709 (1965).

16. M. Tanimoto, Bull. Chem. Soc. Japan 44, 386 (1971).

17. A. V. Jones, J. Chem. Phys. 20, 860 (1952).

CHAPTER VII
C_4 MOLECULE

Introduction

It has been shown in various mass spectrometric measurements that polyatomic molecules up to at least C_5 exist in carbon vapor at high temperatures (1-5). Because of the importance of such polyatomic carbon molecules, Pitzer and Clementi (6) and others (7-10) have made theoretical calculations of the stabilities and thermodynamic properties of the larger species. In these calculations, it is predicted that the most stable structure of C_4 would be a linear system. Clementi (7) has predicted that C_4 should have a $^3\Sigma_g^-$ ground state, and has also estimated the energies of the various excited states for C_4. In the ground state it is expected that C_4 should correspond to the structure :C=C=C=C:, although others (9) predict a ·C≡C-C≡C· type structure. The heat of formation of C_4 has been determined to be 229.8 kcal/mole from mass spectrometric measurements (3,5). The only other experimental parameter determined for C_4 is the infrared vibrational frequency (4) at 2164 cm^{-1} observed at 4^oK in argon matrices.

The object of this research was to investigate further the C_4 molecule by means of ESR and optical

spectroscopy in order to determine the electronic properties of the species isolated at 4°K in various rare gas matrices. The results have been compared to the predicted properties previously mentioned.

Experimental

C_4 was prepared by two completely different techniques. First, by the photolytic decomposition of C_4H_2 and C_4D_2 in argon by means of the previously described H_2/He electrodeless discharge lamp. In this technique, 1% C_4H_2 and C_4D_2 (see C_4H experimental section) in argon gas samples were photolyzed through a lithium fluoride optical window during very slow depositions (~0.1 l-atm/h). The C_4 was then trapped on a sapphire rod for ESR studies or on a sapphire window or cesium iodide window for optical studies which was cooled to 4°K by liquid helium. In the regions of interest, no unidentified impurities were detected.

Another method used to prepare C_4 was by the vaporization of spectroscopic grade graphite after the method of Thompson et al. (4). A tantalum tube, 0.25 in. in diameter, 1.0 in. long, with about 0.008 in. wall thickness, and with a 0.040 in. orifice drilled in the side, was packed with a powdered carbon sample. Tantalum plugs filled the ends and the tube was resistance heated. After heating at about 2400°K for one hour, the tantalum cell was converted to carbide. The cell was then raised

to approximately 2700°K for the vaporization of carbon. In all experiments, variable temperature dewars were employed so that the temperature of the trapped sample could be raised to allow diffusion to occur. Upon raising the temperature to approximately 23°K, significant enhancement of the C_4 signals resulted.

Carbon-13 graphite, 98% enriched, was obtained from Monsanto Company (Mound Laboratory, Miamisburg, Ohio). Natural carbon (99% carbon-12) was obtained from Union Carbide (Carbon Division, Union Carbode Corp.).

Due to the weak signals of C_4 observed in some ESR experiments, a Nicolet Signal Averager (Model 1072 equipped with SW-71A and SD-72A units) was used to enhance the signal to noise ratio (S/N).

ESR Spectra

If C_4 is a linear molecule as predicted, and has a $^3\Sigma_g^-$ ground state, it should exhibit an ESR spectrum as described in the ESR theory section (Chapter III). The theoretical absorption and first derivative spectra for randomly oriented triplets (E = 0) is shown in Figure 27. The ESR spectrum should consist then of five transitions, termed $\Delta M = 2$, z_1, xy_1, xy_2, z_2 in the order of increasing magnetic field in Figure 27. Equations 68 and 69 give the resonant field positions (H_r) at which these transitions should occur for given D and g values. Figure 28a shows the observed ESR spectrum of $^{12}C_4$ at 4°K in argon

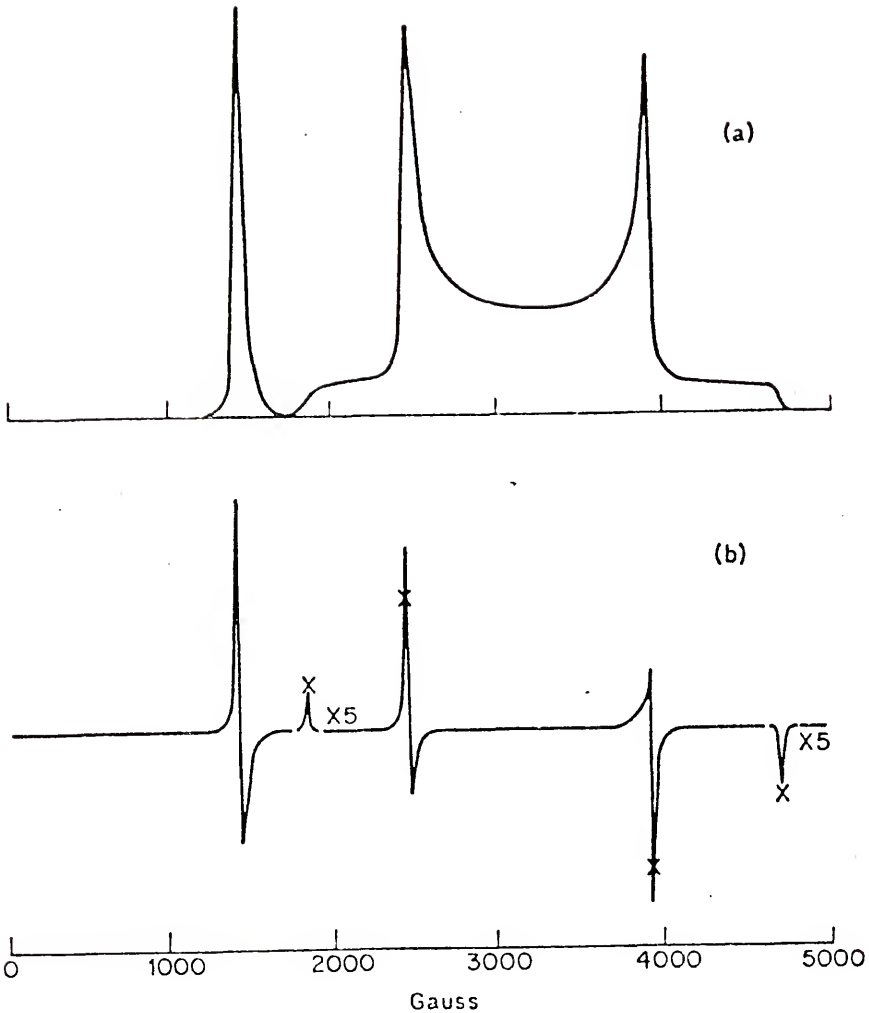

Figure 27: Theoretical absorption and first derivative spectra for randomly orientated triplets (E = 0).

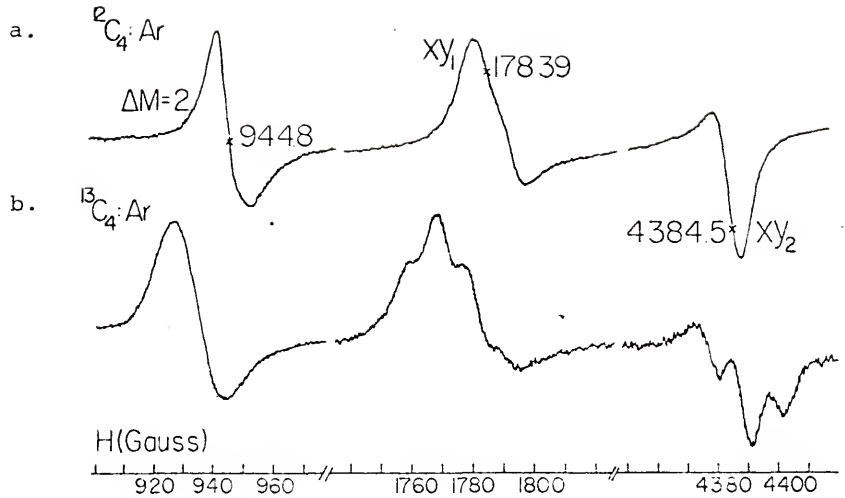

Figure 28: ESR spectra of (a) $^{12}C_4$ and (b) $^{13}C_4$ isolated in argon matrices at 4°K. (See Table XIX for line position of various transitions and cavity frequencies.) Triplet structure in (b) for xy_1 and xy_2 transitions is due to hf interaction.

matrices. Only the three strongest transitions are shown which correspond to the $\Delta M = 2$, xy_1, and xy_2 transitions. No z_1 or z_2 lines were observed in these experiments even though signal averaging was employed. If D is less than $h\nu_o$, the $\Delta M = 1$ signals may be weaker than the $\Delta M = 2$ signal (11) which is the case for C_4. The lines observed for C_4 are very broad as can be seen in Figure 28a. This may also help to account for the non-observance of the weaker z_1 and z_2 lines.

The $\Delta M = 1$ (z_1, z_2, xy_1, and xy_2) transitions occur over a range of several thousand gauss. But the shape of the derivative curve gives special prominence to those resonance fields in which the external field lies along one of the principal magnetic axes of the molecule. These experimentally observed resonances in the randomly oriented samples are due to the relatively few molecules in which one of the three magnetic axes is approximately aligned with the external field.

With ^{13}C was substituted, the spectrum in Figure 28b resulted. The original $^{12}C_4$ lines are split by interaction of the unpaired electrons with the magnetic ^{13}C nuclei. The interaction of the unpaired electrons with the ^{13}C nuclei results in a triplet pattern for each observed ^{12}C line in an approximate ratio of 1:2:1. The measured splitting allows the $A_{\perp}$ value for the end carbons to be calculated. Since no parallel lines were observed, the

value of $A_{||}$ could not be determined. From a comparison of Figure 28 (a) and (b) it can be seen how the hfs broadens each line approximately 10 to 20 gauss with respect to the $^{12}C_4$ lines.

The positions of these lines were found to be dependent on several factors, all of which affected the zero-field parameter, which will be treated in the ESR analysis. The factors include isotopic substitution, temperature, and the effect of different matrix gases.

When ^{13}C was substituted, the observed lines were shifted due to a change in the D value. The $\Delta M = 2$ and xy_1 transitions were shifted down field while the xy_2 transition was shifted up field indicating an increase in the zero field splitting.

Annealing experiments were carried out on $^{12}C_4$ in which the ESR spectra were recorded while the matrix was held at a specified elevated temperature. Figure 29 shows the resulting spectra recorded at approximately 4, 18, and 32°K. Spectra were also recorded at 12 and 24°K but are not shown in Figure 29. The indicated temperature was maintained within about ± 1°K during the recording of the spectra. It can be seen that both the $\Delta M = 2$ and the xy_1 lines are shifted to higher fields while the xy_2 line is shifted to a lower field for increasing temperature. The process is completely reversible in that quenching the matrix to 4°K always

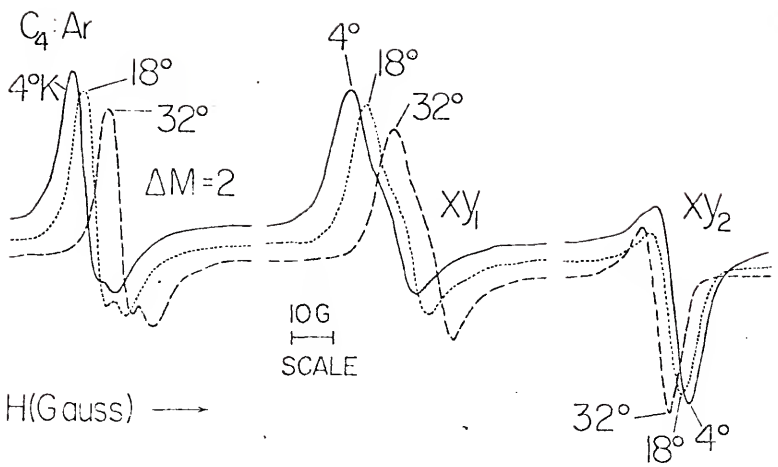

Figure 29: ESR spectra of $^{12}C_4$ isolated in argon matrices at various temperatures. ν = 9.390 GHz, $g_\perp$ = 2.0042(4).

restores the original spectrum. The lines do not appear to be broadened upon increasing the temperature. These shifts indicate a decrease in the D value with an increase in the temperature.

When neon was used as the matrix gas instead of argon, there was an increase in the D value, with the xy_1 and $\Delta M = 2$ transitions moving to lower fields and the xy_2 transition moving to higher fields. It was hoped that neon would improve the band shapes because of decreased matrix gas-triplet molecule interactions but that was not the case.

Some additional features (not shown in Figure 28) were observed near 6000 G when C_4 was prepared by the vaporization of graphite. These were attributed to CCO (12) but as a result of their position, no problems were encountered with overlap. When C_4 was produced by the photolysis of C_4H_2 (C_4D_2) additional features of C_4H, C_4H_3, C_2H and CH_3 were observed near g = 2.00 (see C_4H section, Chapter VI) but again as a result of their position, no analysis problems were encountered.

ESR Analysis

The line positions obtained from the ESR spectra shown in Figure 28 are listed in Table XIX along with the values observed for $^{12}C_4$ in neon. As stated previously no parallel lines were observed in any experiments. As a result of the low yields of C_4 in neon, the line positions were more difficult to determine.

Table XIX

Observed ESR lines in gauss[a] for $^{12}C_4$/Ar, $^{13}C_4$/Ar, and $^{12}C_4$/Ne isolated at 4°K.

	$^{12}C_4$/Ar	$^{13}C_4$/Ar	$^{12}C_4$/Ne
$H_{\Delta M=2}$	944.76	936.64	797.4[b]
H_{xy_1}	1783.93	1772.0	1633.7
H_{xy_2}	4384.46	4388.6	4435.2
H_{z_1}	952.24[b]	938.8[b]	799.5[b]
H_{z_2}	5748.24[b]	5760.4[b]	5892.5[b]

[a] ν = 9.389 GHz for $^{12}C_4$/Ar, 9.387 GHz for $^{13}C_4$/Ar, and 9.377 for $^{12}C_4$/Ne.

[b] predicted from equations 68 (c) and (d) assuming $g_{||} = g_e$.

Using equations 68 (a) - (d) for the line positions, the value of D and $g_{\perp}$ can be solved for by substituting in the observed positions for the xy_1 and xy_2 transitions. D can be given by the equation

$$D = \left(\frac{H_{xy_2}^{\ 2} - H_{xy_1}^{\ 2}}{H_{xy_2}^{\ 2} + H_{xy_1}^{\ 2}} \right) h\nu_o. \qquad (91)$$

Substituting the values given in Table XIX into this equation, it is found that $D(^{12}C_4/Ar) = 0.2242\ (2)\ cm^{-1}$, $D(^{13}C_4/Ar) = 0.2254\ (2)\ cm^{-1}$, and $D(^{12}C_4/Ne) = 0.2381\ cm^{-1}$. Possible explanations for these changes in D will be considered in a later section.

The value of $g_{\perp}$ is given in terms of D by

$$g_{\perp} = \left(\frac{g_e}{H_{xy_2}} \right) [H_o(H_o + D/g_e\beta)]^{1/2}. \qquad (92)$$

From the values of H_{xy_2} and the calculated D values, $g_{\perp}$ was determined to be 2.0042(4) for both cases in argon and 2.0046 for the neon results. Since no parallel lines were observed, $g_{||}$ could not be determined experimentally. However, it is usually found that $g_{||} \simeq g_e$. If this is assumed (i.e. $g_{||} = 2.0023$) then the line positions for H_{z_1} and H_{z_2} can be predicted. The results of these predictions are given in Table XIX.

When ^{13}C was substituted, the observed splitting in Figure 28b resulted. Substituting the observed splitting (ΔH) in equation 77, a value of $A_{\perp}$ = 10.19 Gauss (28.56 MHz) was obtained. No value for $A_{||}$ could be determined. The value for $A_{\perp}$ is expected to be principally caused by the interaction of the unpaired electrons with the nuclear moments of the two equivalent end ^{13}C nuclei from Clementi's MO calculations (7).

The line positions obtained from the ESR spectra shown in Figure 29 were used to calculate the values of D for $^{12}C_4$ at various temperatures. Table XX lists the calculated values of D for 4, 12, 18, 24, and 32 (± 1)^{o}K. Values of $g_{\perp}$ were calculated for each case and, as expected, it was found that $g_{\perp}$ was constant (within experimental results). It can be seen that as the temperature rises, there is a non-linear increase in the value of D.

Optical Spectrum and Analysis

A thorough search was made for the optical spectrum of C_4 from the ultraviolet into the infrared regions. Upon vaporization of graphite the infrared and optical spectra were taken. There was no indication in the infrared of the C_4 vibration, which should appear at 2164 cm^{-1} in argon at 4^{o}K (4). There were transitions observed however for C_3 and CO, as expected. In the optical and ultraviolet regions, there were strong bands of C_3 (13). Upon annealing the sample to 15^{o}K, the

Table XX

Calculated D (cm^{-1}) values for $^{12}C_4$ isolated in argon matrices at various temperatures.[a]

Temperature (^{o}K)	D (cm^{-1})
4(±1)	0.2242
12(±1)	0.2240
18(±1)	0.2238
24(±1)	0.2237
32(±1)	0.2230

[a] $g_{\perp}$ - 2.0042 (4)

infrared indicated the appearance of the C_4 stretching frequency at 2164 cm^{-1} while the optical spectrum showed the appearance of a band system originating at 5206 Å with another member of a progression appearing at 4703 Å to yield a vibrational spacing of 2054 cm^{-1}. Upon further annealing to 20°K, the C_4 transition in the infrared and the new band system reached maximum intensity with the 5206 Å system sharpening considerably. Subsequent annealing affected neither of the systems. Thus, based on the similar appearance and behavior of the new band system with the infrared signal of C_4, this 5206 Å system has been attributed to an electronic transition of C_4. This state then lies approximately 19,200 cm^{-1} above the ground state and has a vibrational spacing of 2054 cm^{-1}. Table XXI lists the observed transition, vibrational frequency and frequency differences.

Examination of the optical regions of interest for experiments in which C_4H_2 was photolyzed with the H_2:He discharge lamp revealed the appearance of a weak band at 5206 Å also. Due to the weak intensity, the second member of the progression was not observed. Similar results were obtained when C_4D_2 was used as the parent species.

The appearance of the 5206 Å system was previously reported by Weltner, et al. (13,14) and it was suggested that the system could be due to C_4, C_5, etc. (14).

Table XXI

Transitions observed for $^{12}C_4$ in argon matrices at $4^{o}K$.

(v',v")	Wavelength (Å)	$\nu(cm^{-1})$	$\Delta G'(cm^{-1})$
(0,0)	5206	19203	
			2054
(1,0)	4703	21257	

Discussion

Optical Transitions

The ground state configuration for C_4 may be written as (7)

$$1\sigma_g^2 1\sigma_u^2 2\sigma_g^2 2\sigma_u^2 3\sigma_g^2 3\sigma_u^2 4\sigma_g^2 4\sigma_u^2 5\sigma_g^2 1\pi_u^4 1\pi_g^2, X^3\Sigma_g^-.$$

The first four orbitals correspond to the atomic $1s^2$ closed shells of the carbon atoms. The electrons in the remaining three σ_g and two σ_u molecular orbitals provide for the σ bonds and two essentially non-bonding pairs. The six remaining electrons are distributed four in the $1\pi_u$ and two in the $1\pi_g$ molecular orbitals. Promotion of a $5\sigma_g$ non-bonding electron is expected to form the first excited state which is predicted (7) to lie approximately 28,000 cm^{-1} above the ground state. This configuration is written as ... $4\sigma_g^2 4\sigma_u^2 5\sigma_g^1 \pi_u^4 \pi_g^3$ (neglecting all other inner electrons) giving rise to a $^3\Pi_g$ inverted state. Due to the g ↮/↛ g electronic selection rule, it is not expected that this state will be observed optically. The next higher excited state predicted by Clementi (7) to lie approximately 34,000 cm^{-1} above the ground state, results from the promotion of a $4\sigma_u$ antibonding electron into the outer $1\pi_g$ molecular orbital. The configuration written ... $4\sigma_g^2 4\sigma_u^1 5\sigma_g^2 1\pi_u^4 1\pi_g^3$ gives rise to a $^3\Pi_u$ inverted excited state. This

presumably is the transition that gives rise to the optical absorptions at 5206 Å (19,000 cm^{-1} above the ground state).

No other transitions were observed that varied with annealing as the 5206 Å system. If the C_4 molecules were in a triple-single-triple bonded structure, it might be expected that another progression would appear in the 5206 Å system with a vibrational spacing indicative of a carbon single bond, but none was observed.

All other excited states predicted by Clementi should appear in the vacuum ultraviolet region.

g Tensor

The shift of $g_\perp = 2.0042$ (4) from the free electron value of $g_e = 2.0023$ indicates that there is mixing of orbital angular momentum from excited states into the ground state wavefunction of C_4. The positive shift, $\Delta g_\perp = +0.0019$ (4), indicates that the lowest-lying excited state that mixes with the ground state should be a $^3\Pi$ inverted state. From the predictions of Clementi (7) the lowest-lying excited state is expected to be the ... $4\sigma_g^2 4\sigma_u^2 5\sigma_g^1 1\pi_u^4 1\pi_g^3$, $^3\Pi_g$ inverted state. Since the orbital angular momentum operator $\underline{L}$ should mix the $^3\Pi_g$ state with the ground $^3\Sigma_g^-$ state, the observed g shift is consistent with the predicted energy level scheme. However, Clementi (7) predicts this state to

lie approximately 28,000 cm^{-1} above the ground state (i.e. it should be observed at approximately 3500 Å in the ultraviolet region). Since the optical studies have indicated that a $^3\Pi_u$ inverted state (predicted to lie higher than the $^3\Pi_g$ state) lies approximately 19,000 cm^{-1} above the ground state, it can be expected that the $^3\Pi_g$ excited state could lie lower than 19,000 cm^{-1} above the ground state. It should be noted that due to the selection rules ($g \not\leftrightarrow g$), the observance of this transition in the optical region is not expected.

Unfortunately, since no parallel lines were observed, the exact value of $g_{||}$ cannot be determined. However, it is not expected that $g_{||}$ should differ much from g_e. If it is assumed that $g_{||} = g_e$, the line positions for the parallel transitions, z_1 and z_2, can be predicted. Using the calculated D values and assuming $g_{||} = g_e$, H_{z_1} and H_{z_2} have been predicted and the values expected are listed in Table XIX. The value of H_{z_1} in every case is very near the observed $\Delta M = 2$ transition. Due to the broadness and intensity of this transition, it is then not expected that the z_1 line should be observed.

From the value of $\Delta g_{\perp} = +0.0019$ (4), a corresponding value of the spin-doubling constant can be estimated. From equation 84,

$$\gamma = -2B\Delta g_{\perp} \tag{84}$$

where B is an average rotational constant. Assuming equal bond distance between the carbon nuclei in C_4 of 1.28 Å, the calculated value of B is 1.72×10^{-1} cm^{-1}. Then γ should be approximately -0.0006 (1) cm^{-1}.

A Tensor

The value of $A_{\perp}(C_{1,4})$ = 28.56 MHz is expected to be predominantly the hyperfine splitting due to the interaction of the unpaired electrons with the two outer carbon nuclei. No parallel lines and therefore no parallel hf splittings were determined making it impossible to determine A_{iso} and A_{dip}. The small value of $A_{\perp}$ indicates that the unpaired electrons have little s-character. This is not surprising considering the predictions of Clementi (7) where the unpaired electrons are in π molecular orbitals which would have little or no electron spin density at the carbon nuclei.

Zero-Field Splitting Parameter (D)

From the value of D for C_4, the energies of the various states may be determined at zero magnetic field. It has been shown that (15)

$$Z = -\frac{2}{3} D, \quad X = Y = \frac{1}{3} D, \text{ and } E = 0 \qquad (93)$$

where X, Y, and Z are the energy levels of the molecule at zero-field as illustrated in Figure 10 and 11. The value of D for $^{12}C_4$ isolated in argon at $4^{o}K$ is

0.2242 (2) cm^{-1} which is equivalent to X = Y = 0.0747 and Z = -0.1495 cm^{-1}. When ^{13}C is substituted, it was found that for $^{13}C_4$ = 0.2254 (2) cm^{-1} with X = Y = .0751 and X = -0.1503 cm^{-1}.

^{13}C substitution then causes the zero-field-splitting to increase from 0.2242 to 0.2254 cm^{-1}. There appear to be two possible explanations for this.

An effect that could alter the D value upon isotopic substitution is the variation in bond length of the C_4 molecule (12). It can be seen from equation 37 that D varies as $1/r^3$ where r is the distance separating the two electronic dipoles. A 1% decrease in the value of r will be seen as a 3% increase in the observed D value. Pierce (16) has observed a slight decrease in the bond length of NNO upon isotopic substitution of ^{15}N. He observed a bond variation of approximately .002 Å or a 0.1% decrease in the overall bond length. A similar decrease in the bond length of C_4 upon ^{13}C substitution would be reflected in a 0.3% increase in the D value. From experimental data, it is observed that the D values of $^{12}C_4$ and $^{13}C_4$ indicate approximately a 0.5% increase in D. This means that if the only effect changing the value of D is the change in bond length, a change of 0.16% is required. Based on the example of NNO, this then is a reasonable explanation.

The usual explanation of isotope effects on D is that the molecules are undergoing torsional oscillation in the matrix (17-20). A restrictive potential is assumed to be involved which is proportional to $(D_g/D_g-D_m)^2$ (where D_g and D_m are the zero-field splitting parameters in the gas and matrix, respectively) and to I^{-1} (the moment of inertia of the molecule) (17). Due to mass effects on the moment of inertia, heavier isotopes reduce motion compared to the lighter isotopes evidenced by an increase in the D value for the heavier isotopes. The results observed for $^{12}C_4$ and $^{13}C_4$ are consistent with such a model (D for $^{12}C_4$ = 0.2242, $^{13}C_4$ = 0.2254). Due to steric factors including the size of rare gas matrix atoms, molecular sizes, and temperature, it was thought unlikely that C_4 would be oscillating when trapped at $4^{o}K$ in the matrix, however, the results do indicate that C_4 is possibly moving in the matrix.

The ESR spectrum of C_4 isolated in argon was measured as a function of temperature in order to gain more information concerning its possible libration in the matrix. As the temperature increased, it would be expected that the D value of a trapped C_4 molecule should approach the gas phase value. Based on the isotope effect and the experimentally determined values for CCO (12), it is expected that D_{gas} of C_4 should be higher than D_{matrix}. However, upon warming the matrix to higher temperatures, it was found that the D value decreased.

Recall (see Table XX) that as the temperature was increased from approximately $4^{o}K$ to $32^{o}K$, the D value decreased non-linearly from 0.2242 to 0.2230 cm^{-1}. This implies an increase in motion of the radical at elevated temperatures, i.e., a lower restrictive potential at higher temperatures.

It is observed in changing the rare gas matrix from neon to argon for C_4, that the D value decreases from 0.2381 cm^{-1} to 0.2242 cm^{-1}. A similar trend was also observed in the case of CCO (12) for changes from neon to argon. From theoretical consideration it was found that the matrix should affect both the electronic spin-spin and the spin-orbit contributions to the D value of the gas molecule (12). The effect of the rare gas on the spin-spin interactions of C_4 may be considered by viewing the rare gas as a force tending to compress the trapped species. As heavier matrices are used with presumably larger substitutional sites, the compression should decrease and the value of the electron dipole-dipole distance should effectively increase, resulting in a decreased value of D. This effect must be reasoned to be very small, however, since there appears to be no present evidence of any increase in D when a triplet molecule is trapped in a matrix. It was also shown (12) that the matrix effect upon the spin-orbit contribution to D is proportional to $-\xi^2$ where ξ is the spin-orbit

coupling constant of the rare gas. Since ξ^2 increases rapidly in going to heavier matrices, it would be expected that D should decrease rapidly from this effect, and this was observed to be very marked for CCO in Kr and Xe (12). This is probably the main reason for the observed decrease in the D value of $^{12}C_4$ from neon and argon matrices.

References - Chapter VII

1. R. E. Honig, J. Chem. Phys. 22, 126 (1954).

2. W. A. Chupka and M. G. Inghram, J. Phys. Chem. 59, 100 (1955).

3. J. Drowart, R. P. Burns, G. DeMaria, and M. G. Inghram, J. Chem. Phys. 31, 1131 (1959).

4. K. R. Thompson, R. L. DeKock, and W. Weltner, Jr., J. Am. Chem. Soc. 93, 4688 (1971).

5. W. C. Steele, U. S. Air Force Syst. Command, Air Force Mater. Lab., Tech Rep., AFML, TR 70-67 (1970).

6. K. S. Pitzer and E. Clementi, J. Am. Chem. Soc. 81, 4477 (1959).

7. E. Clementi, J. Am. Chem. Soc. 83, 4501 (1961).

8. E. Clementi and H. Clementi, J. Chem. Phys. 36, 2824 (1962).

9. S. J. Strickler and K. S. Pitzer in Molecular Orbitals in Chemistry, Physics, and Biology (edited by P. O. Lowdin and B. Pullman) New York: Academic, 1964.

10. R. Hoffman, Tetrahedron 22, 521 (1965).

11. E. Wasserman, L. C. Snyder, and W. A. Yager, J. Chem. Phys. 41, 1763 (1964).

12. G. R. Smith, and W. Weltner, Jr., to be published.

13. W. Weltner, Jr., P. N. Walsh, and C. L. Angell, J. Chem. Phys. 40, 1299 (1964).

14. W. Weltner, Jr. and D. McLeod, Jr., J. Chem. Phys. 45, 3096 (1966).

15. M. Weissbluth in Molecular Biophysics (edited by B. Pullman and M. Weissbluth) New York: Academic, 1965.

16. L. Pierce, J. Mol. Spect. 3, 575 (1959).

17. H. Meyer, M. C. M. O'Brien and J. H. Van Vleck, Proc. Roy. Soc. (London) A243, 414 (1958).

18. H. Kon, J. Am. Chem. Soc. 95, 1045 (1973).

19. R. A. Bernheim, H. W. Bernard, P. S. Wang, L. S. Wood, and P. S. Skell, J. Chem. Phys. 54, 3223 (1971).

20. E. Wasserman, W. A. Yager, and J. Kuck, Chem. Phys. Lett. 7, 409 (1970).

BIOGRAPHICAL SKETCH

Keith Ingram Dismuke, was born on August 27, 1948, in Jackson, Tennessee, and is the son of Mr. and Mrs. George A. Dismuke of Jackson, Tennessee. He graduated from Jackson High School, Jackson, Tennessee, in June, 1966, and entered Union University in Jackson in August, 1966. In June, 1970, he was graduated from Union University with a Bachelor of Science in Chemistry. Since September, 1970, he has pursued a course of study leading to a Doctor of Philosophy degree in Chemistry at the University of Florida, Gainesville, Florida. He is married to Marilyn Lindsey Rose and has one child, Craig Ian.

I certify that I have read this study and that in my opinion it conforms to acceptable standards of scholarly presentation and is fully adequate, in scope and quality, as a dissertation for the degree of Doctor of Philosophy.

William Weltner, Jr., Chairman
Professor of Chemistry

I certify that I have read this study and that in my opinion it conforms to acceptable standards of scholarly presentation and is fully adequate, in scope and quality, as a dissertation for the degree of Doctor of Philosophy.

Wallace S. Brey, Jr.
Professor of Chemistry

I certify that I have read this study and that in my opinion it conforms to acceptable standards of scholarly presentation and is fully adequate, in scope and quality, as a dissertation for the degree of Doctor of Philosophy.

John P. O'Connell
Associate Professor of Chemical Engineering

I certify that I have read this study and that in my opinion it conforms to acceptable standards of scholarly presentation and is fully adequate, in scope and quality, as a dissertation for the degree of Doctor of Philosophy.

Gus J. Palenik
Professor of Chemistry

I certify that I have read this study and that in my opinion it conforms to acceptable standards of scholarly presentation and is fully adequate, in scope and quality, as a dissertation for the degree of Doctor of Philosophy.

Martin T. Vala
Associate Professor of Chemistry

This dissertation was submitted to the Graduate Faculty of the Department of Chemistry in the College of Arts and Sciences and to the Graduate Council, and was accepted as partial fulfillment of the requirements for the degree of Doctor of Philosophy.

March, 1975

Dean, Graduate School